DFT STUDIES ON FUNCTIONAL MATERIALS FOR ADVANCED APPLICATIONS

THESIS

SUBMITTED FOR THE AWARD OF THE DEGREE

OF

Doctor of Philosophy

IN

APPLIED PHYSICS

Submitted by

RAJKAMAL SHASTRI

Enrolment No.: 589/11

Under the Supervision of

Dr. ANIL KUMAR YADAV

BABASAHEB
BHIMRAO
AMBEDKAR
UNIVERSITY

LUCKNOW

प्रज्ञा शील करुणा

ESTABLISHED 1996

DEPARTMENT OF APPLIED PHYSICS
SCHOOL FOR PHYSICAL SCIENCES
BABASAHEB BHIMRAO AMBEDKAR UNIVERSITY
(A CENTRAL UNIVERSITY)
LUCKNOW-226025, U.P. (INDIA)

2019

DECLARATION

I declare that the thesis entitled "**DFT Studies on Functional Materials for Advanced Applications**" has been prepared by me under the supervision of **Dr. Anil Kumar Yadav,** Assistant Professor, Department of Applied Physics, School for Physical Sciences, Babasaheb Bhimrao Ambedkar University, Lucknow. No part of this thesis has formed the basis for the award of any degree, diploma or fellowship previously. I, declare that the material embodied in the present work is based on original research work and the indebtedness to others has been duly acknowledged at relevant places. This is also declared that the thesis is essentially free from any kinds of plagiarism.

(Rajkamal Shastri)

Department of Applied Physics
School for Physical Sciences
Babasaheb Bhimrao Ambedkar University,
Lucknow-226025, U.P., India

Date: 12/03/2019
Place: Lucknow

CERTIFICATE

This is to certify that the thesis titled "**DFT Studies on Functional Materials for Advanced Applications**" submitted by **Mr. Rajkamal Shastri** is an original research work and has not been previously submitted in part or full for the award of any other degree or diploma to this or any other university or institutions.

The thesis submitted to the Babasaheb Bhimrao Ambedkar University, Lucknow, satisfies all the requirements as stipulated in the *Doctor of Philosophy (Ph.D.) regulations -1999 as amended in 2010* and it is fit for the submission and evaluation for the award of Doctor of Philosophy of the University.

Date: 12/03/2019

Supervisor 12/3/19

14/3/19

Head of the Department

ACKNOWLEDGEMENT

First and foremost, I wish to express my profound sense of deepest gratitude and sincere thanks to my honorable and esteemed supervisor ***Dr. Anil Kumar Yadav*** *for the continuous support during my Ph.D. study and related research, for his patience, motivation, and immense knowledge. His guidance helped me in all the time of research and writing of this thesis. I could not have imagined having a better advisor and mentor for my Ph.D. study.*

I convey my sincere thanks to all the faculty members of Applied Physics Department: ***Prof. Devesh Kumar (Head), Prof. B. C. Yadav, Dr. Ramesh Chandra, Dr. Devendra Singh, and Dr. K. B. Thapa*** *for their insightful comments and encouragement, but also for the hard question which incented me to widen my research from various perspectives. A warm thank goes to the departmental Lab Staff for providing friendly and motivating environment during the research work.*

I wish to express my reverence and sense of deep gratitude to ***Prof. S. N. Tiwari (Department of Physics, DDU Gorakhpur University), Prof. Umesh Yadawa (Department of Physics, DDU Gorakhpur University), Prof. Lallan Yadav (Department of Physics, DDU Gorakhpur University), Dr. Divya Srivastava (Department of Physics, Central University of Rajasthan),*** *for their invaluable, insightful comments and suggestions to improve the quality of this work.*

I would like to special thanks to my seniors and friends ***Dr. Rakesh Sonker, Dr. Radheshayam Saroj, Dr. Jitendra Kumar, Dr. Pranav Uppadhaya, Dr. Gaurav Hitkari (DAC, BBAU), Dr. Suresh Kumar, Dr. Ajay Kumar (DAS, BBAU), Mr. Deep Kumar, Mr. Asheesh Kumar, Mr. Gaurav Saxena, Mr. Surya Pratap Goutam, Mr. Ratindra Gautam, Mr. Krishan Pal, Mr. Utkarsh Kumar, Mr. Narindar Kumar, Mr. Diptarka Roy, Mr. Anwesh Pandey, Mr. Ashish Kumar, Mr. Pawan Singh, Ms. Samiksha Sikarwar, Ms. Ruchi Mishra, Ms. Yash Kaur Singh, Mr. Sonu Maurya, Mr. Arvind Rawat, Ms. Rolly Yadav, Ms. Nidhi Awasthi, Ms. Shweta, Ms. Bhavna Pal, Ms. Rajni Chaudhary*** *in for the stimulating*

discussions, and providing a friendly and cooperative environment and for moral support and encouragement throughout this journey.

My deepest gratitude goes to my friend ***Mr. Vivek Kumar Nautiyal (Assistant Professor, Department of Physics, Gaya College, Gaya), Mr. Shivam Kumar Mishra (IPR, Gandhinagar), Mr. Munendra Pal (IIT, Hyderabad),*** *for scientific discussion on various topics and his moral support and encouragement.*

I devote this thesis to my beloved parents ***(Pita Ji Shri Rambachan Ram and Mata ji Smt Kumari Devi)*** *for their lot of love, support and sacrifice from the early first day of my journey of life. I also express my sincere hearty thanks to my sisters* ***Mrs. Kiran, Miss. Premlata Shastri and Miss. Snehlata Shastri*** *and my brother-in-law* ***Mr. Sanjay Kumar (Teacher),*** *for providing me with every kind of support.*

I would like to thanks to uncle ji ***(Shri Jagram Singh)*** *and aunty ji* ***(Smt Kushumlata Singh), Mrs. Anju Singh*** *(Di) and* ***Mrs. Lakshmi aunty*** *(my cook) for their constant moral support during stay at their home.*

Last, but not least, I would like to thank the authors of various research articles and books whose work has been consulted, utilized and cited in my thesis.

I would further like to acknowledge University Grants Commission (UGC) for the financial support, throughout the course of this work.

(Rajkamal Shastri)

ABSTRACT

Considerable effort has been devoted by the researchers on the understanding nanostructures, particularly nanoparticles and nanoclusters and predicting the structures of single stable units, which can offer the possibility of developing cluster assembled materials and nanodevices in recent years. Metals oxides and semicondustors are the materials which are potentially applicable in the field of microelectronics, computer memories, coatings, optics, sensors, catalysis, photovoltaic, energy storage and biomedicine etc. Recent advances in the area of functional materials include the development of porous materials, light-emitting materials, thermoelectric materials, ionic and electronic conducting materials, and nanomaterials etc. With the recent advances in experimental and improved computational techniques, exploration of clusters has been increasing rapidly in the past few decades. Nanoclusters represent the intermediate phase between small molecular species and the bulk state. The knowledge of the atomic structure of nanoclusters is essential as their physical and chemical properties change significantly as size decreases from bulk level to nanoscale. To study the physical properties of such clusters, it is indispensable to have an understanding about cluster evolution and possible structural changes that arise as a function of the nanocluster size because it can lead to the tailoring of novel materials with desirable properties. In view of the enormous potential of transition metal and semiconducting clusters, computational based theoretical investigations have been performed applying *ab initio* (DFT) method in present thesis, to study structural, electronic and vibrational properties of functional materials in form of clusters. Density functional theory (DFT) is one of the most efficient, accurate and cost-

effective methods for the theoretical study of the clusters for the understanding of new properties and phenomena at the atomic and molecular level. The major goal of the thesis is the construction of molecular clusters of semiconducting and transition metals using different possible geometry and to contribute towards fundamental understanding of how clusters can act as a building blocks for constructing nanostructures whose properties may be tailored through the choice of size, composition/doping. These clusters are further optimized in order to obtain the stable cluster of different sizes. To examine the structural and chemical stabilities of the optimized nanoclusters, parameters such as binding energy (BE), highest-occupied and lowest-unoccupied molecular orbital (HOMO-LUMO) gap, ionization potential and electron affinity have been calculated. Moreover, chemical potential (CP), chemical hardness (CH), and dipole moment (DM) vibrational frequencies, infrared intensities (IR Int.), relative infrared intensities (Rel. IR Int.) and Raman scattering activities have also been computed and analyzed. The physical and chemical properties of these clusters have been better discussed for the application point of view and can be of benefit to scientists working with objects of nanoscale for the development of novel materials and technology. The properties of clusters are a function of their clusters size. An important finding of the present study is that the linear stacking of stable units of the ring may undergo to GaN nanowires. Similarly, sideways stacking of several units of rhombus structure may results in nanotube formation.

Overall, observations reveal some important results that can be useful in the development of materials using nanoclusters as building blocks and tailoring the properties of many nanoclusters.

PREFACE

Understanding the functional materials in form of different nanostructures is very important for refining our knowledge about the stimulating and important chemical phenomena occurring in novel materials. The results of theoretical and experimental research suggest that properties of atomic and molecular clusters are directly related to shape, size and geometry of the clusters, and the clusters possess size dependent properties which are quite different from the bulk; and can be used as assembly blocks for building novel materials with inimitable properties. The advancement of computational power provided very efficient methodologies to study different properties of the functional materials in the form of clusters. DFT is one of the most efficient, accurate and cost-effective methods for the theoretical study of clusters for the understanding of new properties and phenomena at the atomic and molecular level. Therefore, in this thesis, computational based theoretical studies applying *ab initio* (DFT) method have been done to investigate the structural, electronic and vibrational properties of functional materials in the form of clusters. The main focus of the thesis is the construction of molecular clusters of some semiconducting and transition metals using different possible geometry and understanding of their properties. In an effort to construct clusters, structural stability and other physical and chemical properties of considered clusters have been better discussed for the application point of view and for the development of novel materials. Entire thesis comprises seven chapters, which are organized as follows.

Chapter one begins with a brief introduction of materials, which explain the need for functional materials and its application for human civilization. In this chapter, we have shed light on the functional materials and their properties in form clusters.

Chapter two presents theoretical and computational methodology used in the thesis. This chapter includes the quantum mechanical calculation methods and its applications. It explains the basis of DFT and the details of its implementation with the main approximations needed to improve it.

In **Chapter three,** we constructed small clusters of CdS (Cadmium Sulfide) taking different possible geometry and studied their structural, electronic and vibrational properties in form of nanoclusters.

Chapter four focuses on the study of ZnO nanoclusters and their structural stability. These nanoclusters were created considering even no. of Zn (Zinc) and O (Oxygen) atoms in ZnO molecules.

Chapter five deals with the DFT study on structural stability and electronic Properties of CoO (Cobalt Oxide) nanoclusters.

In **chapter six,** we have performed a comparative *ab initio* study on structural evolution, stability and electronic properties of undoped and Al-doped GaN and Al-GaN Clusters. Finally, **Chapter seven** presents the conclusion of the entire thesis and further scope of study on such an important class of clusters for advanced applications.

LIST OF ABBREVIATION

1.	**DFT**	Density Functional Theory
2.	**HF**	Hartree Fock
3.	**BE**	Binding Energy
4.	**FBE**	Final Binding Energy
5.	**ZPE**	Zero Point Energy
6.	**GS**	Ground State
7.	**IP**	Ionization Potential
8.	**AIP**	Adiabatic Ionization Potential
9.	**VIP**	Vertical Ionization Potential
10.	**EA**	Electron Affinity
11.	**AEA**	Adiabatic Electron Affinity
12.	**VEA**	Vertical Electron Affinity
13.	**EC**	Electron Correlation
14.	**CdS**	Cadmium Sulfide
15.	**ZnO**	Zinc Oxide
16.	**CoO**	Cobalt Oxide
17.	**GaN**	Gallium Nitride
18.	**HOMO**	Highest Occupied Molecular Orbital
19.	**LUMO**	Lowest Unoccupied Molecular Orbital
20.	**DOS**	Density of State
21.	**DM**	Dipole Moment
22.	**CP**	Chemical Potential
23.	**CH**	Chemical Hardness
24.	**IR**	Infrared
25.	**CFA**	Central Field Approximation
26.	**CI**	Configuration Interaction

LIST OF FIGURES

LIST OF TABLES

CONTENTS

Chapter-1
Introduction

Chapter 1

Introduction

1.1 Introduction

Materials have the capability to offer the structure and the strengths that clamp the development and advancement of society together [1-5]. These materials are more deep-seated in our culture; due to this our daily life is influenced and dependent on materials in myriad ways. In the ancient time, people had been concerned with the problem of only simple materials like clothing, foods and the construction materials for their homes etc. and had access to only a very limited number of materials like stone, wood, clay etc. [6-10]. People are still facing problems of materials, regarding needs for clothes and accommodation such as in old days, but along with this nowadays human being's life become tremendously dependent on an excessive variety of materials, which may be used in transportation, communication, medicals, constructions, clothing, and food production recreation etc. During the end of the 19^{th} century, growth of scientific knowledge was aimed at industrial applications and with the evolution of time, new techniques were discovered for manufacturing innovative materials [11-15]. These materials have unique properties which make them superior from the ordinary natural materials. The properties of materials could be changed by various parameters (like cooling, heating etc.) and the addition of materials or substances which was an evolution in the field of materials science and opened the door for new kinds of materials with various interesting properties [15-25]. The knowledge about the materials in the past years had been allowing designing thousands of different materials with unique characteristics and properties that will prominently affect the world we live in, and fulfill the needs of

modern civilizations. Currently, the interest of scientific communities across the world has been directed towards search of novel materials. The innovative development of materials and their technology make the survival of humankind more comfortable and have been closely connected with the convenience of suitable materials [20-30].

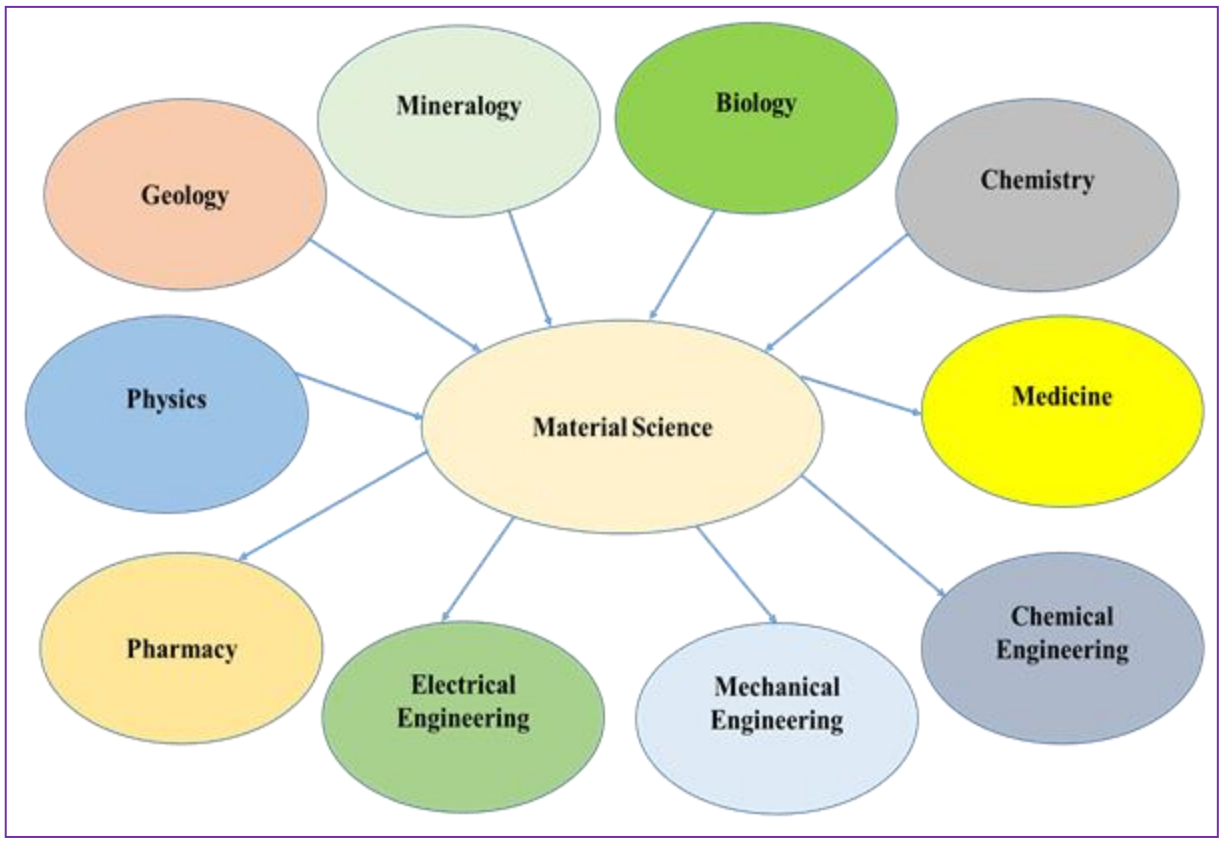

Figure 1.1: Diagram for the related fields of materials science.

1.2 Functional Materials

For a number of centuries, most of the human requirements were fulfilled by the some materials like natural polymer (wool, cotton, asbestos, cellulose) alloys, ceramics, and metals. The innovative period of materials took its birth at the beginning of the twentieth century. This century is the age of new emerging materials (smart materials) which is an essential need for establishing a smart community and systems, which is

further collection of the subsystem of self-retaining, processing, actuation, sensing, feedback, and self-diagnosis [31-39]. In the past few decades, large attention has been paid on the manufacturing of smart materials which can quickly respond to change in surrounding. The manufacturing of such materials is challenging and crucial for the development in the field of electronics, microelectronics, memory devices, surface coating, optoelectronics, sensors, electrical, energy storage, information technology, computer science and engineering, medical, bio-medicine, defense, education, safety engineering and military technologies and transportation. Presently, research community closely focuses on the development of functional materials which will lead the modern science and technology towards the development of smart system and community to make human life much easier in the near future [40, 41]. The term 'functional materials' covers materials, which have capability to execute certain functions and their properties (i.e. chemical and physical) are very sensitive to a change in surrounding such as temperature, pressure, magnetic field, electric field, optical wavelength etc. [40-42]. The properties of functional materials in novel applications lead to outstanding performance characteristics.

1.2.1 Classification of Functional Materials

Functional materials can be classified on the basis of properties (electrical, optical and magnetic) of the materials and its applications in the area of information technology (IT), electrical energy conversion (EEC), biological applications, space technology, sensing, and actuation etc.

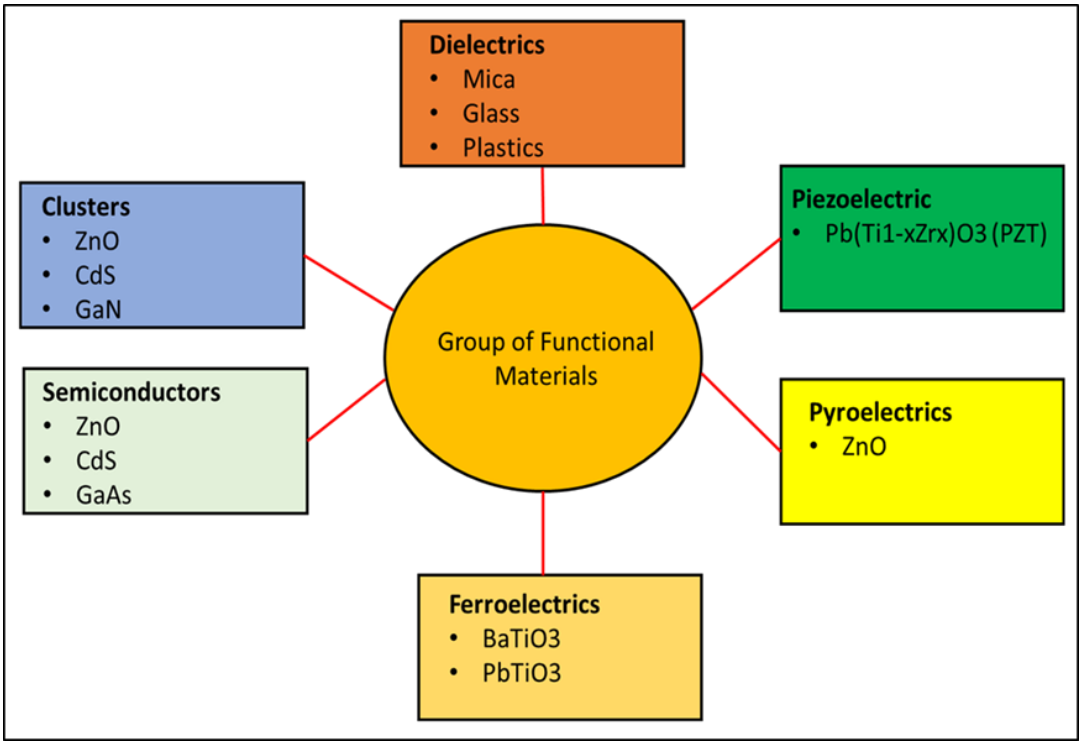

Figure 1.2: Diagram for the various groups of functional materials.

The group of functional materials primarily includes dielectrics, pyroelectrics, piezoelectric, ferroelectrics, ferroelectric relaxors, incipient ferroelectrics, semiconductors, clusters, ionic conductors, superconductors, electro-optics and magnetic materials [43-47].

1.2.2 Applications of Functional Materials

Functional materials are potentially applicable in the field of microelectronics, computer memories, coatings, optics, sensors, catalysis, photovoltaic, energy storage and biomedicine etc. Recent advances in the area of functional materials include the development of porous materials, light-emitting materials, thermoelectric materials, ionic and electronic conducting materials, and nanomaterial [48-55].

1.2.3 Nano Structures of Functional Materials

Nanoscience and nanotechnology is a broad and interdisciplinary area of research that has been growing rapidly worldwide and have received overwhelming interest of the scientific and academic realm in recent years due to its peculiar properties and unlocked the innovative area of research and development for the entire world. The word 'nano' deal with a scale called nano-scale, which belongs to 1 to 100 nm [56-58]. Nanoscience and nanotechnology are primarily concerned with the fabrication, characterization, control and manipulation of materials at the nanoscale. Nanostructures of materials at the nanometer scale not only enrich the specific properties but also exhibit novel physical properties [58-60]. Main reason behind this are quantum confinement effect and an extremely increase in the surface to volume ratio, which are not found in corresponding bulk materials [61-63]. Examples of nanostructured materials are clusters, nanoparticles, nanocrystals, quantum dots, nanowires, and nanotubes etc. [64, 65].

1.3 Clusters

Clusters may be defined as the determinate combinations of atom or molecules containing two to ten lakhs of atoms, which are controlled by the forces like metallic, covalent, Van der Waal and ionic. The small and multi atom particles ($3*10^7$ atoms) are also considered as clusters in clusters science. Clusters signify the intermediate phase between atom and bulk systems and are potentially applicable in various fields of science and technology [66]. Clusters can be prepared experimentally and theoretically by different methods. With the advancement in computational power and techniques, theoretical and experimental data can be correlated appropriately, also cluster science helps much to understand and explain an experiment. Experimentally, they are produced

in molecular beams by the free jet expansions methods. This technique permits precise, detailed and sensitive study which plays an important role in the experimental growth and study of the clusters. It has some limitations and is not appropriate for producing massive clusters. So, this method of clusters production is not relevant for industrial use [67, 68].

1.3.1 Development of Clusters Science (*Brief History*)

The arena of clusters science is rapidly increasing and has opened avenue for interdisciplinary fields of study in last three decades. The scientific community and researchers across the world have devoted considerable efforts to study and understand the clusters and their properties in recent years. The cluster was firstly reported in 1940 as existing in the literature [69]. Colloidal chemistry was very old technique through which clusters were prepared initially. In 1956, optical properties of gold colloidal were investigated by Faraday [70]. Clusters produced by the colloidal method were found to be more stable than those created in molecular beams, and were also in larger amount as far as industrial applications are concerned. Additionally, this technique allows us to control the size, shape, and structure of the clusters for desire applications, which is the foremost significance of this technique [71-73]. During 1980, the need and development of novel materials made the clusters as the new area of research owing to its unique properties. With the great effort by the scientific community, first cluster was created in 1980 which further lead to the development of fullerenes (in 1986) and CNT (carbon nanotube). Clusters have the regular expansion of combined events through which bulk materials can be well explained. One investigation about the cluster is that the collective behavior of materials can be transformed in form of size of a small cluster, which led to the crucial development in the area of clusters science. Some examples of the collective phenomena

exists, such as electrical conductivity, absorption, and refraction of light, the color of the body, and magnetic properties such as ferromagnetic, ferrimagnetic and antiferromagnetic. In last decade, area of clusters science has extended enormously due to the considerable studies devoted to the types of clusters. Clusters establish a link among the atomic, molecular, surface and condensed matter, chemical physics and help to explain many chemical and physical phenomenon in the new atmosphere.

1.3.2 Types of Cluster

Clusters may be classified on the basis of atoms used in their formation and nature of bond present therein. They are mainly designed by the elements available in the periodic table. Stained glass window has been made of copper, silver and gold metal, which are known as coinage metal clusters. Silver clusters are commonly used in photography. Clusters are also found in an atmosphere like water cluster. C_{60} is a well-known carbon nanocluster in form of bucky ball structure [74].

1.3.3 Metal Clusters (MCs)

Clusters which are made from the metallic elements of the periodic table are called metal clusters. These clusters composed of one or more metallic atoms. Generally, alkali, alkaline, and transition metals are used to form metal clusters. The bonds between these clusters are metallic, delocalized and independent of directions, which mainly involve *s*-orbitals; for example, sp-metals, where *s* and *p*-orbitals participate in bonding have nature of the covalent bond. Moreover, in transition metal elements along with *s*- and *p*- orbitals, *d*-orbitals also participate, which has a higher degree of valency and directionality in bonds [75].

1.3.3.1 Alkali Metal Clusters (AMCs)

Clusters made from the first group elements (Li, Na, K etc.) of the periodic table are known as alkali metal clusters. From the literature, it is found that sodium small clusters (less than four atoms) exist in form of planer structures [75]; whereas the clusters containing more than five or six atoms in three-dimensional structures possess fivefold symmetry. In the largest Na clusters, interatomic distances between atoms reduced quickly and approach to bulk nature [42].

The geometrical structure of Na clusters depends on the no. of atoms present. From the available literature, it is investigated that Na containing three atoms (Na_3) has isosceles triangle geometry [77-80], while Na containing four atoms (Na_4) has a rhombus structure [77-83]. When there are five or six atoms in the structures, it has trapezoidal and pentagonal pyramid geometry [77, 79-81]. The other alkali metal clusters like Lithium (Li) and Potassium (K) clusters have hexamers geometry and follow the similar geometry trend as the Na clusters [77, 78, 81, 82, 84, 85].

1.3.3.2 Alkaline-Earth Metal Clusters (AEMCs)

Clusters constructed from the second group elements (Be, Mg, Ca, Ba etc.) of the periodic table are known as alkaline earth metal clusters (AEMCs). The interaction between these clusters is very weak due to the much closed ns^2 outward shell formation. These clusters have three-dimensional structures which contain even four atoms [86]. The structures of the clusters are very compacted and follow solid sphere-packing procedures in small clusters containing very few atoms. The magnesium (Mg) clusters possess the various assemblies of the structures than the alkali metal clusters. Mg_3 clusters containing

three atoms have equilateral triangle geometry, while Mg_4 and Mg_5 have tetrahedron and triangle bipyramidal geometry, respectively [87-92].

1.3.3.3 Transition Metal Clusters (TMCs)

The d-block elements of the periodic table are known as the transition metal element. The clusters composed of the transition metals are known as transition metal clusters (TMCs). These clusters play an important role in catalysis application. Magnetic properties of the transition metals are function of clusters size. When the cluster size is altered the magnetic properties changed and are different from the bulk materials. In these clusters, unfilled d-electrons are more localized in comparison to the *s* and *p*-electrons of simple metals, which are more responsible for the change in the properties of transition metal clusters; and their structural geometry, electronic and magnetic properties are exactly changed in comparison to simple metals like Mg, Ca K, Na, and Al etc. HOMO-LUMO energy gaps in these clusters are very small due to unfilled d-orbitals [42]. The electronic properties of such metals clusters are very much different from those of the surface metal. The structural stability of these clusters does not follow any regular pattern. Most of the transition metal clusters prefer 3-dimensional structure having only four atoms in their structures [42]. Parks at al. performed the icosahedral growth in Nickel (Ni) clusters [93]. Excitingly, sometimes it is found that thirteen atoms clusters behave as magic clusters. These properties of clusters vary from cluster to cluster; and such behavior is observed in alkaline earth metal clusters which reveal that the d-orbital electrons make icosahedral development. Theoretical investigations of TMCs applying first principle method are very lesser in comparison to the studies on s-p bonded

structure. The main reason behind this is that the TMCs involve d-orbital electrons. The tight-binding method was used for the investigation on some transition metal elements like neutral and charged Fe and Ti clusters applying the simulation technique [94]. These clusters show icosahedral structures in the range of thirteen to nineteen atoms. It was found that the hexagonal isomer of Ti_{22} possesses lowest energy. These calculations predict that the clusters containing 7, 9, 13, and 19 atoms are magic clusters, which were also compared with experiment [95]. These results were found in good agreement with a collision-induced dissociation study [96], which predict that the positively charged clusters having 7, 13, and 19 numbers of atoms are more stable than the any other cluster. Fe clusters are more interesting due to having unique magnetic properties [97-99]. Its reactivity strongly depends on the size of small clusters [100]. A good agreement was found with a change in IP (ionization potential). Panas et al. correlate the ionization potential with the electronic structures of these clusters [101]. A good correlation was found with the variation in ionization potential. Conceicao et al. established a good agreement with the variance of the ionization potential and affinity [102]. The dissociation energy of positively charged clusters was measured by Lian et al. [103]. Postor et al. established a good agreement in IP with the measured value by applying tight-binding method considering the bcc-type structures [104]. Using photoelectron microscopy, Wang et al. [105] have studied the electronic structures of Fe clusters. Better correlation was found between the theoretical and experimental results for the clusters containing the number of atoms more than 9 and have bcc structures [106].

1.3.4 Ionic Clusters (ICs)

These clusters are formed with the combination of cations and anion atoms having static charge and depend on its stoichiometry wherein binding of the constituents involves the electrostatic interaction between the positively and negatively charged species. The polarities of bonds depend on the electronegativity variance between the atoms, and it increases when electronegativity is increased in compound clusters [107]. In this case, bonds are defined as ionic in character. For example, the clusters composed of sodium (Na) and chlorine (Cl), zinc (Zn) and oxygen (O), gallium (Ga) and nitrogen (N) etc.

1.3.5 Rare Gas Clusters (RGCs)

The clusters which are made of inert gas elements of the periodic table are known as rare gas or inert gas clusters. Rare gas elements (from He to Rn) are situated in the last group of the periodic table [107]. Formation of these clusters is possible only at low temperature and atoms are held together by very weak force which is known as Van der Waal. Moreover, the interatomic attraction is proportional to its atomic mass and when atomic mass increases, the attraction between atoms also increases.

1.3.6 Molecular Clusters (MCs)

Molecular clusters are those clusters which possess aggregates of molecules such as CO_2, NH_3, H_2O, and TiO_2 etc. These clusters can be built by repeating unit of a molecule. Further, they are classified as homo molecular clusters and hetero molecular clusters. In a homo molecular cluster, the molecule is of the same type, while heteromolecular cluster contain different molecules. In clusters of molecules, the constituent molecules are held together by different types of bonds such as Van der Waal

and hydrogen bonds and the interactions originating from the dipole-dipole and higher order multipolar interactions. Hence, studies of these clusters are of great importance from a chemical and physical point of view [107].

1.3.7 Semiconductor Clusters (SCs)

Semiconductor clusters (SCs) are made up of atoms belonging to group IV elements of the periodic table, such as carbon (C), Silicon (Si), Germanium (Ge), Selenium (Se) and tellurium (Te). Other semiconductor clusters are constructed by combining IIIrd and Vth, IInd and VIth and IIIrd and Vth group's atoms, for example- Gallium arsenide (GaAs), ZnO and GaN, respectively. In these clusters, atoms are connected through strong and directional covalent bonds. In SCs, HOMO-LUMO gaps are the function of clusters size, and when there is variation in HOMO-LUMO energy gaps the properties of photoluminescence of the materials changed [106]. The discovery of nanotubes [108] lead to the formation of miniature devices and can be used as Hydrogen (H) storage resources [109]. Silicon (Si) clusters were studied both experimentally and theoretically due to its unique photoemission properties [110]. From the available literature, it is found that silicon clusters containing four, six, seven and ten number of atoms have closed-shell structures and energy band gap nearly about 1 to 1.5 eV, same as Germanium (Ge) clusters. Highest occupied molecular orbital (HOMO), lowest unoccupied molecular orbital (LUMO) and ionization potential (IP) investigated for the silicon, germanium, and tin clusters for the number atoms less than twenty (N<20) have higher values of ionization potentials, and there was a quick decrease for the clusters containing twenty-two atoms (N = 22) [111, 112-114]. From photodissociation [115-118] and collision-induced dissociation [119-121] experiments, it was observed that

the clusters, which contain ten atoms in the clusters are more stable than the any other cluster. The vibrational behaviors and structures of small Ge and Si clusters have been investigated through infrared [122] and Raman spectroscopies [123]. The mobility of cationic clusters, such as Si and Ge clusters were measured by Jarroled and coworkers and their experiment established the existence of isomers. They also stated that when Si clusters contain near about 27 atoms in the clusters (N = 27), its structure vary from the rectangular to spherical shape, whereas Ge atom clusters also show this structural change from prolate to spherical one when it contain approximately 70 atoms (N ≈ 70). There are two types of allotropes of tin (Sn): first is α-Sn and other is β-Sn. The nature of α-Sn is semiconducting and possesses diamond-like structure, very stable at the temperature below 286 K. β-Sn shows metallic nature and possesses bcc tetragonal structures. Its structure is stable under extensive surrounding. The experiments show that the magic behaviors of the clusters of Pb, Si or Ge depend on growth conditions of these clusters [124-126]. Ion mobility measurement [127] predict the prolate type structure of Sn clusters similar to Si clusters; when it contain 35 to 65 atoms in the clusters, its structure transit from prolate to spherical structures. The formation energy of isolated Sn clusters has been measured by Bachels et al. through calorimetric measurement [128]. The small Sn clusters have a high melting temperature comparable with Sn in bulk form [129]. It is also found that larger clusters of Sn with radius of 5 to 50 nm have a lower melting point of temperature. So, it is concluded that there exists critical size of clusters below which Sn clusters have a higher melting temperature as compared to the bulk materials. This unique behavior of the Sn clusters is similar to clusters of another elements, which are very important for the development of novel technology. The theoretical analyses on Sn

clusters have been performed by different methods: quantum chemical [130, 131], Hartree-Fock (HF), tight binding (TB) [124, 132], and density functional theory (DFT) based method to find out the lowest possible energy and structures. Andreoni and coworkers [133, 134] performed local density approximation (LDA) study on small clusters of Ge and Si from the ab initio molecular dynamics method with norm-conserving pseudopotentials, and found these to have similar structures [106].

1.4 Properties of Metal Clusters

1.4.1 Ionization Potential (IP)

The ionization potential (IP) is defined as the minimum energy required in removing one electron from the neutral cluster. Ionization potential can be determined by the equation in form of the total energy of the neutral and ionized clusters is given below-

$$IP\ (X_n) = E\ (X_n^+) - E\ (X_n) \qquad \text{…….1.1}$$

Where IP (X_n) is ionization potential, E (X_n^+) is the energy of the cation clusters; E (X_n) is the energy of the neutral clusters [135, 136].

1.4.2 Electron Affinity (EA)

Electron affinity (AE) is defined as the energy evolved after adding one electron, which will be the binding energy of one additional electron in the cluster and is calculated by the equation given below-

$$AE\ (X_n) = E\ (X_n) - E\ (X^-_n) \qquad \text{…..……1.2}$$

where AE (X_n) is electron affinity, E (X_n) is the energy of the neutral clusters;

E (X_n) is the energy of the anion clusters [137].

1.4.3 Hardness and Reactivity of Clusters

The reactivity of metal clusters is contingent on the kinetics reaction. Consideration of the reactivity of the metal clusters is a very difficult task. Reactivity of the metal clusters changes in accordance with their size, geometry and electronic structure, and is calculated from the expression given below-

$$\textbf{Chemical hardness (K)} = \frac{Ionization\ potential\ (IP)\ -\ Electron\ Affinity\ (EA)}{2} \quad \ldots.1.3$$

The above relation can be understood as the variations in the energy difference of the clusters are owing to the small change in the number of the electron with retaining nucleus stable locus [138, 139].

1.5 Importance and Interesting Facts about the Clusters

Clusters of a variety of molecules have has become a subject of keen interest of the scientific world due to their inimitable properties, which are entirely different from those of the bulk phase. Two decades ago, there were no techniques available to determine the properties of clusters. But nowadays, with the recent advancement in powerful computational tools and experimental techniques clusters can be investigated by both the way theoretically as well as experimentally. Clusters are not only the mediator between the atomic or molecular and bulk system, but it also supports to understand the evolution from molecular to bulk behavior of matter. Moreover, it helps to achieve the chemical reaction through novel methods. Clusters may provide new ways to build and understand the properties of novel materials. Some of them are subject intense interest of research among researchers. One of the reasons behind the unique properties of clusters is the variance in the structure and structural size of small clusters. It is found that there are

many types of small clusters which prefer their stability based on structures like cubic, the octahedron, and polyhedron etc. Interestingly, the icosahedron with twenty-face and twelve-vertex are highly stable structures. It is very difficult to build the infinite, repeating array of atoms in icosahedron rather than atoms arranged in the cube and octahedral. Quasi crystals are the infinite array of an icosahedron but it does not have the regular, repeating structures, which can be linked with the crystals. The novel materials can be formed by implanting microclusters of one material in a host of unlike but associated materials. Considering this technique some research is going on to introduce some exceptional properties into material for the advanced purpose. The icosahedral clusters of silicon (Si) can be condensed to form a bulk structure. The C_{60} buckminsterfullerene structure is the combination of twelve 5-membered rings and twenty 6-membered rings build from sixty carbon atoms at every corner. C_{60} is helpful to form salt-like compounds. K_3C_{60} is the compound which can be obtained with the help of C_{60} molecule, and at low temperature, it shows superconductive behavior [140, 141].

References

[1] J. F. Shackelford, *Introduction to Materials Science for Engineers,* Pearson Education, New Jersey (2009).

[2] M. F. Ashby, D. R. H. Jones, *Engineering Materials 1, An Introduction to Their Properties and Applications,* 2nd edition, Pergamon Press, Oxford, (1996).

[3] R. L. Fleischer, *Tracks to Innovation,* Springer, New York, 31(1998).

[4] C. J. McMahon, C. D. Graham, *Introduction to Engineering Materials: The Bicycle and the Walkman*, Merion Books, Philadelphia, (1992).

[5] G. T. Murray, *Introduction to Engineering Materials-Behavior, Properties, and Selection,* Marcel Dekker, Inc., New York, (1993).

[6] D. R. Askeland, *The Science and Engineering of Materials,* 3rd edition, Brooks/Cole Publishing Co., Pacific Grove, CA, (1994).

[7] R. W. Cahn, ArtiJice, Artefacts, *100 Essays in Materials Science* (Institute of Physics Publishing, Bristol and Philadelphia), 3, 14 (1992).

[8] COSMAT Materials and Man's Needs: Materials Science and Engineering. Summary Report of the Committee on the Survey of Materials Science and Engineering (National Academy of Sciences, Washington, DC) pp. 1, 39 (1974).

[9] W. D. Callister, *Materials Science and Engineering-An Introduction*, Wiley, New York, Weinheim (2011).

[10] K. M. Ralls, T. H. Courtney, and J. Wulff, *Introduction to Materials Science and Engineering*, John Wiley & Sons, New York, (1976).

[11] J. P. Schaffer, A. Saxena, S. D. Antolovich, T. H. Sanders, Jr., and S. B. Warner, *The Science and Design of Engineering Materials,* 2nd edition, WCB/McGraw-Hill, New York, (1999).

[12] J. F. Shackelford, *Introduction to Materials Science for Engineers,* 5th edition, Prentice Hall, Inc., Upper Saddle River, NJ, (2000).

[13] C. R. Barrett, W. D. Nix, and A. S. Tetelman, *The Principles of Engineering Materials,* Prentice Hall, Inc., Englewood Cliffs, NJ, (1973).

[14] R. A. Flinn, and P. K. Trojan, *Engineering Materials and Their Applications,* 4th edition, John Wiley & Sons, New York, (1990).

[15] Jacobs, J. A. and T. F. Kilduff, *Engineering Materials Technology,* 3rd edition, Prentice Hall, Upper Saddle River, NJ, (1996).

[16] M. Ohring, *Engineering Materials Science,* Academic Press, San Diego, CA, (1995).

[17] W. F. Smith, *Principles of Materials Science and Engineering,* 3rd edition, McGraw-Hill Book Company, New York, (1995).

[18] L. H. Van Vlack, *Elements of Materials Science and Engineering,* 6th edition, Addison-Wesley Publishing Co., Reading, MA, (1989).

[19] M. B. Bever, Metallurgy and Materials Science and Engineering at MIT: 1865-1988 (privately published by the MSE Department) (1988).

[20] R. W. Cahn, Nature 225, 693 (1970).

[21] M. E. Fine, Annu. Rev. Mater. Sci. 24, 1 (1994).

[22] L. Hoddeson, E. Braun, J. Teichmann, and S. Weart, *Out of the Crystal Maze,* (Oxford University Press, Oxford) (1992).

[23] J. P. Frankel, *Principles of the Properties of Materials*, McGraw-Hill, New York, (1957).

[24] Y. Furukawa, *Inventing Polymer Science* (University of Pennsylvania Press, Philadelphia) (1998).

[25] J. J. Harwood, *Emergence of the field and early hopes, in Materials Science and Engineering in the United States,* ed. Roy, R. (Pennsylvania State University Press), 1 (1970).

[26] J. D. Verhoeven, *Fundamentals of Physical Metallurgy*, Wiley, Inc., New York (1994).

[27] A. Tetelman, C. R. Barrett, and W. D. Nix, *The Principles of Engineering Materials,* Prentice-Hall, Englewood Cliffs, NJ (2005).

[28] G. Weidmann, P. Lewis, N. Reid, *Structural Materials,* Butterworth, London (1990).

[29] D. A. Porter, K. E. Easterling, *Transformations in Metals and Alloys,* Nelson Thornes, Cheltenham (2009).

[30] J. H. Hollomon, J. Metals (AIME), 10, 796 (1958).

[31] N. F. Mott, *The Beginnings of Solid State Physics,* Proc. Roy. SOC (1980).

[32] P. A. Psaras, H. D. Langford, *Advancing Materials Research* (National Academy Press, Washington DC) 35 (1987).

[33] M. Riordan, and L. Hoddeson, *Crystal Fire: The Birth of the Information Age*, W.W. Norton, New York (1997).

[34] R. L. Sproull, Annu. Rev. Muter. Sci. 17, 1 (1987).

[35] D. Hull, and D. J. Bacon, *Introduction to Dislocations,* Butterworth-Heinemann, Oxford (2011).

[36] G. E. Dieter, *Mechanical Metallurgy,* McGraw-Hill, London (1988).

[37] R. E. Smallman, R. J. Bishop, *Modern Physical Metallurgy & Materials Engineering,* Butterworth-Heinemann, Oxford (2014).

[38] T. H. Courtney, Mechanical Behavior of Materials, McGraw-Hill, London (2013).

[39] W. O. Baker, J. Mater. 2, 917 (1967).

[40] Z. L. Wang and Z. C. Kang, Functional and Smart Materials Structural Evolution and Structure Analysis, Plenum Press, New York (1998).

[41] A. Tiwari and L. Uzun *Advanced Functional Materials,* wiley (2015).

[42] P. Jena and A. W. Castleman, Nanoclusters: a bridge across disciplines, Elsevier, (2010).

[43] W. Wong-Ng and C. J. Rawn Crystals, 7, 279 (2017).

[44] M. Penza, A. L. Spetz, A. R. Rodriguez and M. Meyyappan, *Functional materials for environmental sensors and energy systems,* Beilstein J. Nanotechnol., 8, 2015–2016 (2017).

[45] C. A. Wilkie, G. Geuskens, *Handbook of research on functional materials: principles, capabilities, and limitations,* Toronto; New Jersey, Apple Academic Press, (2014).

[46] H. Fredriksson, U. Åkerlind, Physics of Functional Materials, John Wiley, England (2008).

[47] W. Cao, H. H. Cudney, and R. Waser, Proc. Natl. Acad. Sci. 96, 8330 (1999).

[48] L. P. Cook, G. Brewer, W. Wong-Ng, Structural Aspects of Porphyrins for Functional Materials Applications. Crystals, 7, 223 (2017).

[49] M. Barsukova, T. Goncharova, D. Samsonenko, D. Dybtsev, A. Potapov, Crystals 6, 132 (2016).

[50] M. Qi, W. A. O' Brien, C. A. Stephenson, V. Patel, N. Cao, B. J. Thibeault, M. Schowalter, A. Rosenauer, V. Protasenko, H. G. Xing, et al. Crystals, 7, 157 (2017).

[51] Tesla Debuts Electric Car for the Masses, CBC News, 2009-03-27. Available online:http://www.cbc.ca/news/technology/tesla-debuts-electric-car-for-the-masses-1.816478 (2017).

[52] L. A. Bendersky, H. Tan, K. B. Karuppanan, Z. P. Li, A. C. Johnston-Peck, Crystals, 7, 127 (2017).

[53] D. Zhao, F. X. Ma, C. K. Nie, J. Wang, L. Zhang, Y. Fan, Crystals, 7, 129 (2017).

[54] Z. X. Wang, H. K. Li, G. M. Cai, Z. P. Jin, 31, 110 117 (2016).

[55] M. A. McGuire, Crystals, 7, 121 (2017).

[56] Drexler, K. Eric, *Nanosystems: Molecular Machinery, Manufacturing, and Computation*, New York: John Wiley & Sons (1992).

[57] H. Gleiter, Acta mater., 48, 1 (2000).

[58] Quan Li, *Functional Organic and Hybrid Nanostructured Materials: Fabrication, Properties, and Applications,* Wiley-VCH Verlag, Weinheim, 12, 69469 (2018).

[59] B. S. Murty, P. Shankar, B. Raj, B. B. Rath, J. Murday, *Nanoscience and Nanotechnology*, Springer (2013).

[60] E. L. Wolf, *Nanophysics and Nanotechnology: An Introduction to Modern Concepts in Nanoscience,* WILEY-VCH Verlag, Weinheim (2006).

[61] M. Daniel, D. Astruc, Chem. Rev., 104 293 (2004).

[62] P. Weaver, *The Technique of Lithography*, London: B.T. Batsford, p. 49 (1964).

[63] P. B. A Meggs, *History of Graphic Design*, John Wiley & Sons, p. 146 (1998).

[64] H. K. Bisoyi, Q. Li, *Liquid crystals, in Kirk-Othmer Encyclopedia of Chemical Technology*, John Wiley & Sons,, pp. 1–52 (2014).

[65] Q. Li, *Liquid Crystals Beyond Displays: Chemistry, Physics, and Applications*, John Wiley & Sons, New Jersey, (2012).

[66] L. D. Marks, Rep. Prog. Phys. 57, 603 (1994).

[67] G. Schmid, V. Maihack, F. Lantermann and S. Peschel, J. Chem. Soc., Dalton Trans., 589 (1996).

[68] G. M. Francis, I. M. Goldby, L. Kuipers, B. von Issendorf and R. E. Palmer, J. Chem. Soc., Dalton Trans. 665 (1996).

[69] M. Faraday, Phil. Trans. R. Soc. Lond., 147, 145 (1857).

[70] G. Schmid, Chem. Rev., 92, 1709 (1992).

[71] T. S. Ahmadi, Z. L. Wang, T. C. Green, A. Henglein and M. A. El-Sayed, Science, 272, 1924 (1996).

[72] R. L. Whetten, J. T. Khoury, M. M. Alvarez, S. Murty, I. Vezmar, Z. L. Wang, P. W. Stephens, C. L. Cleveland, W. D. Luedtke and U. Landman, Adv. Mater. 8, 428 (1996).

[73] J. Jortner, Z. Phys. D 24, 247 (1992).

[74] H. W. Kroto, J. R. Heath, S. C. O'Brien, R. F. Curl, R. E. Smalley, nature, 318, 163 (1985).

[75] Roy L. Johnston, Atomic and Molecular Clusters, Taylor & Francis, New York, (2002).

[76] G. Durand, F. Spiegelman, A. R. Allouche, Eur. Phys. J. D, 24, 19 (2003).

[77] F. Spiegelmann, D. Pavolini, J. Chem. Phy., 89, 4954 (1988).

[78] J. Flad, G. lgel, M. Dolg, H. Stoll, H. Preuss, Chem. Phys., 75, 331 (1983).

[79] V. Bonac~ic'-Koutecky, P. Fantucci, J. Koutecky, Phys. Rev. B, 37, 4369 (1988).

[80] J. L. Martins, J. Buttet, R. Car, Phys. Rev. B, 31, 1804 (1985).

[81] G. Pacchioni, H. O. Beckmann, J. Koutecky, Chem. Phys. Lett., 87, 151 (1982).

[82] T. A. Dahlseid, M. M. Kappes, J. A. Pople, M. A. Ratner, J. Chem. Phys. 96, 4924 (1992).

[83] J. Chen, D. M. Brink, L. T. Wille, J. Phys. B, 23, 885 (1990).

[84] B. K. Rao, P. Jena, Phys. Rev. B, 32, 2058 (1985).

[85] I. Boustani, W. Pewestorf, P. Fantucci, V. Bonac~ic'-Koutecky, J. Koutecky, Phys. Rev. B, 35, 9437 (1987).

[86] C. Schmidt, P. B. Allen, T. Baruah, M. Pederson arXiv:cond mat/0411009v1.

[87] T. J. Lee, A. P. Rendell, P. R. Taylor, J. Phys. Chem., , 94, 5463 (1990).

[88] F. Reuse, S. N. Khanna, V. de Coulon, J. BuRet, Phys. Rev. B, 41, 11743 (1990).

[89] V. Kumar, R. Car, Z. Phys. D, 19, 177 (1991).

[90] C. W. Jr. Bauschlicher, P. S. Bagus, B. N. Cox, J. Chem. Phys., 77, 4032 (1982).

[91] R. A. Chiles, C. E. Dykstra, K. D. Jordan, J. Chem. Phys., 75, 1044 (1981).

[92] G. Pacchioni, J. Koutecky, J. Chem. Phys., 77, 5850 (1982).

[93] E. K. Parks, B. J. winter, T. D. Klots, S. J. Riley: J. Chem. Phy. 94, 1882 (1991).

[94] A. Taneda, Y. Kawazoe: Materials Transactions, JIM 40, 859 (1999).

[95] T. D. Kolts, B. J. winter, E. K. Parks, S. J. Riley: J. Chem. Phy. 95, 8919 (1991).

[96] L. Lian, C.-X. Su, P. B. Armentrout: J. Chem. Phys. 97, 4084 (1992).

[97] W. A. de Heer, P. Milani, A. Chatelain, Phys. Rev. Lett. 65, 488 (1990).

[98] S. N. Khanna, S. Linderoth, Phys. Rev. Lett. 67, 742 (1991).

[99] J. L. Chen, C. S. Wang, K. A. Jackson, M. R. Pederson, Phys. Rev. B 44, 6558 (1991).

[100] M. E. Geusic, M. D. Morse, R.E. Smalley: J. Chem. Phys. 82, 590 (1985); R. L. Whetten, D. M. Cox, D. J. Trevor, A. Kaldor: Phys. Rev. Lett. 54, 1494 (1985); M. D. Morse, M. E. Geusic, J. R. Heath, R. E. Smalley: J. Chem. Phys. 83, 2293 (1985); E. K. Parks, K. Liu, S. C. Richtsmeier, L. G. Pobo, S. J. Riley: J. Chem. Phys. 82, 5470 (1985); S. C. Richtsmeier, E. K. Parks, K. Liu, L.G. Pobo, S. J. Riley: J. Chem. Phys. 82, 3659 (1985); P. J. Brucat, C. L. Pettiette, L. S. Zheng, M. J. Craycraft, R. E. Smalley: J. Chem. Phys. 85, 4747 (1986); D. M. Cox, K. C. Reichmann, D. J. Trevor, A. Kaldor: J. Chem. Phys. 88, 111 (1988); E. K. Parks, G.C. Nieman, L.G. Pobo, S.J. Riley: J. Chem. Phys. 88, 6260 (1988).

[101] I. Panas, P. Siegbahn, U. Whalgren, *In the Challenge of d and f Electrons*, American Chemical Society, Washington, D. C., 125 (1989).

[102] J. Conceiao, R. T. Laaksomen, L. S. Wang, T. Guo, P. Norlander, R. E. Smal-Ley, Phys. Rev. B, 51, 4668 (1995).

[103] L. Lian, C. X. Su, P. B. Armentrout, J. Chem. Phys. 97, 4072 (1992).

[104] G. M. Pastor, J. Doranates-Davila, K. H. Bennemann: Chem. Phys. Lett. 148, 459 (1988).

[105] L. S. Wang, H. S. Cheng, J. Fan: J. Chem. Phys. 102, 9480 (1995).

[106] Y. kawazoe, Y. Kondow, K. Ohno, *Clusters and Nanomaterials: Theory and experiments*, Springer, New York, (2002).

[107] Roy L. Johnston, Atomic and Molecular Clusters, Taylor & Francis, New York, (2002).

[108] S. Iijima: Nature (London) 354, 56 (1991).

[109] C. Liu, Y.Y Fan., M. Liu, H.T. Cong, H.M. Cheng, M.S. Dresselhaus: Science, 286, 1127 (1999).

[110] O. Cheshnovsky, K.J. Taylor, J. Conceicao, R.E. Smalley: Phys. Rev. Lett., 64, 1785 (1990).

[111] H. Kawamata, Y. Negishi, R. Kishi, S. Iwata, M. Gomei, A. Nakajima, K. Kaya: J. Chem. Phys. 105, 5369 (1996); Y. Negishi, H. Kawamata, F. Hayakawa, A. Nakajima, K. Kaya: Chem. Phys. Lett., 294, 370 (1998).

[112] R. Kishi, Y. Negishi, H. Kawamata, S. Iwata, A. Nakajima, K. Kaya: J. Chem. Phys., 108, 8039 (1998).

[113] K. Fuke, K. Tsukamoto, F. Misaizu, M. Sanekata: J. Chem. Phys**.,** 99, 7807 (1999).

[114] S. Yoshida, K. Fuke, J. Chem. Phys. 111, 3880 (1999).

[115] K. D. Rinnen, M. L. Mandich, Phys. Rev. Lett., 69, 1823 (1992).

[116] L. A. Bloomfield, R. R. Freeman, W. L. Brown: Phys. Rev. Lett., 54, 2246 (1985).

[117] L. A. Bloomfield, M. E. Guesic, R. R. Freeman, W. L. Brown, Chem. Phys. Lett., 121, 33 (1985).

[118] Q. L. Zhang, Y. Liu, R. F. Curl, F. K. Tittel, R. E. Smalley, J. Chem. Phys., 88, 1670 (1988).

[119] W. Begemann, K. H. Meiwes-Broer, H. O. Lutz: Phys. Rev. Lett. 73, 2248 (1986).

[120] M. F. Jarrold, E. C. Honea: J. Phys. Chem**.,** 95, 9181 (1991).

[121] J. M. Hunter, J. L. Fye, M. F. Jarrold, J.E. Bower: Phys. Rev. Lett., 73, 2063 (1994).

[122] S. Li, R. J. Van Zee, W. Weltner Jr., K. Raghavachari, Chem. Phys. Lett., 243, 275 (1995).

[123] E.C. Honea, A. Ogura, C. A. Murray, K. Raghavachari, W. O. Sprenger, M. F. Jarrold, W. L. Brown, Nature, London, 366, 42 (1993).

[124] K. Laihing, R.G. Wheeler, W. L. Wilson, M. A. Duncan: J. Chem. Phys., 87, 3401 (1987).

[125] T. P. Martin, H. Schaber, J. Chem. Phys. 83, 855 (1985).

[126] M. Watanabe, Y. saito, S. Nishigaki, T. Noda, Jpn. J. App. Phys. Part 1 **27**, 344 (1988); Y. Saito, T. Noda; Z. Phys., D, 12, 225 (1989).

[127] A. A. Schvartsburg, M. F. Jarrold: Phys. Rev. A, 60, 1235 (1999).

[128] T. Bachels, R. Schäfer, H. J. Güntherodt, Phys. Rev. Lett., 84, 4890 (2000).

[129] A. A. Schvartsburg, M. F. Jarrold: Phys. Rev. Lett., 85, 2530 (2000).

[130] K. Raghavachari, C. M. Rohlfing: J. Chem. Phys., 89, 2219 (1988); J. Chem. Phys., 94, 3670 (1991).

[131] G. Pacchioni, J. Koutecky: J. Chem. Phys., 84, 3301 (1986).

[132] M. Menon, K. R. Subbaswamy, Phys. Rev. B 47, 12754 (1993); P. Ordejon, D. Lebedenko, M. Menon: Phys. Rev. B 50, 5645 (1994); J. Pan, M.V. Ramakrishna: Phys. Rev. B, 50, 15431 (1994).

[133] W. Andreoni: Phys. Rev. B, 45, 4203 (1986).

[134] P. Ballone, W. Andreoni, R. Car, M. Parrinello, Europhys. Lett., 8, 73 (1989).

[135] L. D. Marks, Rep. Prog. Phys., 57, 603 (1994).

[136] G. Schmid, V. Maihack, F. Lantermann and S. Peschel, J. Chem. Soc., Dalton Trans., 589 (1996).

[137] G. M. Francis, I. M. Goldby, L. Kuipers, B. von Issendorf and R. E. Palmer, J. Chem. Soc., Dalton Trans. 665 (1996).

[138] M. Faraday, Phil. Trans. R. Soc. Lond., 147, 145 (1857).

[139] J. A. Alonso, *Structure and Properties of Atomic Nanoclusters*, Imperial College Press, (2005).

[140] E. Roduner, Chem. Soc. Rev., 35, 592 (2006).

[141] H. Haberland, Clusters of Atoms and Molecules, *Theory, Experiment, and Clusters of Atoms*, Springer-Verlag, (1994).

Chapter-2
Computational Methodology

Chapter 2

Computational Methodology

2.1 Introduction

This chapter briefly presents a small glimpse of theoretical quantum chemical methods which are essentially based on the density functional theory (DFT). In the area of computational molecular modelling, excessive development and sophistication have been seen due to the advancement in electronic structure theory and computer technology from the last few decades. Currently, several computational methodologies are available; suitability of each approach depends on properties of interest and the size of the system. They have been very helpful in quantitative understanding of structure-property and performance relationships, thereby providing guidelines in designing experiments, creating experimentally testable hypotheses and elucidating unanswered questions and phenomena. The molecular modelling techniques concern with the geometrical position of nuclei of stable molecules. These techniques calculate relative energies and structures, dipole moment, polarizability, atomic charge, vibrational frequencies, infrared, Raman and NMR spectra, bond length, thermodynamical, molecular orbitals and magnetic properties etc. of a molecular and atomic system. The *ab initio* is one of the most popular technique, which does not rely on any experimental data and can be directly derived using the Schrödinger wave equation. The Hartree-Fock (HF) and Density functional theory are the most commonly used *ab initio* methods. HF method considers central field approximation (CFA) without taking into account of electron correlation. There are some other methods available within the *ab initio* method which consider electron-electron

correlations like Möller Plesset (MP), Configuration Interaction (CI), Density Functional Theory (DFT) etc. Density functional theory is one of the most popular and successful quantum mechanical theories which, in a nut shell, transform a system of many interacting particles into a functional of the ground state density, density being function of position coordinates. This fundamental difference leads to a significant reduction in computational difficulty, which makes the method of great practical use in the calculation of the electronic structure of atoms, molecules, solids and nano-materials, in the ground state.

2.2 Quantum Mechanical Method

The electronic properties of the atom and molecules are governed by the solution of many-body problems. In principle, to solve a many-electron system we have to incorporate the many-electron wave function into the Schrödinger equation. In quantum mechanics (QM), the wave function (Ψ) which is the solution of the Schrödinger equation, contains all probable information of a molecular system [1, 2].

2.2.1 Schrödinger Wave Equation

Properties of materials at the nanoscale are governed by the laws of quantum mechanics. The behavior of atoms and electrons in a system evolving with time is described by the time-dependent Schrödinger equation (Schrödinger, (1926)) which is given as-

$$i\hbar \frac{\partial}{\partial t} \Psi = \hat{H} \Psi \qquad \text{.....2.1}$$

where *i* is imaginary number, $\hbar$ is the reduced Planck constant, Ψ is the multi-electron wave function of the system, and $\hat{H}$ is the Hamiltonian operator, which characterizes the total energy of any given wave-function and takes different forms depending on the

situation. The symbol $\frac{\partial}{\partial t}$ indicates a partial derivative with respect to time *t.* In order to obtain a stationary situation, the Hamiltonian is independent of time and the time-independent Schrödinger equation simply takes the form-

$$\hat{H}\,\Psi = E\,\Psi \qquad \text{.....2.2}$$

where $\hat{H}$ is Hamiltonian operator of the system and E is the energy eigenvalue of operator H. Ψ is known as wave function, and $\Psi^{*}\Psi$ gives the probability density [3]. Hamiltonian operator representing the total energy, is a sum of kinetic and potential energies of the nuclei and electrons respectively-

$$\hat{H} = \hat{T}_n + \hat{T}_e + \hat{V}_{ne} + \hat{V}_{ee} + \hat{V}_{nn} \qquad \text{.....2.3}$$

where the operator $\hat{T}$ represents the kinetic energy and $\hat{V}_{ne}$ describes external potential generated by nucleons-electron interactions, while $\hat{V}_{ee}$ and $\hat{V}_{nn}$ are the potentials produced by electron-electron and nuclei-nuclei interactions, respectively. Basically, Schrödinger equation describes the single electron system (Hydrogen like atoms), while solving Schrödinger equation for many electron system is a very complicated task. In order to simplify this problem, we need to deal with the various approximations. Born-Oppenheimer approximation is one of the most used approximations for solving the complex Schrödinger equation. Born-Oppenheimer approximation permits the wave function of the system to break into its electronic and nuclear components and consequently allows solving the both parts of the problem independently. Solution of this approximation gives effective electronic energy which depends on relative nuclear coordinates. In this approximation, it is assumed that nucleus is heavier than the electron,

and due to this electrons can move very fast in comparison to nucleons and come to the lower energy state configuration given by nuclear position.

2.2.2 Born-Oppenheimer Approximation

This approximation is used to separate the motion of the heavy nuclei of a molecule from the much faster dynamics of the electrons [4]. The general form of the Hamiltonian is given as follows-

$$\hat{H}_{mol} = \hat{T}_{el} + \hat{V}_{el-el} + \hat{T}_{nuc} + \hat{V}_{nuc-nuc} + \hat{V}_{el-nuc} \quad \text{.....2.4}$$

Where the kinetic energies for the electrons and nuclei are represented by $\hat{T}_{el}$ and $\hat{T}_{nuc}$ respectively and can be described as follows-

$$\hat{T}_{el} = \sum_{j=1}^{N_{el}} \frac{p_j^2}{2m_e} \quad \text{.....2.5}$$

and

$$\hat{T}_{nuc} = \sum_{j=1}^{N_{nuc}} \frac{p_j^2}{2M_j} \quad \text{.....2.6}$$

where m_e, M are the masses of electron and nucleus, respectively. $\hat{V}_{el-el}$, $\hat{V}_{nuc-nuc}$, $\hat{V}_{el-nuc}$ are the potentials that describe the electron-electron, nucleus-nucleus and electron-nucleus interactions, respectively. Above potentials are governed by the coulomb interaction given as-

$$\hat{V}_{el-el} = \frac{1}{2}\sum_{i\neq j} \frac{e^2}{|r_i - r_j|} \quad \text{.....2.7}$$

$$\hat{V}_{nuc-nuc} = \frac{1}{2}\sum_{i\neq j} \frac{Z_i Z_j e^2}{|R_i - R_j|} \quad \text{.....2.8}$$

and

$$\hat{V}_{el-nuc} = -\sum_{i,j} \frac{Z_i Z_j e^2}{|r_i - R_j|} \quad \text{.....2.9}$$

The Born-Oppenheimer approximation greatly simplified the previous Hamiltonian (eq. 2.2) by introducing the nuclear coordinate R. This is due to the fact that the large mass difference between electrons and nuclei, the electrons will be able to respond instantaneously to any change in the nuclear configuration. Now the Hamiltonian has the form as follows-

$$\hat{H}_{el}(\mathrm{R}) = \hat{T}_{el} + \hat{V}_{el-el} + \hat{V}_{el-nuc} \qquad \text{…….2.10}$$

The electronic energies E^{el} and wave function φ (r, R) are the solution of the Schrodinger equation- (eq. 2.2) that depends parametrically on the nuclear geometry as-

$$\hat{H}_{el}\left|\varphi_n(r,R)\right\rangle = E_n^{nl}(R) + \left|\varphi_n(r,R)\right\rangle \qquad \text{…….2.11}$$

on adding the inter nuclear repulsion, the solution of the electronic part of the Schrodinger equation for different nuclear coordinates (R) results in the potential hyper surface V(R) which is invariant with respect to the electronic coordinates. A potential term arising due to the interaction between the different electronic states [3] is neglected. This potential results from the non-adiabatic coupling operator. A single adiabatic potential energy surface can be written as-

$$V_n(R) = E_n^{nl}(R) + \hat{\mathrm{V}}_{nuc-nuc} \qquad \text{…….2.12}$$

The elimination of the non-adiabatic electronic coupling is the core of the Born Oppenheimer approximation, which leads to a nuclear Schrodinger equation-

$$\hat{H}_{nuc}\left|\Psi_n(R)\right\rangle = \left[\hat{T}_{nuc} + V_n(R)\right]\left|\Psi_n(R)\right\rangle = E_n^{nuc}\left|\Psi_n(R)\right\rangle \qquad \text{…….2.13}$$

This explains the geometry of the nuclei in the mean field produced by the speedy electrons. Each electronic state is associated with different nuclear potential. Therefore,

in Born-Oppenheimer approximation, the dynamics of the nuclei is well defined by the nuclear potential V(R).

2.3 Hartree-Fock (HF) Method

Hartree-Fock (HF) method is used to determine the ground state wave function and to calculate the ground state energy of many-body systems. It breaks the Schrödinger equation for many-electron into many one electron equation. The wave function is considered to be a product of one–electron wave function as given in equation 2.14-

$$\Psi(r_1, r_2, r_3, ...r_n) = \varphi_1(r_1)\varphi_2(r_2)\varphi_3(r_3).....\varphi_n(r_n) \qquad \text{…….2.14}$$

Since electrons are fermions hence the wave function should be antisymmetric wave function with respect to the interchange of any set of space-spin coordinates. This is accomplished by writing the wave function in the form of determinant, termed as Slater determinant. In the H-F method, the wave function of an 'N' electron system is described by a single Slater determinant of N dimension, Ψ_{SD}. The elements of determinant are one-electron wave functions (molecular orbitals (MO) (ϕ_i (i))) [6, 7].

$$\Psi_{SD} = \frac{1}{\sqrt{N!}} \begin{vmatrix} \phi_1(1) & \phi_2(1) & \ldots\ldots\ldots & \phi_N(1) \\ \phi_1(2) & \phi_2(2) & \ldots\ldots\ldots & \phi_N(2) \\ \ldots. & \ldots. & & \ldots. \\ \phi_1(N) & \phi_2(N) & \ldots\ldots\ldots & \phi_N(N) \end{vmatrix}$$

Since these one electron wavefunctions are orthonormal and form a complete set, hence we can express these one-electron wavefunctions (ϕ_i(i)) as a superposition of the basis functions [8].

$$\phi_i = \sum_{\mu}^{M} C_{\mu i} \chi_{\mu i} \qquad \text{…….2.15}$$

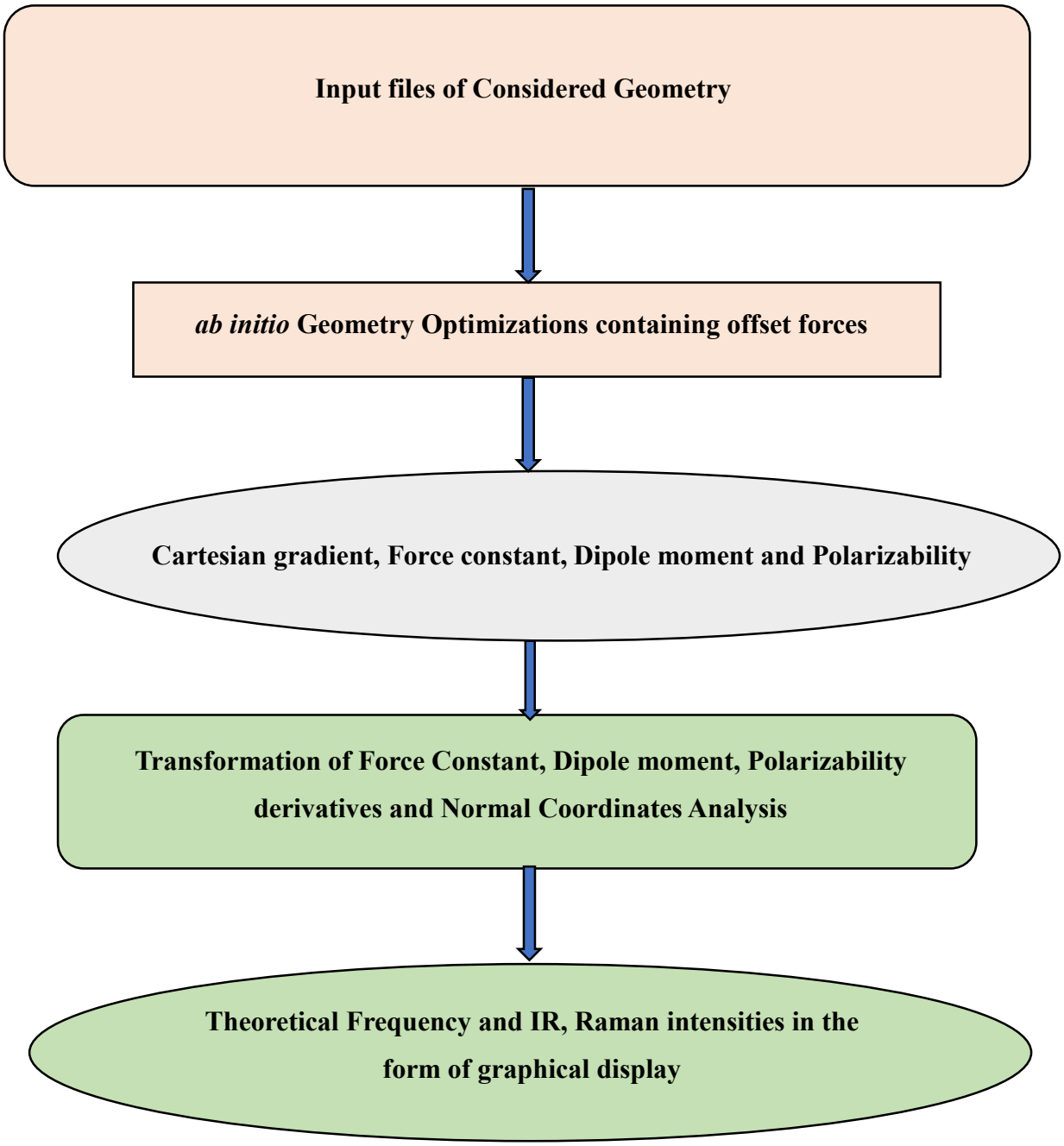

Figure 2.1: Flow diagram of program used in the quantum chemical calculations.

Where, $C_{\mu i}$ are the expansion coefficients of the basis functions $\chi_{\mu i}$ and 'M' is the total number of basis functions. The energy of the system is given by the following equation-

$$E = \left\langle \Psi \middle| \hat{H} \middle| \Psi \right\rangle \qquad \text{…….2.16}$$

where Ψ is the normalized wave function, Ĥ is molecular Hamiltonian.

2.3.1 Variational Theorem- This theorem gives the upper bound to energy that is used to minimize the energy for determining the coefficients. Mathematically,

$$\frac{\partial E}{\partial C_{\mu i}} = 0; \text{for all } \mu \text{ and i} \qquad \text{…….2.17}$$

In the HF method, the consequence of allowing a one-electron Hamiltonian i.e. Fock operator is to reduce the many-electron systems into a one-electron system. This can be done via establishing the mean field approximation i.e. an electron seeking a mean potential $v_{HF}(i)$ of the other electrons. The Fock operator is given as,

$$\hat{f}_i = -\frac{1}{2}\nabla_i^2 - \sum_A^O \frac{Z_A}{r_{iA}} + v_{HF}(i) \qquad \text{…….2.18}$$

'O' is the number of atoms in the molecule.

$$v_{HF}(i) = \sum_i^N (\hat{J}_i(i) - \hat{K}_j(i)) \qquad \text{…….2.19}$$

The operators that describe the electron repulsion term contain two-terms, named as Coulomb $\hat{J}_j(i)$ and exchange integral $\hat{K}_j(i)$ respectively.

$$J_j(1) = \left\langle \phi_j(2) \middle| \frac{1}{r_{12}} \middle| \phi_j(2) \right\rangle \qquad \text{…….2.20}$$

$$\hat{K}_j(1)\phi_i(1) = \left\langle \phi_j(2) \middle| \frac{1}{r_{12}} \middle| \phi_j(2) \right\rangle \phi_i(1) \qquad \text{…….2.21}$$

By solving the following equation, the one-electron wave function ($\phi\ (i)$) is thus obtained,

$$f_i\phi_i = \varepsilon_i\phi_i\ ;\ \mathrm{i} = 1, 2, ..., \mathrm{N} \qquad \text{…….2.22}$$

where ε_i are the molecular orbital energies.

The variational condition produces a set of algebraic equations for the coefficient $c_{\mu i}$ known as the Roothaan- Hall equations [13-14].

$$\sum_{\nu=1}^{M}(F_{\mu\nu} - \varepsilon_{\mu\nu})c_{\mu i} = 0 \qquad \text{…….2.23}$$

or it can be rewritten as-

$$FC = SC\varepsilon \qquad \text{…….2.24}$$

Where, (μ = 1, 2, …M), M is the number of basis functions. μ, ν, λ and σ are indices of the basis functions χ_μ, χ_ν, χ_λ, and χ_σ ,respectively.

F is the Fock matrix in the Equation (2.23) with $F_{\mu\nu}$ matrix elements; ε represents a diagonal matrix with the molecular orbital energies (ε_i) as the diagonal elements. S represents the overlap matrix and $S_{\mu\nu}$ are the overlap matrix elements.

$$S_{\mu\nu} = \langle\mu|\nu\rangle \qquad \text{…….2.25}$$

$$F_{\mu\nu} = H_{\mu\nu}^{core} + \sum_{\mu=1}^{N}\sum_{\sigma=1}^{N}P\lambda\sigma\left[\langle\mu\nu|\lambda\sigma\rangle - \frac{1}{2}\langle\mu\lambda|\nu\sigma\rangle\right] \qquad \text{…….2.26}$$

Where $H_{\mu\nu}^{core}$ represents the matrix having the energy of each electron exclusively in the field of the nuclei as below-

$$H_{\mu\nu}^{core} = \left\langle\mu\left|-\frac{1}{2}\nabla^2 - \sum_{A=1}^{0}\frac{Z_A}{r_{1A}}\right|\nu\right\rangle \qquad \text{…….2.27}$$

where, Z_A is the atomic number of atom A and the matrix $P_{\lambda\sigma}$ contains the one-electron densities, given by-

$$P_{\lambda\sigma} = 2\sum_{i=1}^{occ} c_{\lambda j}^{*} c_{\sigma i} \qquad \text{.....2.28}$$

Since it is difficult to solve the Roothaan-Hall equations explicitly due to the non-linearity of equations, hence we need an iterative method to solve it. The Hartree-Fock method requires an initial guess to calculate the orbital coefficients and this function is used to calculate energy and a new set of coefficients, which is again used to obtain a new set, and so on. This procedure iteratively repeated till the energies and orbital coefficients remain constant for two consecutive iterations i.e. it reaches self-consistency, which is known as the self-consistent field (SCF) procedure.

2.4 Electron Correlation (EC)

Instead of electron-electron interaction, the HF method takes care of the mean effect of electron-electron repulsion. In HF theory, the probability of finding an electron around an atom is determined by the electron to nucleus distance, not by the distance between two electrons. The pairing or correlation of electrons between them is termed as electron correlation [10, 11-13]. The electron-electron repulsion energy is reduced by considering an electron correlation. Generally, it is of three types: a) exchange b) dynamic and c) non-dynamic electron correlation. Since the description of HF theory incorporates an exchange-correlation, which arises due to pairs of electrons having parallel spin, therefore, the HF function must be anti-symmetric as per requirement of Pauli principle. It vanishes because of the same spin of two electrons having the same spatial coordinates. This basic correlation prevents two parallel–spin electrons from being found at the same

position in space; this is often called Fermi correlation. In the HF method, the calculated energy is different from the exact energy of the system due to the exclusion of Coulomb correlation. This difference is termed as correlation energy (E_{corr}).

$$E_{corr} = E_{exact} - E_{HF} \quad \text{.....2.29}$$

There are some other theoretical methods presented within the ab initio method which considers electron-electron correlations, which are referred to as post-self-consist field methods due to considering electron correlation rectification in Hartree-Fock model. Some popular model which considers electron correlation correction are CI (configuration interaction), MCSCF (multi configurational self-consistent field), MPn (Møller-Plesset perturbation theory) and CC (coupled cluster theory). Out of these theoretical models, hybrid density functional theory (DFT) is mostly used due to cost-effectiveness and better accuracy.

2.5 Basis Set

A basis set is a set of mathematical function which is used to designate the shape of the orbital in an atom and it is considered for theoretical calculations. The linear combination of this function approaches the molecular orbital and whole wave function. Basis set play a very important role in the accuracy of the result. For more accurate calculation, we need to select an appropriate basis set according to type of calculation to be done. The large basis set gives more accurate result but it takes much CPU time and also very expensive. In general, two types of basis sets are more famous in ab initio method, first one is STO (slater type orbitals) and another is GTO (Gaussian type orbitals) [14, 15]. STO basis set is a very simple type and tells about the exact eigen function of hydrogen like atoms and has exponential form. STO is a good basis for MOs

(molecular orbitals) due to having a direct physical explanation. An STO has a functional form for an s-type atomic orbital-

$$S(r) = N_s e^{\zeta r^2} \qquad \text{…….2.30}$$

where 'r' represents the radial distance from the nucleus, N_s, represents the normalization constant, and ζ is an orbital exponent, which is governed by the size of the orbital. Along with the advantage, STO has some shortcomings also, such as for self-consistent field (SCF) maximum required integral must be calculated numerically. So, computationally it is very expensive, while the GTO basis set is comfortable with the wave function for computation point of view. GTO for s-type atomic orbital with the similar orbital exponent as STO can be written in the form-

$$g(r) = N_g e^{\zeta r^2} \qquad \text{…….2.31}$$

where N_g is the normalization constant, r is the radial distance from the nucleus, N_s, is normalization constant, and ζ is an orbital exponent.

The minimal basis set is teeny basis set and expresses the single basis function for each type of employed orbital in the detached atoms [16]. These basis sets are used for the very huge molecules, qualitative results, and in certain cases quantitative results. STO-3G is most popular minimal basis set, which is mostly used. In STO-3G, 3G represents the three Gaussian type orbitals, and the shape of a slater type orbitals is approximated by basis set using a single compression of 3-GTO. One such compression would then be used for each orbital, which better define a minimal basis set. STO-nG basis set is minimal basis set in which n GTOs are used to represent each orbital. In general, n represent 2 to 6 (n = 2-6). The other type of basis set is Pople basis set, which

is written in the form of 6-31G [17, 18]. In 6-31G, single contraction of six GTO primitives is used for each core orbitals. Two contraction, one with three primitives and other is for one primitive, are used to describe each valence shell orbital. For organic molecules, such types of the basis set are very useful. Some times Pople basis set is changed by imposing 1 or 2 asterisks (*) like 6-31G* or 6-31G**. The single asterisk (*) indicates that a set of primitives d has been added to atoms other than hydrogen, while two asterisks (**) means that a set of p-primitives has also been added to hydrogen as well, which is called polarization function.

Polarization function provides more stretchability to the wave function for modification of the form of the orbital. Sometimes we see these basis set with the positive sign such as 6-31+G* or 6-31++G*. Here one positive sign (+) represents the addition of a diffuse function to the atoms except for the hydrogen, while the two positive sign (++) indicates that diffuse functions are added for all the atoms. Basis sets with diffuse functions are also termed as augmented basis sets. These diffuse functions are mostly used with anions and have greater electron density distribution. These diffuse functions are primitives with minor exponents, therefore, express the nature of the wave function distant from the nucleus. Long distances interactions, like Van der Waals, can be well explained through these diffuse functions. The addition of the diffusion function transforms relative energies of the several geometries connected with these systems [17, 19]. In the variational principle, electronic energy of the molecular system proceeds towards the precise value very closely with the rise in the number of basis function. Moreover, double Zeta (DZ) type basis set is very convenient for geometry optimization. This basis set involves two basis functions, each minimal basis function for detached

atoms [20]. Some other important basis set which involve an effective core potential (ECP). These ECP are used for the consideration of a large number of electrons in transition metal (TM) [21]. For example- in iron (Fe) atom, the core electrons are 1s, 2s and 2p, which are mostly not contributed in the bond creation, hence these are not much affected with respect to atomic orbital. The effective core potential module sometimes also holds relativistic rectification in the energy to refine the energy calculation [22]. LANL2DZ is known as Los Alamos National Laboratory basis set developed by Hay and Wadt [23-25]. It is combination of effective core potential (ECP) and valence basis set. This basis set is particularly used to study the clusters or compounds which contain heavy atoms. These basis functions were achieved by the proper procedure of pseudo-orbitals with Gaussian functions [26].

2.6 Density Functional Theory (DFT)

Density Functional Theory (DFT) describes the energy as a functional of electron density of the molecule (ρ) [27]. A functional is defined as a function of a function, and the energy of the molecule is a functional of the electron density. Determination of electron density is more prominent as it is independent of the variation of the number of electrons; whereas the number of electrons increases the wave-function calculation method becomes more sophisticated to calculate.

The Hohenberg Kohn theorem [28] described that the external potential is a functional of the ground-state density; it means that the density is used as a parameter to describe the interactions between electrons. In Kohn Sham (KS) theory [29], the ground state energy is formulated as a simple expression-

$$E[\rho] = T_s[\rho] + V_{ne}[\rho] + J[\rho] + E_{xc}[\rho] \qquad \text{.....2.32}$$

where the forms of some of the functionals are explicitly known. The kinetic energy for the KS non-interacting reference system is-

$$T_s[\rho] = \sum_i \left\langle \phi_i \left| -\frac{1}{2}\nabla^2 \right| \phi_i \right\rangle \qquad \text{.....2.33}$$

in terms of $\{\phi_i\}$, the set of one electron KS orbitals. The electron density of the KS reference system is given by-

$$\rho(r) = \sum_i |\phi_i(r)|^2 \qquad \text{.....2.34}$$

The other two known energy components are the nucleus electron potential energy, expressed in terms of the external potential due to the nuclei-

$$\nu(r) = -\sum\nolimits_A (Z_A / |r - R_A|) \qquad \text{.....2.35}$$

$$V_{ne}[\rho] = \int \rho(r)\nu(r)dr \qquad \text{.....2.36}$$

and the classical electron-electron repulsion energy is-

$$J[\rho] = \frac{1}{2}\int\int \frac{\rho(r)\rho(r')}{|r - r'|} dr dr' \qquad \text{.....2.37}$$

The exchange-correlation functional, E_{xc} [ρ], although no explicit form is available, can be expressed in the constrained search formulation for density functional [30].

$$\begin{aligned} E_{xc}[\rho] &= \min_{\Psi\to\rho} \langle \Psi | T + V_{ee} | \psi \rangle - T_S[\rho] - J[\rho] \\ &= \left(T[\rho] - T_s[\rho]\right) + \left(V_{ee}[\rho] - J[\rho]\right) \end{aligned} \qquad \text{.....2.38}$$

It can also be expressed elegantly through the adiabatic connection [31, 32]

$$E_{xc}[\rho] = \int_0^1 \langle \Psi_\lambda | V_{ee} | \Psi_\lambda \rangle d\lambda - J[\rho] \qquad \text{.....2.39}$$

On the basis of techniques, DFT is categorized into three types: (a) LDA (*Local density approximation*) methods- in this approximation method the density of the electrons is identical all over the molecule, (b) GCA (*Gradient corrected approximation*) methods-in this method electron density is not uniform thought the molecular system. (c) A hybrid method, this method combines the additional features of HF and DFT` with the improvement of accuracy, hence it is called a hybrid method. DFT is a more superior method than the any other method presented within *ab initio* due to providing high accuracy in computational results without consuming extra time [33, 34]. DFT method becomes more advance (hybrid) with the consideration of Beck three-parameter [35]. The hybrid DFT method offers the comparisons of computationally calculated value with the experimentally known parameters such as ionization energies (IE), electron affinities (EA) with higher accurateness. Beck led three hybrid parameters in DFT method for approximating the exchange and correlation functions and optimized the value of these fit parameters (K, L, and M) for evaluating the experimental data in the trial set. There are numerous options available for linking the various exchange and correlation functional. In current period, the B3LYP is the most prevalent method as it offers good result with accuracy [35-37]. Principally, the hybrid density functional method B3LYP has the following form as-

$$E_{xc}^{B3LYP} = KX_X^{Slater} + (1-K)E_X^{HF} + L\Delta E_X^{Becke} + E_C^{VWN} + M\Delta E_C^{LYP} \qquad \text{.....2.40}$$

It considers the LDA functions of Slater and Vosko-Will-Nusair, the HF exchange, a refinement term to the exchange due to Beck and Lee-Yang-Parr correction for non- local

correlation factors. The coefficient K, L, and M are the appropriate parameters obtained through fitting the energies of B3LYP/6-31G* calculation against experimentally obtained ionization energies and electron affinities. So, the B3LYP method has become one of the extensive used methods in science over the past decade, because these fit-parameters have created an accurate and low-cost computational method. These hybrid and non-hybrid DFT such as B3LYP have been revealed to be extremely accurate with 15% HF exchange, useful for geometry optimization and versatile for a computational chemist. M06-2X belongs to M06-class functional which relies on spin densities, spin density gradients, spin kinetic energy density and for non-local hybrid functional, Hartree-Fock exchange. It is a hybrid Meta functional, based on GGA approximation has excellent performance for main group chemistry. M06-2X is global hybrid functional with 54% HF exchange and very important for non-covalent interaction, kinetics and main group thermochemistry [38]. CAM-B3LYP includes the hybrid abilities of B3LYP and consider for long-range correction. It is very useful for the estimation of polarizability of the large chain, excitation to Rydberg states and charge transfer excitations [39]. Furthermore, CAM-B3LYP is a hybrid functional with 19% HF exchange.

2.7 Geometry Optimization

Geometry optimization is a key component of most computational chemistry studies that are concerned with the structure and/or reactivity of molecules. The molecule of minimum energy is obtained by the procedure known as geometry optimization. Initial deduction of the geometry further applies for the computation of the energy and wave functions, which is further modified iteratively until (I) the minimum energy is not

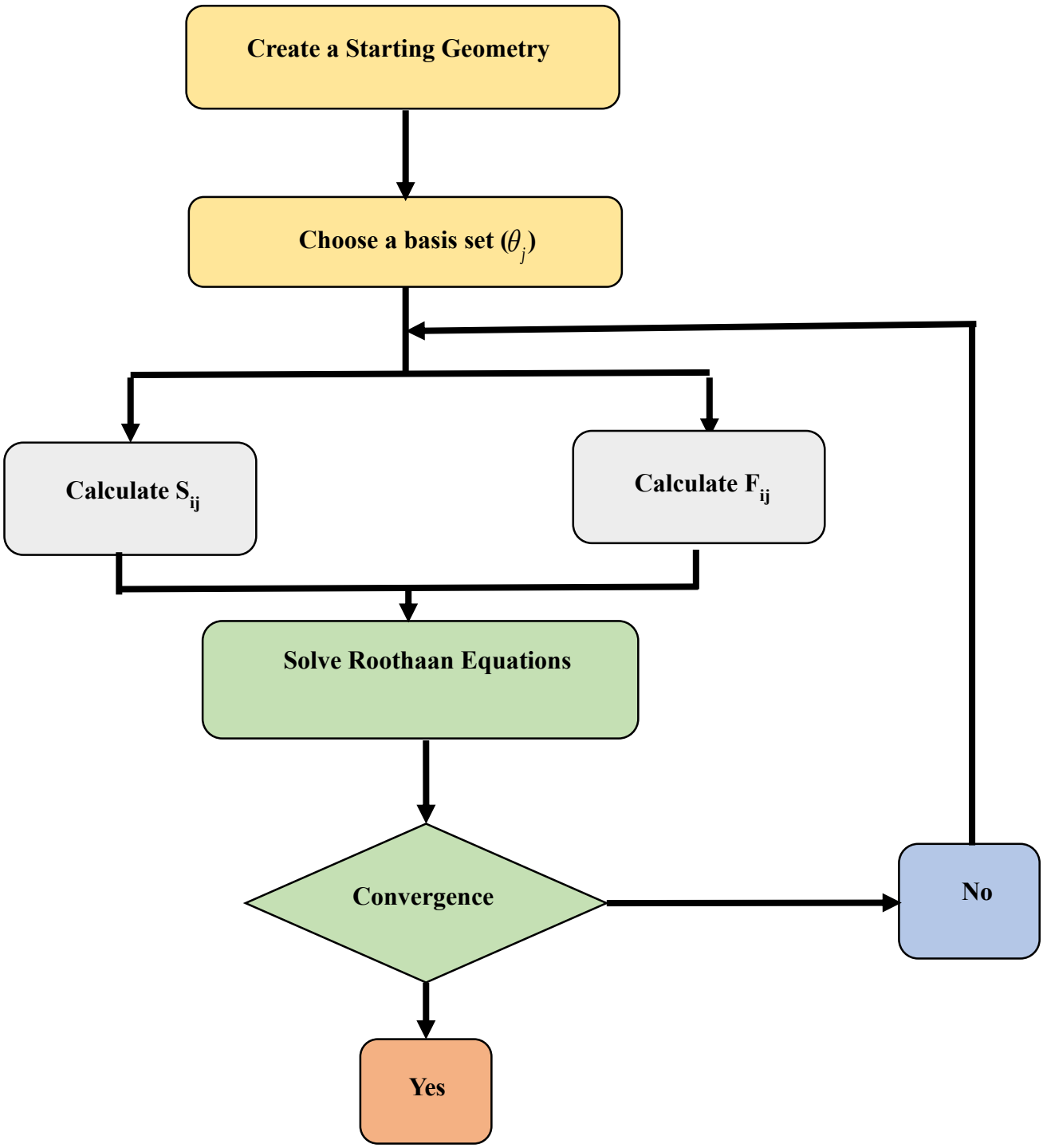

Figure 2.2: Flowchart for a typical quantum mechanical calculation.

achieved and (II) forces within the molecules are zero. Non-rigid molecules may have many energy minimum; therefore, some effort may be required to obtain the global minimum. Optimization is generally used to locate minimum on a potential energy surface (PES) and can expect the equilibrium structure of the molecule for the unknown or unconfirmed structures of molecules.A point on a PES where the forces are zero is called a stationary point and these are the points generally located during an optimization. To move the calculation process across the PES, we have to provide an input geometry. The energy, gradient and the force constant are estimated at every point and these constant identify the curvature of the surface at the same point, consequently gives the appropriate information which is helpful for regulating the next step. To determine whether the geometry optimization has found a minimum or a transition state, it is necessary to perform frequency calculations. A transition state is a point that links two minima on the PES and is characterized by one imaginary frequency. The eigenvector from the Hessian matrix determines the nature of the imaginary frequency and indicates a possible reaction coordinate. A minimum energy structure will have no imaginary frequencies.

2.8 Dipole Moment Calculation

In order to calculate the dipole moment (μ) of the molecules, we have used the Gaussian 09 based on the finite field approach. Following Buckingham's definitions [40], total dipole moment in the Cartesian frame is given by:

$$\mu = (\mu_x^{\,2} + \mu_y^{\,2} + \mu_z^{\,2})^{1/2} \qquad \text{…….2.41}$$

2.9 Frequency Calculations

Infrared and Raman spectra of molecules can be predicted for any optimized molecular structure. The position and relative intensity of vibrational bands can be collected from the output of a frequency calculation. This information is independent of experiment and can, therefore, be used as a tool to confirm peak positions in experimental spectra or to predict peak positions and intensities when experimental data is not available. Calculated frequencies are based on the harmonic model, while real vibrational frequencies are anharmonic. This adequately explains the difference between the calculated and experimental frequencies.

The Raman intensities were calculated from the Raman activities obtained from the Gaussian 09 program, using the following relationship derived from the intensity theory of Raman scattering [41, 42].

$$I_i = [f(\nu_0 - \nu_i)^4 S_i] / [\nu_i \{1 - \exp(-hc\nu_i / kT)\}] \quad \text{.....2.42}$$

Where ν_0 being the exciting wavenumber in cm^{-1}, ν_i the vibrational wave number of the i^{th} normal mode, h, c, and k are the Planck constant, the speed of light in vacuum and Boltzmann constant respectively, f is a suitably chosen common normalization factor for all peak intensities.

References

[1] L. I. Shiff, *Quantum Mechanics,* McGraw- Hill, NewYork, Fifth Ed. (1968).

[2] E. Schroedinger, Ann. Physik, 79, 361 (1926).

[3] L. Pauling, E. B. Wilson, *Introduction to Quantum Mechanics,* McGraw-Hill, New York (1935).

[4] M. Born, R. Oppenheimer, Ann. Phys., 84, 457 (1927).

[5] V. May, O. K¨uhn. *Charge and Energy Transfer Dynamics in Molecular Systems.* Wiley-VCH, Berlin, (2000).

[6] J. C. Slater, Phys. Rev., 34, 1293 (1929).

[7] J. C. Slater, Phys. Rev., 35, 509 (1930).

[8] C. C. J. Roothaan, Rev. Mod. Phys., 23, 69 (1951).

[9] C. G. Hall, Proc. Roy. Soc., A 205, 541 (1951).

[10] W. J. Hehre, *A Guide to Molecular Mechanics and Quantum Chemical Calculations, Wavefunction,* Inc.: Irvine, CA (2003).

[11] A. Szabo, N. S. Ostlund, *Modern Quantum Chemistry: Introduction to Advanced Electronic Structure Theory,* McGraw-Hill: New York, (1982).

[12] K. Raghavachari, J. B. Anderson, J. Phys. Chem., 100, 12960 (1996).

[13] M. Head-Gordon, J. Phys. Chem., 100, 13213 (1996).

[14] T. Helgaker, P. R. Taylor, *Modern Electronic Structure Theory,* Part II (D. 92 Yarkony ed.), World Scientific, pp. 727 (1995).

[15] S. F. Boys, Proc. Roy. Soc., (London), A 200, 542 (1950).

[16] W. J. Hehre, R. F. Stewart, J. A. Pople, J. Chem. Phys., 51, 2657 (1969).

[17] J. S. Binkley, J. A. Pople, J. Am. Chem. Soc., 102, 939 (1980).

[18] M. J. Frisch, J. A. Pople, Binkley, J. Chem. Phys., 80, 3265 (1984).

[19] W. J. Hehre, R. Ditchfield, J. A. Pople, J. Chem. Phys., 56, 2257 (1972).

[20] T. H. Dunning Jr. and P. J. Hay, Modern Theoretical Chemistry, Ed. H. F. Schaefer III, Vol. 3, pp. 1, Plenum, New York (1977).

[21] H. Hellmann, J. Chem. Phys., 3, 61 (1935).

[22] P. J. Hay and W. R. Wadt, J. Chem. Phys., 82, 270 (1985).

[23] W. R. Wadt and P. J. Hay, J. Chem. Phys. 82, 270 (1985).

[24] W. R. Wadt and P. J. Hay, J. Chem. Phys. 82, 284 (1985).

[25] W. R. Wadt and P. J. Hay, J. Chem. Phys. 82, 299 (1985).

[26] S. Chiodo, N. Russo, E. Sicilia, J. Chem. Phys. 125, 104107 (2006)

[27] T. Ziegler, Chem. Rev., 91, 651 (1991).

[28] P. Hohenberg, W. Kohn, Phys. Rev., B, 136, 864 (1964).

[29] W. Kohn, L. J. Sham, Phys. Rev., A, 140, 1133 (1965).

[30] M. Levy, Proc. Natl. Acad. Sci. U. S. A., 76, 6062 (1979).

[31] D. C. Langreth, J. P. Perdew, Phys. Rev. B, 26, 2810 (1982).

[32] J. Harris, R. O. Jones, J. Phys. F, 4, 1170 (1974).

[33] A. J. Cohen, P. Mori-Sánchez, W. Yang Chem. Rev., 112, 289 (2012).

[34] G. Zhang, C. B. Musgrave J. Phys. Chem. A, 111, 1554 (2007).

[35] A. D. Becke, J. Chem. Phys., 98, 5648 (1993).

[36] D. Kumar, N. Sastry, S. D. Visser, Chem. Eur. J., 17, 6196 (2011).

[37] A. K. Vardhaman, C. V. Sastri, D. Kumar, S. D. Visser, Chem. Commun., 47, 11044 (2011).

[38] T. Yanai, D. P. Tew. N. C. Handy, Chem. Phys. Lett., 393, 51 (2004).

[39] Y. Zhao and D.G. Truhlar, Theor. Chem. Account, 120, 215 (2006).

[40] A. D. Buckingham, Adv. Chem. Phys., 12, 107 (1967).

[41] G. Keresztury, S. Holly, J. Varga, G. Besenyei, A. Y. Wang, and J. R. During, Spectro. Acta, 49, 2007 (1993).

[42] G. Keresztury, *Raman Spectroscopy Theory-Handbook of Vibrational Spectroscopy*, John Wiley & Sons, New York, (2002).

Chapter-3

Size Dependent Structural, Electronic and Vibrational Properties of Cd_mS_n (m+n=2–6) Nanoclusters: A DFT Study

Chapter 3

Size Dependent Structural, Electronic and Vibrational Properties of Cd_mS_n (m+n = 2–6) Nanoclusters: A DFT Study

3.1 Introduction

Nanoclusters represent the intermediate phase between small molecular species and the bulk state. The knowledge of the structure of nanoclusters is essential because their properties are highly sensitive to the size and composition; and physical and chemical properties change significantly as size decreases from bulk level to nanoscale. Two basic reasons namely, quantum confinement effect and higher surface to volume ratio are viewed as vital for the dramatic change in their physical and chemical properties. Therefore, to study the physical properties of such clusters, it is central to have an understanding about cluster evolution and possible structural changes that arise as a function of the cluster size and composition because it can lead to the tailoring of novel materials with desirable properties [1]; size of the electronic devices have been reduced [2, 3]. The basic idea behind a structural study of the nanocluster is the assumption that it will follow structure with minimum energy. Therefore, global minimization techniques are used to predict the structure of nanoclusters. II-VI semiconductors such as ZnS, CdSe, and CdTe are of enormous technological importance in different branches of science and technology. These semiconductors are widely used in solar cells, electronic sensors, hydrogen generation, photocatalysis and biological detections [4-9]. Among the II-VI semiconductors, cadmium sulfide (CdS) is an important inorganic semiconductor owing to its unique photoelectric properties. It holds particle-size-dependent electronic spectrum

[10, 11] which could show the influence of size quantization effects. Its potential applications have been exhibited in many fields such as the nonlinear optics [12] the photo electrochemical cells and heterogeneous photocatalysis [13, 14] etc. There have been many theoretical studies using different computational approaches and experimental studies which are focused on the clusters of various compositions having important and promising applications [3-8]. For binary clusters $(CdS)_n$, a number of theoretical studies have been performed for the geometrical structure of the lowest total energy isomers [15-30]. It turns out from previous studies that the $(CdS)_n$ structures (n = 4–7) , obtained in different studies as the lowest energy states are often not the same. Specifically, controversy is found in the structure of the lowest total energy state of $(CdS)_4$; three different structures were obtained. First one is cubic structure as predicted by Gurin et al. [21], second a ring non-planar structure [22] a state with the square geometry [23].

To the best of our knowledge, no detailed DFT calculations have been performed on CdS nanoclusters with an unequal number of m and n considering the various properties. And hence, in this chapter, DFT computations have been applied to systematically investigate structural stability, electronic properties, adiabatic and vertical ionization potential (IP) and electron affinity (EA), HOMO-LUMO, Density of states (DOS) and vibrational behavior of Cd_mS_n (m+n = 6) clusters as a function of the cluster size.

3.2 Computational Methods

Theoretical methods used in the present study are based on first principle calculations within the density functional theory. Density functional theory (DFT) is one of the promising and efficient methods to investigate electronic, optical properties and

structural stability of nanostructures. Several structures were constructed for each Cd_mS_n cluster, and the geometrical structures reported have been fully optimized using the hybrid gradient-corrected functional (B3LYP) with the combination of LANL2DZ basis set within density functional theory frame in the Gaussian-09 code [31]. LANL2DZ incorporating effective core potential (ECP) has been used as the basic basis set in this study for the most precise calculation. Minimum energy for each structure is achieved by relaxing the atomic positions. GaussSum 3.0 [32] has been used for the evaluation of the density of states (DOS) spectrum. For the visualization of molecular orbitals, chemcraft software was used [33]. In order to determine the stability of nanocluster, the binding energy (BE) of the nanocluster is defined by the equation as given below-

$$BE = [mE(Cd) + nE(S) - E(Cd_mS_n)]/(m+n) \quad \ldots\ldots\ldots 3.1$$

Where, E(Cd), E(S), and $E(Cd_mS_n)$ are the total energy of isolated atoms Cd, S and Cd_mS_n clusters, respectively, (m+n) is the total number of Cd and S atoms. This binding energy is termed as the binding energy (BE) per atom. For more accurate calculation of binding energy of a system, the zero point vibrational energy is subtracted from the earlier calculated BE value [34]. Therefore, the harmonic vibrational frequencies and the corresponding zero point energy (ZPE) have also been calculated for all optimized structures. The stability of nanocluster finally is considered on the basis of final binding energy (FBE) thus obtained. The harmonic vibrational frequencies of each optimized structures are evaluated by analytical differentiation of gradients. In all fully optimized structures, the convergence of the system energy was obtained up to 10^{-7} meV and the forces of 10^{-3} eV/Å on each atom were achieved.

3.3 Results and Discussion

3.3.1 Geometries and Stabilities of Cd_mS_n Clusters

The exact determination of equilibrium structures for the clusters under consideration is a fundamental requirement for the discussion of clusters properties and the variation of the chemical bond with the size of the cluster. There may be existent various possible structures for a given number of atoms which are rather close in energy. It is, therefore, significant to evaluate the sensitivity of a given property with respect to structural changes and for identifying a stable cluster in a specific composition, it is key to investigate different parameters, such as, binding energy (BE), HOMO-LUMO gap, ionization potential, and electron affinity etc. with the change in cluster size during the growth process. First-principles calculations were carried out on the various Cd_mS_n (m+n = 2-6) clusters to obtain the stable isomers in each size range. The optimized most stable structures are presented in figure 3.1, while the symmetry, multiplicity of the ground state, HOMO-LUMO gap, binding energies and the final binding energy for all the optimized structures are listed in table 3.1. The stable isomers of Cd_mS_n clusters (m+n = 2-6) possess linear, trigonal, rhombic, bent and star geometries, respectively, which are quite comparable to other reports. The aforementioned properties of most stable structures of Cd_mS_n nanoclusters are given in table 3.2. The calculated bond lengths of Cd-Cd, Cd-S, and S-S for the most stable structures are appended in table 3.3. Detailed discussion of the considered nanoclusters is given in the following.

CdS dimer: Figure 3.1 (a) shows only possible linear structure of the CdS cluster. The calculated value of final binding energy is 2.38 eV and the Cd-S bond length is 2.648 Å. This equilibrium distance is much similar to the value (2.36 Å) computed by Chu et al.

[35] and experimental result 2.52 Å [36]. The multiplicity of the ground state of this cluster is of the triplet in nature.

Cd_mS_n (m+n = 3): For the three-atom cluster, three structures were obtained. These are the S-terminated linear structure, S-centred linear structure, and trigonal structure. For Cd_2S configuration, ground states of the linear and trigonal structures are of singlet and triplet in nature, whereas for CdS_2 configuration the predicted ground states for the linear and triangular structures are triplet and triplet, respectively.

Cd_2S: For the Cd_2S configuration, it is clear from table 3.1 that the trigonal structure symmetry and the triplet ground state has maximum FBE (3.05 eV). The other two structures, linear Cd-Cd-S, and Cd-S-Cd have lower FBEs in comparison to the trigonal Cd_2S structure. Furthermore, obtained Cd-S and Cd-Cd bond lengths for the trigonal structure are 2.59 Å and 4.06 Å, respectively as can be seen in table 3.3.

CdS_2: A similar structures to that of the Cd_2S are predicted for this cluster also. Among these, trigonal structure of CdS_2 with C_S symmetry has FBE of 2.22 eV and is predicted to be most stable. The other two structures, linear S-Cd-S, and Cd-S-S are less stable in comparison to the trigonal CdS_2 structure by energy difference of 0.06 eV. The equilibrium geometry for the triangular CdS_2 structure has a Cd-S bond length of 2.76 Å and S-S bond length of 2.26 Å.

Cd_mS_n (m+n = 4): Calculations show that the four atom structured clusters have the singlet ground states. For the Cd_mS_n (m+n=4) cluster, three configurations, namely Cd_2S_2, Cd_3S, and CdS_3 have taken. These three configurations of CdS contain nine geometry whose descriptions are given below-

Cd_2S_2: Five different configurations have been investigated for the Cd_2S_2 nanoclusters;

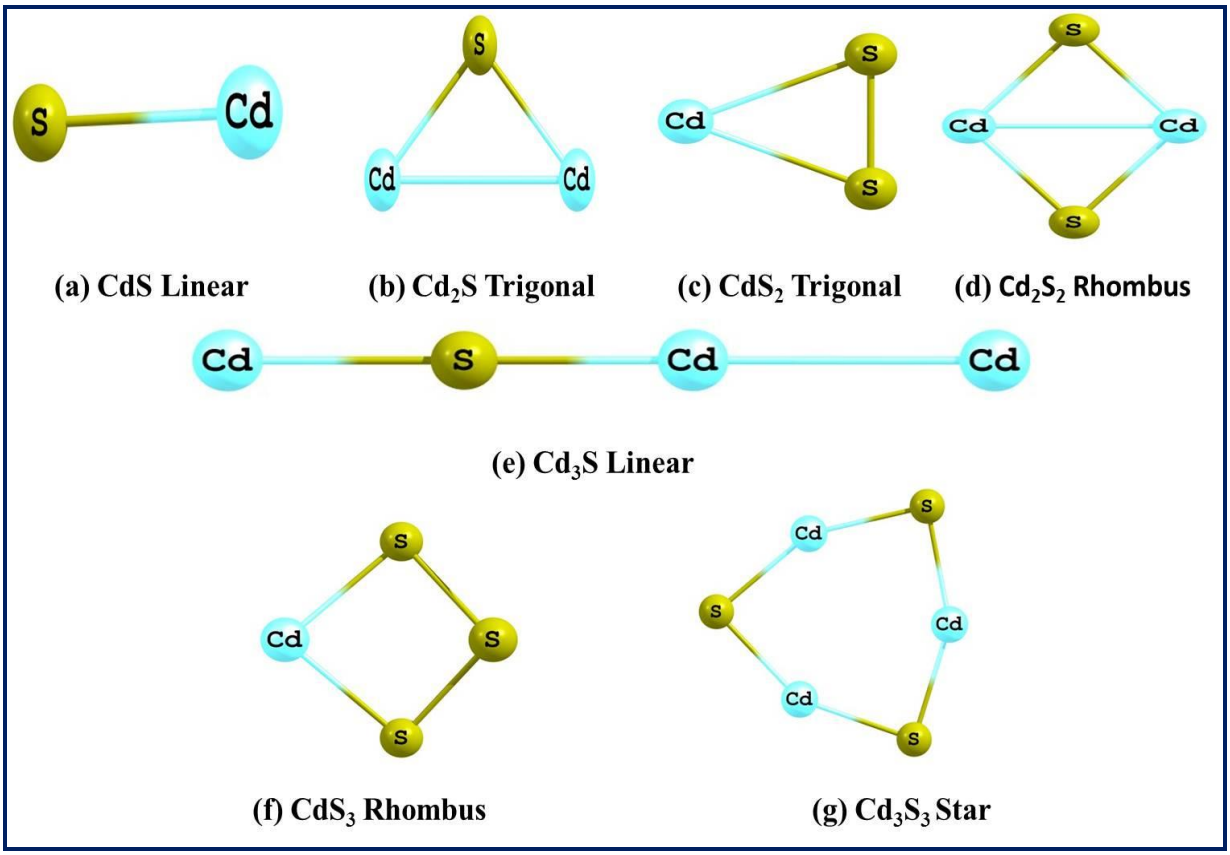

Figure 3.1: Most stable structures of Cd_mS_n (m+n=2-6) nanoclusters.

two linear structures with Cd-S-S-Cd and S-Cd-Cd-S geometry, two bent structures (Cd-S-Cd-S, Cd-S-S-Cd) and a rhombus structure. From table 3.1, it is evident that the rhombus structure having C_1 symmetry and ground state of singlet is the most stable structure as it has maximum FBE of 1.88 eV. Further, our results demonstrate that the Cd-S and Cd-Cd bond lengths 2.56 Å and 2.96 Å respectively are very close to the experimental data (2.57 Å) and the results of Chu et al. [35] (2.50 Å). Cd3S: Three structures for a four-atom cluster were tried. These are the two linear chains Cd-Cd-S-Cd and Cd-Cd-Cd-S, and rhombus geometries. From table 3.1, it seems logical that the linear (Cd-Cd-S-Cd) geometry with C_1 symmetry has a maximum final binding energy of 0.82

Table 3.1: Symmetry, multiplicity of the ground state (GS), binding energy per atom (BE), zero point energy (ZPE), final binding energy (FBE) and HOMO-LUMO gap for all the configuration for the Cd_mS_n (m+n = 2-6) nanocluster.

Nanocluster	Configuration	Symmetry	GS Multiplicity	BE (eV)	ZPE (eV)	FBE (eV)	HOMO-LUMO (eV)
CdS	Linear Cd-S	C_{*v}	3	2.39	0.01	2.38	α =4.69 β=3.00
Cd_2S	Linear Cd-S-Cd	C_{*v}	1	1.09	0.03	1.06	α =1.99
	Trigonal	C_S	3	3.08	0.03	3.05	α =3.90 β=2.36
CdS_2	Linear S-Cd-S	D_{*h}	3	2.21	0.05	2.16	α =5.53 β=0.98
	Trigonal	C_S	3	2.26	0.04	2.22	α =3.94 β=1.89
Cd_2S_2	Bent Cd-S-Cd-S	C_1	1	1.63	0.07	1.56	α =0.65
	Linear Cd-S-S-Cd	C_1	1	1.57	0.06	1.51	α =0.90
	Linear S-Cd-Cd-S	C_1	1	1.60	0.05	1.55	α =1.99
	Bent Cd-S-S-Cd	C_1	1	1.57	0.06	1.51	α =1.28
	Rhombus	C_1	1	1.97	0.08	1.88	α =2.23
Cd_3S	Linear Cd-Cd-S-Cd	C_1	1	0.86	0.04	0.82	α =1.73
	Rhombus	C_1	1	0.75	0.0	0.75	α =1.19
CdS_3	Bent S-S-Cd-S	C_1	3	2.23	0.08	2.15	α =4.33 β=2.05
	Rhombus	C_1	1	3.33	0.09	3.24	α =1.82 β=1.82
Cd_3S_3	Hexagon (Caze)	C_1	1	1.55	0.09	1.46	α =2.40
	Hexagon (Star)	C_1	1	2.34	0.14	2.20	α =3.33

Table 3.2: Symmetry, multiplicity of the ground state (GS), binding energy per atom (BE), zero point energy (ZPE), final binding energy (FBE) and HOMO-LUMO gap for all the most stable configuration for the Cd_mS_n (m+n = 2-6) nanoclusters.

Nanocluster	Configuration	Symme-try	GS Multi-plicity	BE (eV)	ZPE (eV)	FBE (eV)	HOMO-LUMO (eV)	Other (eV)
CdS	Linear Cd-S	C_{*v}	3	2.39	0.01	2.38	α =4.69 β=3.00	
Cd_2S	Trigonal Cd-S-Cd	C_S	3	3.08	0.03	3.05	α =3.90 β=2.36	
CdS_2	Trigonal S-Cd-S	C_S	3	2.26	0.04	2.22	α =3.94 β=1.89	
Cd_2S_2	Rhombus	C_1	1	1.97	0.08	1.89	α =2.23	2.34[21]
Cd_3S	Linear Cd-Cd-S-Cd	C_1	1	0.86	0.04	0.82	α =1.73	
CdS_3	Rhombus	C_1	1	3.33	0.09	3.24	α =1.82 β=1.82	
Cd_3S_3	Hexagon (Star)	C_1	1	2.34	0.14	2.20	α =3.33	

Table 3.3: Bond lengths (Å) for all the most stable configurations of Cd_mS_n (m+n = 2-6) nanoclusters.

Nanocluster	Configuration	Bonds	Bond Length Å (Present)	Bond Length Å Other
CdS	Linear Cd-S	Cd-S	2.65	2.295[21] , 2.36[35], 2.52[36]
Cd_2S	Trigonal Cd-S-Cd	Cd-S Cd-Cd	2.59 4.06	
CdS_2	Trigonal S-Cd-S	Cd-S S-S	2.76 2.26	
Cd_2S_2	Rhombus Cd-S-S-Cd	Cd-S Cd-Cd S-S	2.56 2.96 4.18	2.490[21], 2.50[35], 2.57[36]
Cd_3S	Linear Cd-Cd-S-Cd	Cd-S Cd-Cd	2.46 3.24	
CdS_3	Rhombus S-S-Cd-S	Cd-S S-S	2.58 2.32	
Cd_3S_3	Hexagon (Star)	Cd-S Cd-Cd	2.49 3.43	2.416[21]

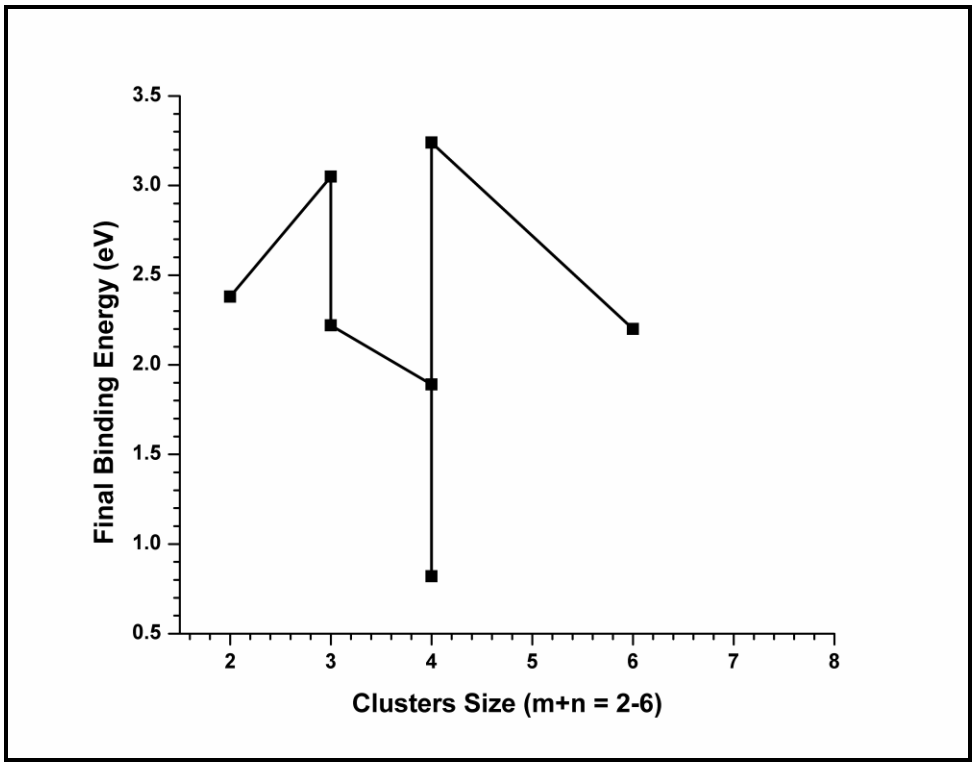

Figure 3.2: Final binding energy vs cluster size of Cd_mS_n (m+n = 2-6) nanoclusters.

eV and is most stable. The computed values of Cd–S and Cd–Cd bond lengths for the most stable structure are found to be 2.46 Å and 3.24 Å, respectively.

CdS_3: For CdS_3, three different geometries linear chain (Cd-S-S-S), bent (S-S-Cd-S) and rhombus have been considered. It was found that rhombus structure having final binding energy 3.24 eV is the most stable structure. The calculated values of Cd-S and S-S bond lengths were found to be 2.58 Å, 2.32 Å, respectively as shown in table 3.3.

Cd_3S_3 (m+n = 6): The ground state of six atom nanoclusters was predicted as a singlet. For Cd3S3 configuration, two linear (Cd-S-Cd-S-Cd-S-Cd-S-Cd-S-Cd-S, Cd-Cd-Cd-S-S-S-S) and two hexagon (Cage, Star) structures have been considered. For these four nanocluster structures, it was found that the hexagon (Star) is the most stable structure because it has maximum FBE of 2.20 eV. The calculated Cd-S bond length is 2.49 Å and for the Cd-Cd, bond length was found to be 3.43 Å. This value of Cd-S bond length

closely approach the data (2.43 Å) deduced by the computations of Chu et al. [35]. Moreover, the most stable structure has C_1 symmetry and a very important one. It was observed that the Cd-Cd bond length is increasing with the size of clusters except for the Cd_2S nanocluster.

3.3.2 Electronic Property: HOMO-LUMO and DOS of CdS Nanoclusters

The HOMO–LUMO energy gap depends upon the chemical connection and reaction between atoms and molecules. The computed energy gap between the highest occupied molecular orbital (HOMO) and the lowest unoccupied molecular orbital (LUMO) i.e. HOMO-LUMO gap.

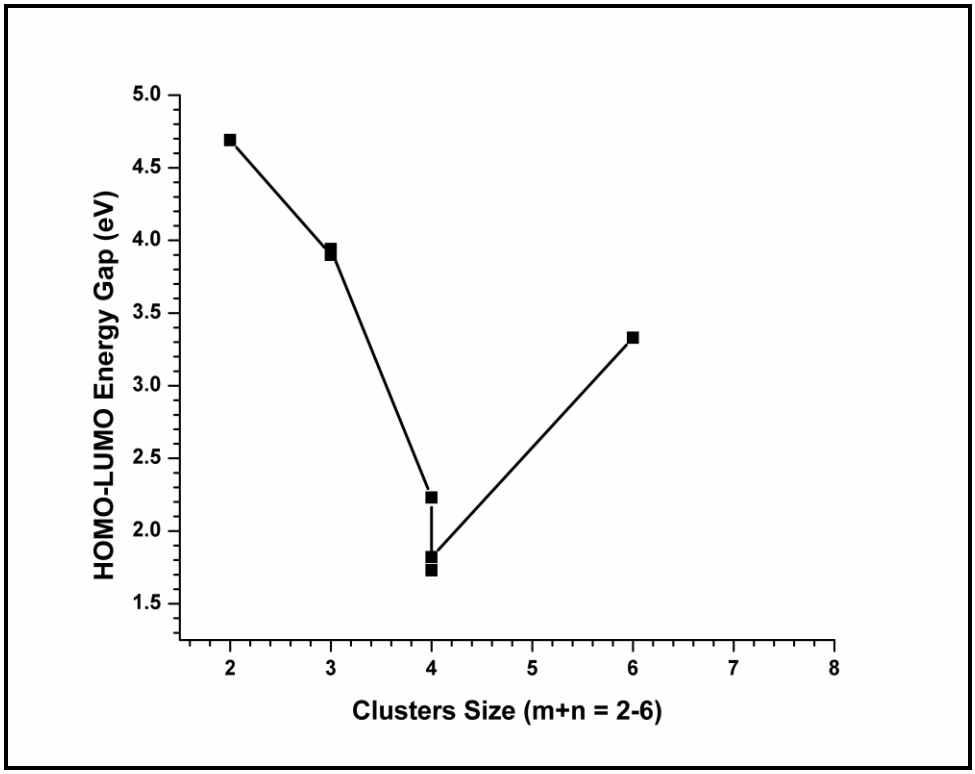

Figure 3.3: HOMO-LUMO gap vs cluster size of Cd_mS_n (m+n = 2-6) nanoclusters.

The studied structures are presented in table 3.1. It may be pointed out that the HOMO-LUMO gaps decrease with a number of S atoms. Figure 3.3, shows our calculated HOMO-LUMO energy gap as a function of cluster size.

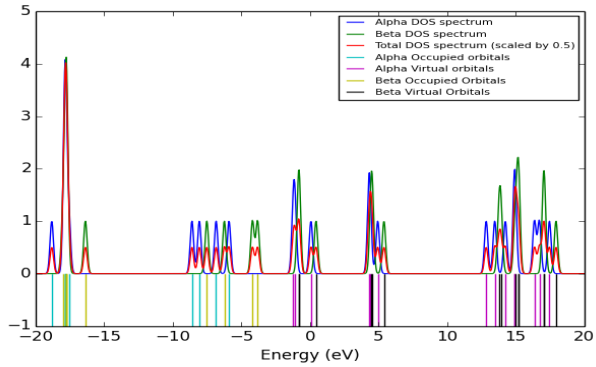

(a) CdS Linear

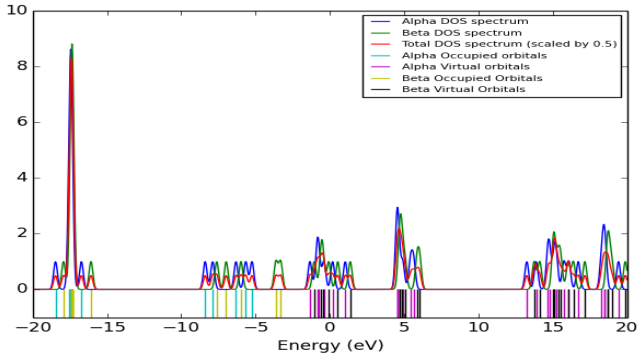

(b) Cd_2S Trigonal

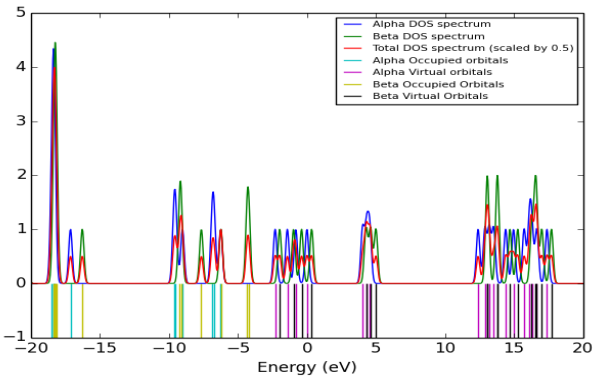

(C) CdS_2 Trigonal

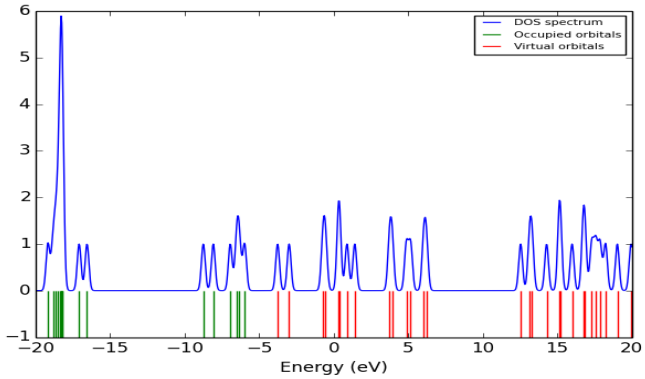

(d) Cd_2S_2 Rhombus

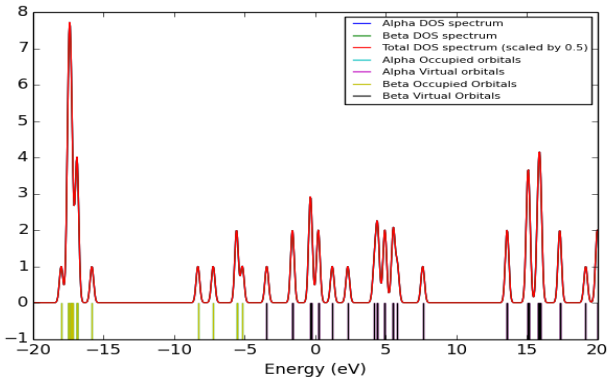

(e) Cd_3S Linear

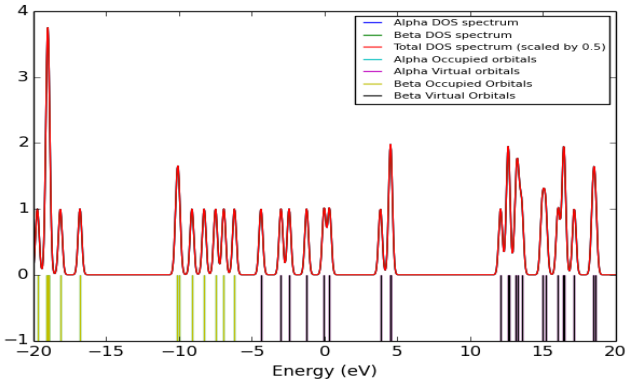

(f) CdS_3 Rhombus

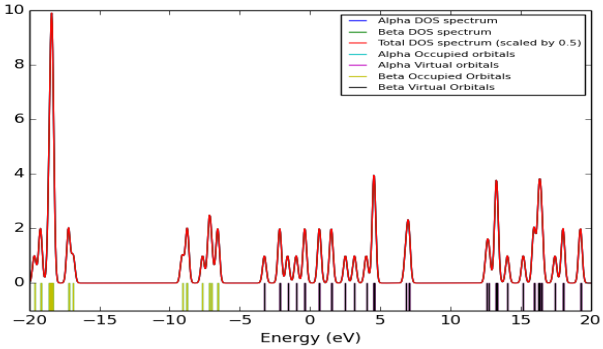

(g) Cd_3S_3 Star

Figure 3.4: DOS, HOMO-LUMO energy diagram for all the most stable configuration of the Cd_mS_n (m+n = 2-6) nanoclusters.

Nanocluster	Configuration	HOMO	LUMO
CdS	Linear (Cd-S)	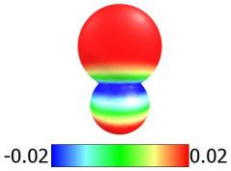	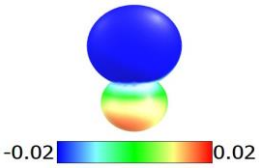
Cd_2S	Trigonal (Cd-S-Cd)	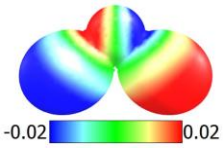	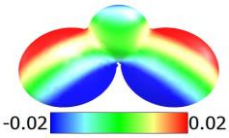
CdS_2	Trigonal (S-Cd-S)	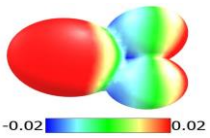	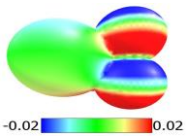
Cd_2S_2	Rhombus (Cd-S-S-Cd)	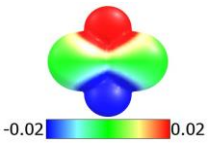	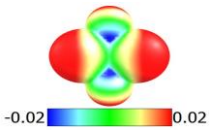
CdS_3	Rhombus (S-S-Cd-S)	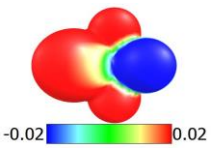	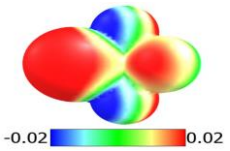
Cd_3S	Linear (Cd-Cd-S-Cd)	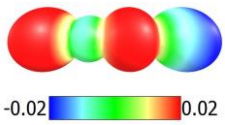	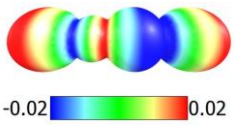
Cd_3S_3	Hexagon (Star)	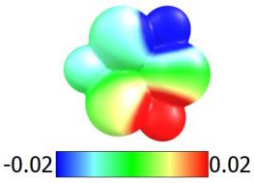	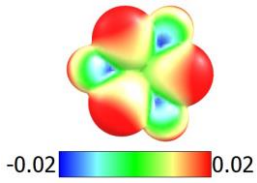

Figure 3.5: HOMO-LUMO energy visualization for all the most stable configuration of the Cd_mS_n (m+n = 2-6) nanoclusters.

Table 3.4: Adiabatic and vertical ionization potential (IP) and electron affinity (EA) in eV for all the most stable configurations of Cd_mS_n (m+n = 2-6) nanoclusters.

Configuration	Ionization potential (IP)		Electron affinity (EA)	
	Adiabatic (eV)	Vertical (eV)	Adiabatic (eV)	Vertical (eV)
Linear Cd-S	8.31	8.41	1.99	1.94
Trigonal Cd-S-Cd	7.04	7.13	2.13	1.88
Trigonal S-Cd-S	8.28	8.63	2.22	2.07
Rhombus Cd-S-S-Cd	7.88	7.95	2.09	2.03
Linear	7.30	7.34	2.02	1.95
Rhombus S-S-Cd-S	8.02	8.22	2.54	2.38
Hexagon (Star)	9.64	9.65	1.88	1.74

Here, mostly high energy gap indicates that the clusters are more stable as already noted from the calculated FBEs. The information about the electronic properties of CdS nanocluster can be derived with the help of HOMO-LUMO gap. Herein, by increasing the size of the nanocluster by adding number of atoms, it was observed that HOMO-LUMO gap is decreasing rapidly up to cluster size (m+n = 4) and attains a maximum value (4.69 eV) for CdS. Further, when there is an increase in the cluster size by adding some more no. of atoms, the HOMO-LUMO gap is rising up to the cluster size (m+n = 6). The high value of the energy gap reveals that the electrons in the valance band need more energy to go the conduction band. Furthermore, from the figure 3.4 of DOS, it is very clear that due to the overlapping of Cd atoms with S atoms in the nanocluster, density of charge is very low in occupied orbital than the in virtual orbital. In the nanoclusters, the geometry of the clusters is also affected due to the density of charges in

a virtual and occupied orbital. From figure 3.4, it is evident that the DOS is much more depending on the geometry and number of the atoms present in the nanocluster. It is observed that for the same and maximum number of m and n i.e. (m+n = 4), the amplitude of peak is maximum rather than the other nanoclusters, which can be seen in figure 3.4. HOMO-LUMO energy visualization for all the most stable configuration of the Cd_mS_n (m+n = 2-6) nanoclusters has been displayed in figure 3.5.

3.3.3 Ionization Potential and Electron Affinity

The ionization potential (IP) and the electron affinity (EA) of a cluster are very important properties from the theoretical point of view. They are experimentally accessible and provide a direct measure for the type of bonding involved in a cluster. The ionization potential (IP) is defined as the amount of energy required to remove an electron from a nanocluster. In the present study, adiabatic ionization potential (AIP) has been calculated by taking the energy difference between the neutral and the ionized nanoclusters after finding the most stable structure for the ionized nanoclusters using the optimization procedure. The electron affinity (EA) is defined as the energy evolved when an electron is added to a neutral cluster. The adiabatic electron affinity (AEA) has been evaluated by finding the energy difference between the neutral and the anionic nanocluster. The anionic nanocluster is relaxed to its most stable state. The adiabatic and vertical IPs and EAs for the most stable structures are listed in table 3.4. To the best of our knowledge, experimental data and earlier calculation are available very scarcely for comparison of IP of Cd_mS_n clusters.

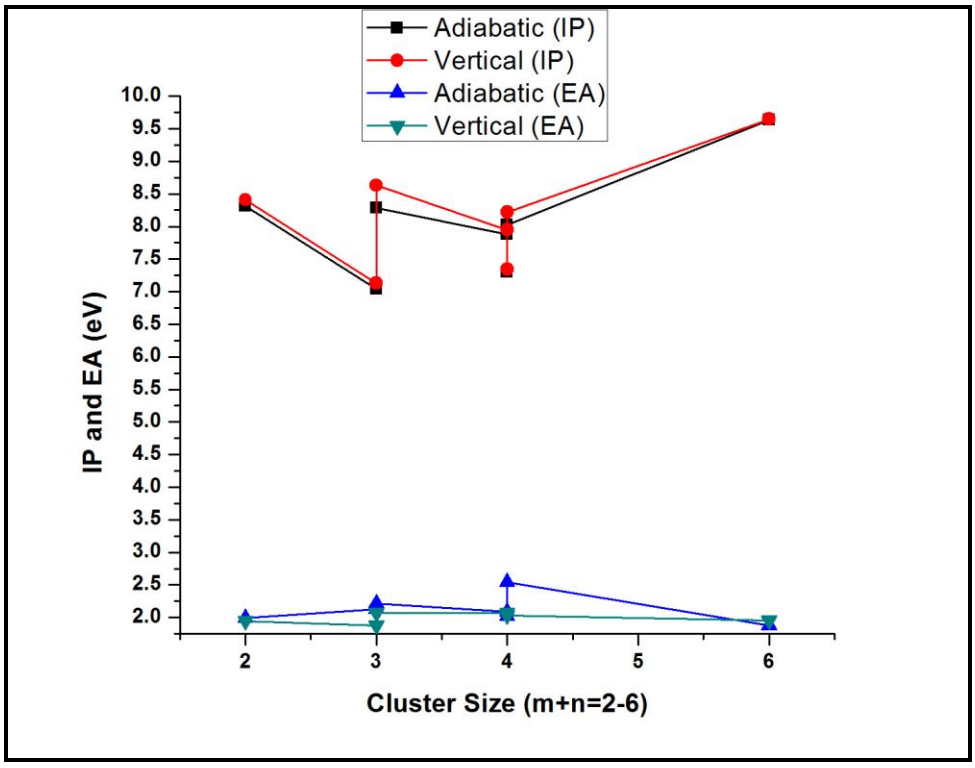

Figure 3.6: Ionization potential and electron affinity vs cluster size of Cd_mS_n (m+n = 2-6) nanoclusters.

A zigzag behavior can be seen in the variation of both IP and EA with nanocluster size. However, a similar trend was noted also for the corresponding ZnSe clusters from the literature [37]. Variation of the adiabatic and vertical IPs and EAs for the most stable structures is depicted in figure 3.6. It is interesting here to compare the ionization potential of the hexagon (star, figure 1g) geometry has the highest value of adiabatic IP and vertical IP, which are 9.64 eV and 9.65 eV and for the trigonal structure of the configuration, Cd_2S has lowest values of the adiabatic and vertical ionization energy. A perusal of table 3.4 shows that the values of the adiabatic and vertical electron affinity for rhombus geometry of CdS_3 configuration are highest i.e. 2.54 eV and 2.38 eV, respectively. For the cluster size Cd_2S_2, calculated vertical ionization energy is 7.95 eV which is in good agreement with 8.10 eV evaluated by Sanville et al. [21] and the

experimental (7.26 eV) photoelectric thresholds for bulk CdS Swank [38]. The hexagon (star) structure has the lowest value of adiabatic and vertical EA which are 1.88 and 1.74 eV respectively.

3.3.4 Vibrational Frequencies

Investigation of vibrational frequencies is a very significant parameter in exploring the local minimum in structures. It is observed that even for a small number of atoms in a cluster there are plenty of possible structures which may represent local minima on the energy hypersurface. In order to decide whether or not there is a local minimum, it is necessary to determine the harmonic vibrational frequencies and to check if any of these is zero or takes an imaginary value. In the present investigation, the vibrational frequencies are calculated using the B3LYP- DFT/LANL2DZ method for the most stable nanoclusters. For the determination of vibrational frequencies, the second derivative of the total energy of the system with respect to the atomic displacements is found out. The obtained above calculated physical quantities for the most stable clusters are listed in table 3.5. The above physical properties have not been reported by any other worker. The above properties have discussed for each nanocluster in the following section: For CdS, the stretching mode frequency of 209.5 cm^{-1} was obtained which is both IR and Raman active. For Cd_2S trigonal (Cd-S-Cd) structure, the calculated frequencies are 41.26 cm^{-1}, 203.25 cm^{-1}, 253.08 cm^{-1}. From table 3.5, it is evident that the highest stretching-frequencies are both highly IR and Raman active. The lower frequency 41.26 cm^{-1} originates from the bending vibration of Cd-S bond, etc. For CdS_2 trigonal (S-Cd-S) structure, the frequencies 39.42 cm^{-1}, 199.18 cm^{-1} and 449.82 cm^{-1} were obtained wherein the highest frequency of 449.82 cm^{-1} corresponds to the Cd-S stretching vibration. In this

Table 3.5: The calculated vibrational frequencies (cm^{-1}), infrared intensities (IR Int. in km mol^{-1}), relative IR intensities (Rel. IR Int.) and Raman scattering activities (Raman activity in $Å^4$/amu) for most stable configurations of Cd_mS_n (m+n = 2-6) nanoclusters.

Nanocluster	Configuration	Properties	Values
CdS	Linear Cd-S	Frequency IR Int. Rel. IR Int. Raman activity	209.53 2.34 1 49.59
Cd_2S	Trigonal Cd-S-Cd	Frequency IR Int. Rel. IR Int. Raman activity	41.26, 203.25, 253.08 0.35, 3.38, 24.17 0.01, 0.14, 1 11.52, 52.29, 21.29
CdS_2	Trigonal S-Cd-S	Frequency IR Int. Rel. IR Int. Raman activity	39.42, 199.18, 449.82 0.02, 23.82, 0.67 0.00, 1, 0.03 33.16, 16.25, 46.37
Cd_2S_2	Rhombus Cd-S-S-Cd	Frequency IR Int. Rel. IR Int. Raman activity	96.86, 128.65, 196.16, 208.96, 309.97, 310.99 20.10, 0.00, 0.00, 25.14, 44.97, 0.00 0.45, 0.00, 0.00, 0.56, 1, 0.00 0.00, 8.87, 2.64, 0.00, 0.00, 67.69
Cd_3S	Linear Cd-Cd-S-Cd	Frequency IR Int. Rel. IR Int. Raman activity	6.82, 46.52, 48.22, 50.37, 130.00, 303.36 0.61, 16.33, 2.76, 17.29, 9.74, 79.67 0.01, 0.21, 0.03, 0.230.12, 1 3.10, 2.31, 0.72, 1.12, 18.55, 40.56
CdS_3	Rhombus S-S-Cd-S	Frequency IR Int. Rel. IR Int. Raman activity	102.56, 136.69, 240.27, 283.79, 370.78, 379.18 4.89, 3.17, 3.46, 2.12, 8.58, 10.83 0.45, 0.29, 0.32, 0.20, 0.79, 1 13.12, 30.36, 10.57, 36.62, 6.82, 16.61
Cd_3S_3	Hexagon (Star)	Frequency IR Int. Rel. IR Int. Raman activity	59.85, 62.49, 70.37, 70.61, 94.83, 100.67, 262.90, 263.35, 290.11, 293.75, 337.61, 338.35, 0.01, 0.03, 4.47, 4.51, 27.80, 0.01, 13.42, 13.68, 0.01, 0.01, 72.32, 72.33 0.00, 0.00, 0.06, 0.06, 0.38, 0.00, 0.19, 0.19, 0.00, 0.00, 0.99, 1 0.70, 0.71, 3.18, 3.21, 0.00, 2.74, 11.79, 11.77, 97.73, 0.02, 0.05, 0.04

case frequency, 199.18 cm^{-1} is found to highly IR reactive in comparison to others. For the rhombus Cd_2S_2, (Cd-S-S-Cd) structure, there are six frequencies. The two highest frequencies (310.99 cm^{-1}, 309.97 cm^{-1}) appear due to the stretching of the two S atoms. The remaining four frequencies originate from the mixed vibration of Cd and S atoms and highest frequency is not IR active. For Cd_3S, linear configuration Cd_3S has 6 frequencies and the highest frequency 303.36 cm^{-1} corresponds to the Cd-S stretching vibration which is both IR and Raman active. The rhombus CdS_3 has the highest frequency 379.18 cm^{-1}, rhombus CdS_3 has the highest frequency 379.18 cm^{-1} and found to be less IR reactive in comparison to the linear Cd_3S configuration. 12 frequencies were obtained for the Cd_3S_3 hexagonal cage structure, in all. The upper two frequencies 337.61 cm^{-1} and 338.35 cm^{-1} are due to the stretching vibration of S atom close to the Cd atom and lower frequencies 59.85 cm^{-1}, 62.49 cm^{-1}, 70.37 cm^{-1}, and 70.61 cm^{-1} correspond to twisting vibration of the whole cluster.

3.4 Conclusion

In conclusions, DFT approaches were used for the detailed theoretical characterization of the most stable isomers of the Cd_mS_n clusters. The calculated properties include bond lengths, adiabatic and vertical ionization potentials and electron affinities, charge on atoms and dipole moments for the Cd_mS_n nanoclusters. The results reveal that the nonlinear structured nanoclusters are most stable in comparison to linear one depending on FBE. It is found that Cd_2S trigonal structure is most stable structure among the all the considered nanoclusters. In general, nanoclusters with high FBEs have a large number of S atoms. It is observed that the value of HOMO-LUMO gap decreases with a number of S atoms. Further, the IP and EA both show zigzag behavior with the

clusters size. Vibrational properties were studied for the most stable structured only in which, except Cd_2S_2 and Cd_3S_3 all are IR active at the vibrational frequencies. For the most stable structure, calculated lowest and highest frequencies are 102.56 cm^{-1}, and 397.18 cm^{-1} and both are infrared active. The results of the present systematic study should be useful in modelling and understanding the growth of cadmium-based clusters at the nanoscale. Complete identification and characterization of clusters are mandatory for improving the use of their potentialities in fundamental and applied areas. The outcome should motivate new experimental studies on this important class of clusters.

References

[1] S. M Woodley, R. Catlow, Nat. Mater, 7, 937 (2008).

[2] H. J. Himmel, N. Hebben, Chem. Eur. J, 11, 4096 (2005).

[3] S. M. Sheehan, G. Meloni, B. F. Parsons, N. Wehres, D. M. Neumark, J. Chem. Phys, 124, 064303 (2006).

[4] C. B. Murray, D. J. Norris, M. G. Bawendi, J. Am. Chem. Soc., 115, 8706 (1993).

[5] C. Ricolleaui, L. Audinet, M. Gandais, T. Gacoin, Eur. Phys. J. D, 9, 565 (1999).

[6] Manna Liberato, C. Erik Scher, L.S. Li, Paul Alivisatos Pau, J. Am. Chem. Soc., 124, 7136 (2002).

[7] B. Song, L. Ling, P. L. Cao, Chin. Phys., 13, 489 (2004).

[8] D. Vogel, P. Kruger, J. Pollmann, Phys. Rev. B, 52, 14316 (1995).

[9] A. Tomasulo and M. V. Ramakrishna, J. Chem. Phys. 105, 3612 (1996).

[10] R. Rossetti, S. Nakahara, L. E. Brus, J. Chem. Phys. 80, 4464 (1983).

[11] R. Rossetti, J. L. Ellison, J. M. Gibson, L. E. Brus, J. Chem. Phys., 79, 1086 (1984).

[12] N. Herron, Y. Wang, M. M. Eddy, G. D. Stucky, D. E. Cox, K. Moller., T. Bein, J. Am. Chem. Soc., 111, 530 (1989).

[13] P. K. Mahapatra, C. B. Roy, Electrochim. Acta, 29, 1439 (1984).

[14] A. P. Alivisatos, J. Phys. Chem., 100, 13226 (1996).

[15] M. C. Troparevsky, J. R.Chelikowsky, J.Chem. Phys., 114, 943 (2001).

[16] P. Deglmann, R. Ahlrichs, K. Tsereteli, J. Chem. Phys., 116, 1585 (2002).

[17] J. O. Joswig, G. Seifert, T. A. Niehaus, M. Springborg. J. Phys. Chem. B, 107, 2897 (2003).

[18] J. M. Matxain, J. M. Mercero, J. E. Fowler, J. M. Ugalde, J. Phys. Chem. A, 108, 10502 (2004).

[19] G. Maroulis, C. Pouchan, J. Phys. Chem. B, 107, 10683 (2003).

[20] S. Karthikeyan, E. Deepika and P. Murugan, J. Phys. Chem. C, 116, 5981 (2012).

[21] Sanville, A. Burnin, J. J. BelBruno, J. Phys. Chem. A, 110, 2378 (2006).

[22] V. S. Gurin, Z. Phys. D, 42, 65 (1997).

[23] H. Zeng, R. R. Vanga, D. S. Marynick, Schelly, Z. A. J. Phys. Chem. A, 112, 14422 (2008).

[24] P. Karamanis, C. Pouchan, Chem. Phys. Lett., 474, 162 (2009).

[25] J. O. Joswig, M. Springborg. G. Seifert, J. Phys. Chem. B, 104, 2617 (2000).

[26] J. Frenzel, J. O Joswig, P. Sarkar, G. Seifert, M. Springborg, Eur. J. Inorg. Chem., 3, 585 (2005).

[27] J. Frenzel, J. O. Joswig, G. Seifert, J. Phys. Chem. C, 111, 10761 (2007).

[28] C. E. Junkermeier, J. P. Lewis, G. W. Bryant, Phys. Rev. B, 77, 205125 (2008).

[29] G. L. Gutsev, O. Neal, R.H. Belay, K.G. Weatherford, C. A. Chem. Phys. 368, 113 (2010).

[30] C. He-Ying, L. Zhao-Xia, Q. Guo-Li, K. De-Guo, W. Si-Xin, L. Yun-Cai, D. Zu-Liang, Chin. Phys. B, 17, 247 (2008).

[31] M. J. Frisch, G. W. Truck's, et-al, Gaussian, Inc., Wallingford CT, (2009).

[32] N. M. O'Boyle, A. L. Tenderholt, K. M Langner, J. Comp. Chem., 29, 839 (2008).

[33] Chemcraft 1.8, http://www.chemcraftprog.com

[34] R. Shastri, D. Kumar, D. Kumar, A. K. Yadav, IARJEST, 2, 94 (2015).

[35] H.-Y. Chu, Z.-X. Liu, G.-L. Qiu, D.-G. Kong, S.-X. Wu, Y.-C. Li, Z.-L. Du, Chin. Phys. B, 17, 2478 (2008).

[36] V. S. Gurin, J. Phys. Chem., 100, 869 (1996).

[37] P. S. Yadav, D. K. Pandey, Appl. Nanosci., 2, 351 (2012).

[38] R. K. Swank, Phys. Rev., 153, 844 (1967).

Chapter-4

Quantum Chemical Studies on Zn_mO_n (m+n=2–8) Even Nanocluster's Stability

Chapter 4

Quantum Chemical Studies on Zn_mO_n (m+n=2–8) Even Nanocluster's Stability

4.1 Introduction

Materials play a very significant role in the development of science and technology. These materials are deep-seated in human life and making the daily life of human very comfortable. With the fast development of modern science and technology, it is crucial to discover new advanced functional materials, which possess versatile properties. Semiconductors are very common material, which plays a very important role in the field of electronics and technology. Owing to the need for speed and technology, many of the materials are being discovered and are using to serve the purpose. So, there is a requirement of such material to the world which possesses some unique properties such as larger band gap, higher electron mobility, and higher breakdown field. Zinc Oxide (ZnO) can be a better optional material. ZnO, II-VI group semiconductor, electronically play a very important role due to the wide band gap. It has direct band gap energy of 3.37 eV and large binding energy, 60 meV at the room temperature, very well satisfying the aforesaid properties [1]. ZnO has high mechanical, thermal and chemical stability, and is very promising candidate in field of nanoscience because it is very cheap, nontoxic and biocompatible in comparison with Cd (cadmium) based semiconductors materials like CdSe or CdTe [2]. ZnO is kind of semiconductor, which exhibit quantum confinement effect [3]. In recent time, ZnO-based low dimensional materials have produced great scientific interest because of their encouraging applications in the area of nanoscale

optoelectronic devices, photocatalysis, photovoltaic solar cells, quantum devices, UV electronics, spintronic devices and sensor applications [4-11]. It has been commonly used in its polycrystalline form over a hundred years in a wide range of applications and has emerged as a prominent material with potential optoelectronics, involves polycrystalline or nanostructured ZnO [12-18]. Various theoretical studies have been performed on $(ZnO)_n$ clusters for the different range of clusters size, which shows that fullerene like structures are more stable in small sized clusters [19]. Wang et al. have predicted the hollow cage structures formed by $(ZnO)_n$ (n = 2) squares and $(ZnO)_3$ hexagons (n = 3) [20]. Cusco et al. have discussed the temperature dependence of the Raman scattering of ZnO at 80K to 750K [21]. Lucas et al. have reported the nanobelts of ZnO nanostructure using the combination of Raman spectroscopy and AFM and they found dual growth modes of the nanostructure [22]. The computational study may be a useful and dominant instrument for overcoming the existing disadvantages and predicting the theoretical concept of such type of semiconductor material systems. Theoretical investigation of ZnO nanoclusters will provide vital information for understanding the growth mechanisms of geometry and stability of ZnO nanoclusters having the lowest energy of formation. Density functional theory (DFT) is a reliable theoretical method to study nanoclusters, particularly in the prediction of the structures that lie between molecular and bulk system. This allows for much possible geometry and it is challenging to find a truly global minimum energy structure. Though, there are a number of theoretical studies performed to investigate the properties of ZnO clusters [23-25], to best of our knowledge no precise quantum calculations have been performed, for considered nanoclusters using density functional theory (DFT) calculations and basis set. Therefore, the theoretical

study of these systems is required. In the present chapter, ZnO nanocluster is being stabilized up to (m+n = 2-8), only for even nanoclusters for different structures and their structural stability, dipole moment, HOMO-LUMO energy gap, binding energy per atom, DOS, Ionization potential, Electron affinity and vibrational behavior of these nanoclusters have been calculated and discussed.

4.2 Computational Techniques

For optimization of ZnO nanocluster and to calculate their ground and excited state properties, the DFT method have been used. Structural optimizations (i.e. the geometrical parameters) have been completed with no constraints imposed on the nanocluster structures during the optimization. Various possible structures have constructed for each ZnO cluster. For geometry optimization and vibrational analysis, B3LYP level of DFT method, Beck's three parameters with correlation function (Lee-Yang-Parr), and relativistic effective core potential with double zeta basis set, LANL2DZ as implemented in Gaussian 09 programme suit [26] are used. DFT is one of the promising and efficient methods to investigate the electronic, optical and structural stability of nanoclusters. Also, Gauss Sum 3.0 [27] has been used for the evaluation of the density of states (DOS) spectrum.

4.3 Results and Discussion

4.3.1 Geometries and Stability of ZnO Nanoclusters

This section deals with the structural stability of ZnO nanoclusters. The first principal calculation has been applied for various ZnO cluster to get the stable isomer in each size. For stability of nanocluster, the binding energy of the nanocluster is defined by

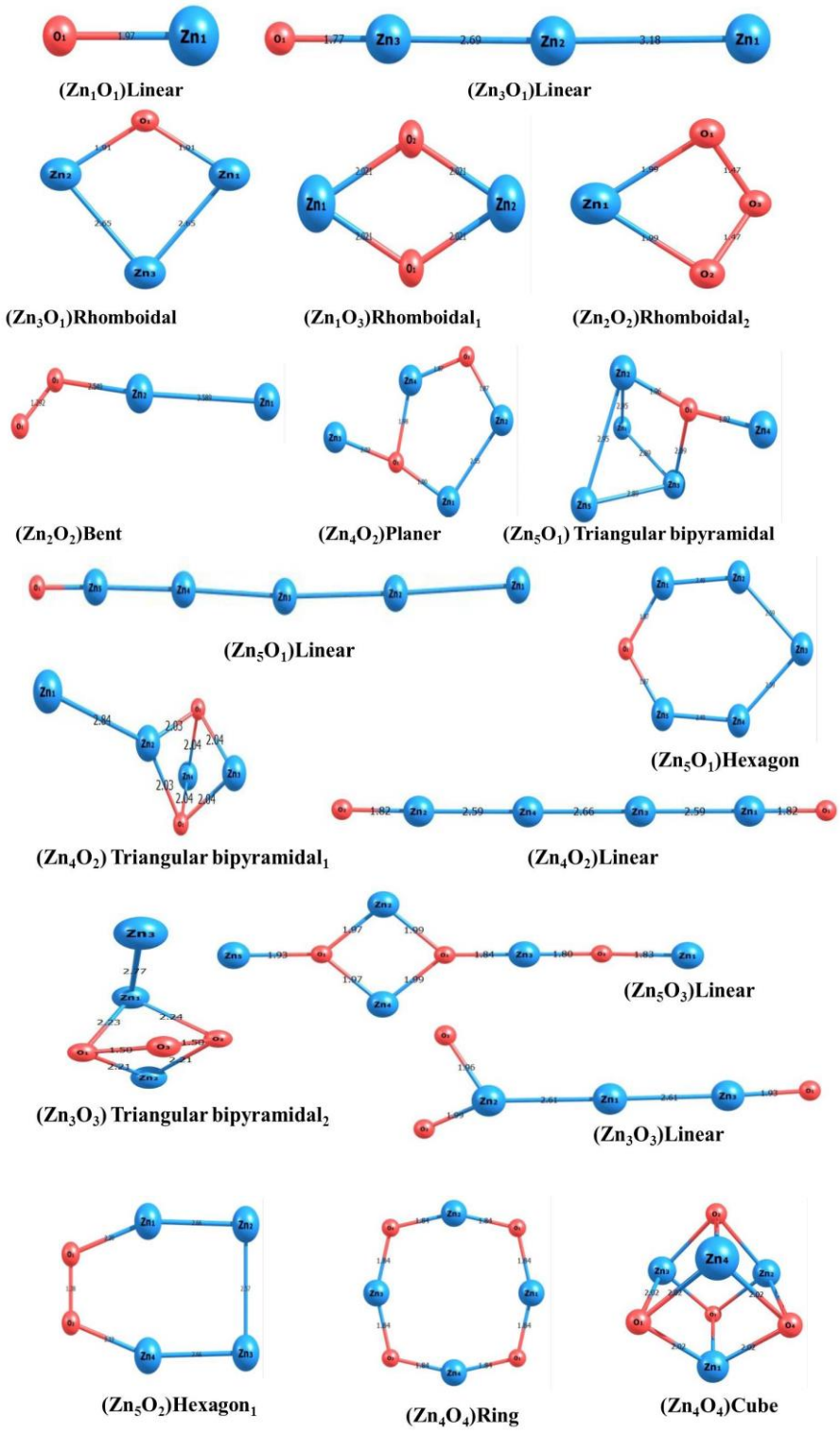

Figure 4.1: Optimized structures of Zn_mO_n (m+n = 2-8) nanoclusters.

the equation-

$$BE = [mE(Zn) + nE(O) - E(Zn_mO_n)]/(m+n) \quad \text{…....5.1}$$

where, E(Zn), E(O), and $E(Zn_mO_n)$ are the total energy of isolated atoms ZnO and Zn_mO_n clusters, respectively, and m+n is the total number of Zinc (Zn) and Oxygen (O) atoms. This is termed as the binding energy (BE) per atom. For more precise computation of binding energy of a system, the zero-point vibrational energy (ZPE) is subtracted from the previous calculated binding energy value. Calculated values of final binding energy, HOMO-LUMO gap and dipole moment are shown in table 4.1. In the following section, most sable nanoclusters of each even sized clusters have been discussed.

Zn_mO_n (**m+n = 2**) nanocluster contains only linear possible structure having bond length 1.97 Å and final binding energy is 0.10 Hartree (E_h). Ground state multiplicity of ZnO is a triplet and dipole moment is 2.71 Debye. For this linear ZnO molecule, theoretical bond length, 1.73 Å and 1.71 Å, is reported by A. Jain et al. [28] and B. L. Wang et al. [29] which is slightly lower than the calculated results.

For the nanocluster size (**m+n = 4**) of Zn_mO_n, five geometries have considered including trigonal, linear, bent and rhomboidal, and optimized. Out of these five geometries, ZnO_3 $rhomboidal_1$ nanocluster has a maximum final binding energy of 0.13 E_h. So, it will be the most stable structure among these five nanocluster structures. The bond length between Zn-O and O-O are 1.99 Å and 1.47 Å respectively, and the bond angle between Zn-O-O is 85.84°. However, ZnO_3 has singlet ground state multiplicity and dipole moment 5.84 Debye. For Zn_mO_n (**m+n = 6**), nine structures are optimized which possess the different geometry including linear, planer, triangular bipyramidal and hexagon. Out of these nine, Zn_4O_2 having planer geometry is found to be most stable

Table 4.1: The symmetry, multiplicity of the ground state (GS), final binding energy (FBE), HOMO-LUMO gap and dipole moment for Zn_mO_n (m+n = 2-8) nanoclusters.

Nanocluster (No. of atoms)	Configuration	Symmetry	Multiplicity	FBE (E_h)	HOMO-LUMO Gap (E_h)	Dipole Moment (Debye)
ZnO_ (2)	**Linear**	**C*V**	**Singlet**	**0.10**	**0.09**	**2.71**
Zn_3O_ (4)	Linear	CS	Singlet	0.04	0.07	11.94
Zn_2O_2	Bent	C_1	Triplet	0.11	0.07	1.64
Zn_3O	Rhomboidal	C_1	Singlet	0.05	0.04	2.62
ZnO_3	**$Rhomboidal_1$**	**CS**	**Singlet**	**0.13**	**0.08**	**5.84**
Zn_2O_2	$Rhomboidal_2$	C2V	Triplet	0.12	0.05	0.29
Zn_4O_2 (6)	**Planer**	**C_1**	**Singlet**	**0.50**	**0.07**	**3.87**
Zn_5O	Triangular Bipyramidal	C_1	Singlet	0.15	0.07	0.60
Zn_4O_2	Triangular $Bipyramidal_1$	C_1	Singlet	0.06	0.07	3.03
Zn_3O_3	Triangular $Bipyramidal_2$	C_1	Singlet	0.04	0.07	1.84
Zn_5O	Hexagon	C_1	Singlet	0.01	0.01	2.31
Zn_4O_2	$Hexagon_1$	C_1	Triplet	0.12	0.01	3.96
Zn_5O	Linear	CS	Singlet	0.02	0.07	14.74
Zn_4O_2	$Linear_1$	CS	Triplet	0.12	0.05	0.14
Zn_3O_3	$Linear_2$	C_1	Triplet	0.10	0.08	2.04
Zn_4O_4 (8)	Ring	C_1	Singlet	1.08	0.15	0.00
Zn_4O_4	Cube	C_2H	Singlet	1.06	0.11	0.00
Zn_5O_3	**Linear**	**C_1**	**Triplet**	**1.24**	**0.03**	**2.08**

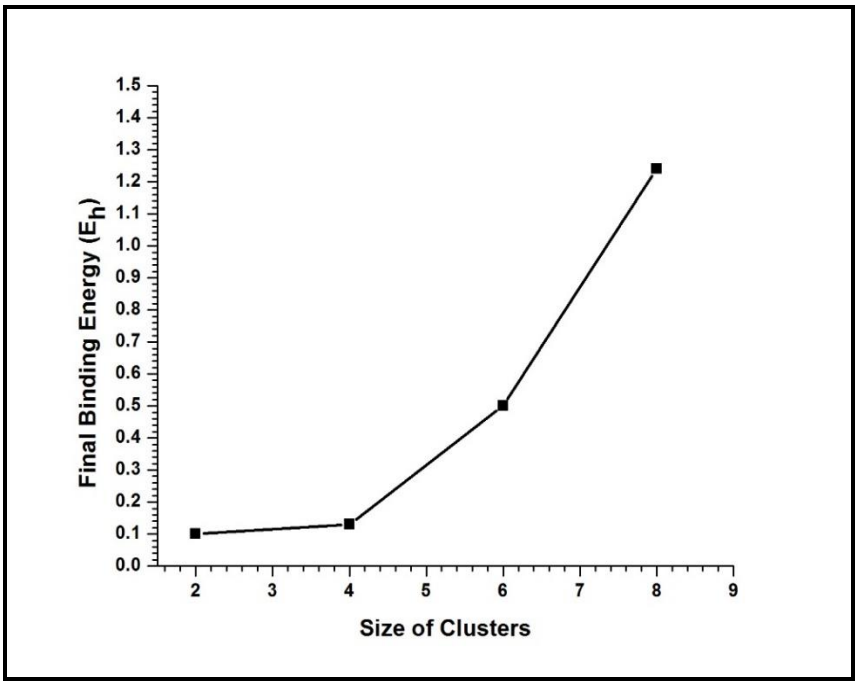

Figure 4.2: Final binding energy vs cluster size of Zn_mO_n (m+n = 2-8) nanoclusters.

because it has maximum final binding energy. The bond length between Zn_4-O_2 and O_2-Zn_2 is 1.87 Å, which is similar while between Zn_3-O_1 and O_1-Zn_4 is different. The angle between Zn_3-O_1-Zn_4 and Zn_1-O_1-Zn_4 is 86.52° and 105.39° respectively. The ground state multiplicity of Zn_4O_2 is singlet and FBE is 0.50 E_h. The dipole moment is 3.87 Debye. For Zn_mO_n (**m+n = 8**), only three structures are optimized which are shown in figure 4.1. The structural geometry- including linear, ring, and cube, are optimized. Out of these three structures, Zn_5O_3 structure (rhomboidal linear) is found to be most stable because it has a maximum final binding energy of 1.24 E_h. The bond lengths between O_1-Zn_2, O_1-Zn_4, and Zn_2-O_2, O_2-Zn_4 are 1.97 Å and 1.99 Å respectively while between Zn_5-O_1, O_2-Zn_3, Zn_3-O_2, and O_3-Zn_1 are 1.93 Å, 1.84 Å, 1.80 Å, and 1.83 Å respectively. Bond angle between Zn_2-O_1-Zn_4 and Zn_2-O_1-Zn_4 is 90.37° and 89.23°. The ground state multiplicity of Zn_2O is singlet and dipole moment is 0.00 Debye. All the most stable configurations of

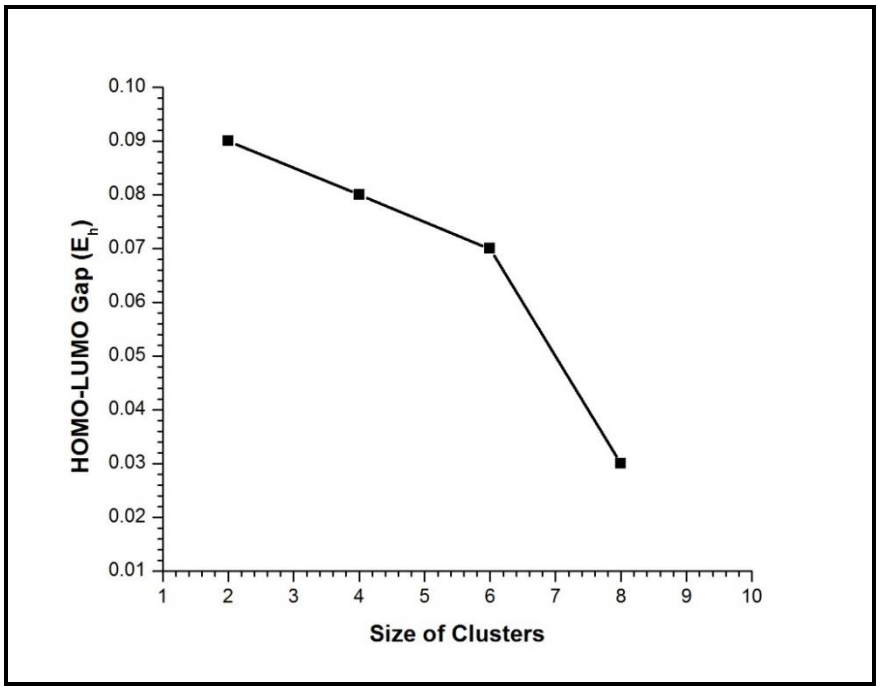

Figure 4.3: HOMO-LUMO gap vs cluster size of Zn_mO_n (m+n = 2-8) nanoclusters.

ZnO nanoclusters are shown boldly in table 4.1, while structures are depicted in figure 4.1. The variation of final binding energy (FBE) of most stable structures with the cluster size is shown in figure 4.2. From the figure, it is clear that the binding energy is increasing with increasing the number of atoms in the clusters. Binding energy is minimum for Zn_mO_n (m = 1, n = 1) configuration and maximum for Zn_mO_n (m = 5, n = 3). On the basis of binding energy, it can state that Zn_5O_3 linear structure is most stable among all considered nanocluster.

4.3.2 Electronic Property: HOMO-LUMO Gap and DOS

The HOMO-LUMO gap is defined as the energy difference between the highest occupied and lowest unoccupied molecular orbitals. It depends upon the chemical reaction between atoms and molecules and structural geometry. The calculated energy gap between the highest occupied molecular orbital (HOMO) and the lowest unoccupied molecular orbital (LUMO) i.e. HOMO-LUMO gap for all the studied nanostructures is

shown in table 4.1 whereas for the most stable structures it is shown bolded in the table. Further, the graph is plotted between the total number of atoms in nanocluster i.e. the size of the cluster and HOMO-LUMO energy gap for the most stable configuration of Zn_mO_n on the basis of lower binding energy. Figure 4.3 shows the calculated energy gap as a function of cluster size.

It is evident from figure 4.3 that with the increase of cluster size, the HOMO-LUMO gap is decreasing. For Zn_mO_n (m = 1, n = 1) and Zn_mO_n (m = 5, n = 3), it is found maximum and minimum which are 0.09 E_h and 0.03 E_h respectively. With the help of these values of HOMO-LUMO, the information about the electronic properties of ZnO nanocluster can be known.

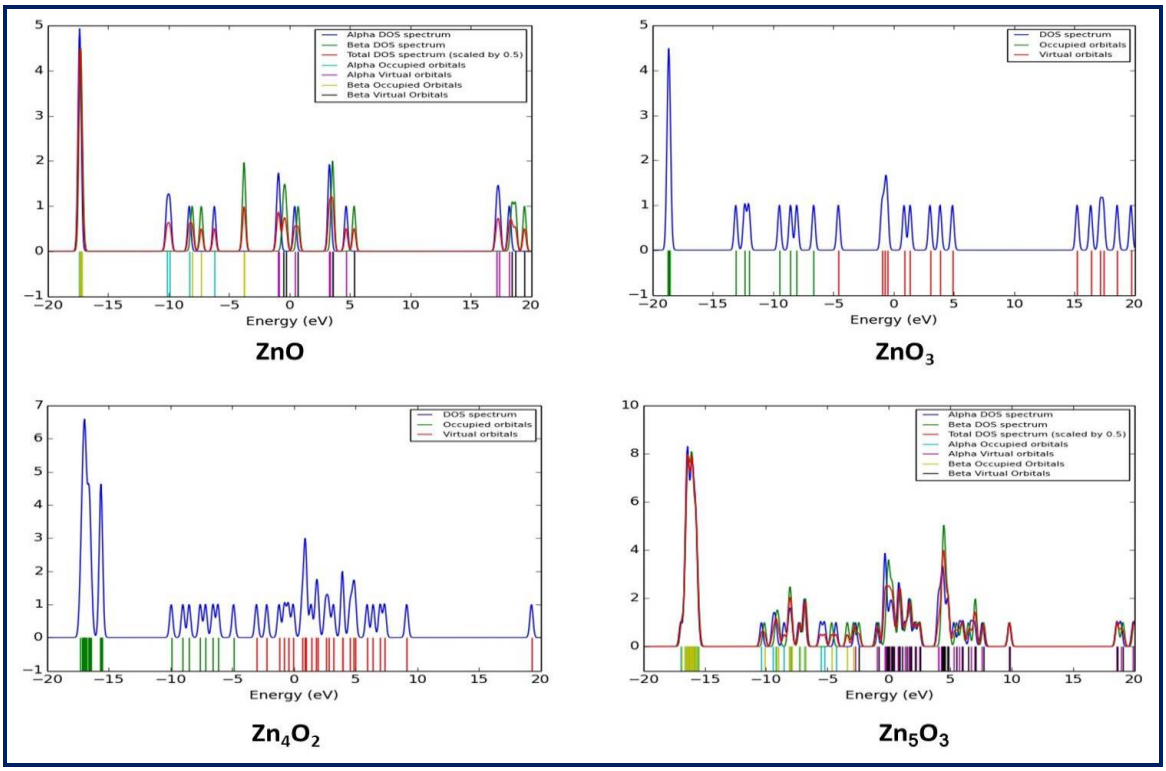

Figure 4.4: DOS, HOMO-LUMO energy diagram of most stable Zn_mO_n (m+n = 2-8) nanoclusters.

The high value of the energy gap reveals that the electrons in the valance band needed more energy to go the conduction band. The density of the state is much more depending on the geometry and number of the atoms present in the nanocluster. Figure 4.4, reveals that the ZnO and Zn_5O_3 both contain spin up and spin down electron because alpha and beta molecular orbital are presented in DOS diagram. In the case of ZnO_3 and Zn_4O_2, only alpha molecular orbital exists in a particular range of energy which is clear from the figure. HOMO-LUMO energy visualization for all the most stable configuration of the Zn_mO_n (m+n = 2-8) nanoclusters is displayed in figure 4.4.

4.3.3 Ionization Potential (IP) and Electron Affinity (EA)

From the theoretical point of view, ionization potential (IP) and the electron affinity (EA) of a nanocluster are very important properties. They are experimentally accessible and provide a direct measure for the type of bonding involved in a cluster. The ionization potential (IP) is well-defined as the amount of energy required to remove an electron from a nanocluster. In the present study, adiabatic ionization potential (AIP) has been calculated by taking the energy difference between the neutral and the ionized nanoclusters after finding the most stable structure for the ionized nanoclusters using the optimization procedure. The electron affinity (EA) is defined as the energy evolved when an electron is added to a neutral cluster. In the current study, AEA is evaluated by finding the energy difference between the neutral and the anionic nanocluster. The anionic nanocluster is relaxed to its most stable state. The graph is drawn for the most stable nanoclusters, between IP, EA and cluster size as shown in figure 4.5. To the best of our knowledge, experimental data and earlier calculation are available very scarcely for comparison of IP and EA of the considered configuration of Zn_mO_n nanoclusters. From

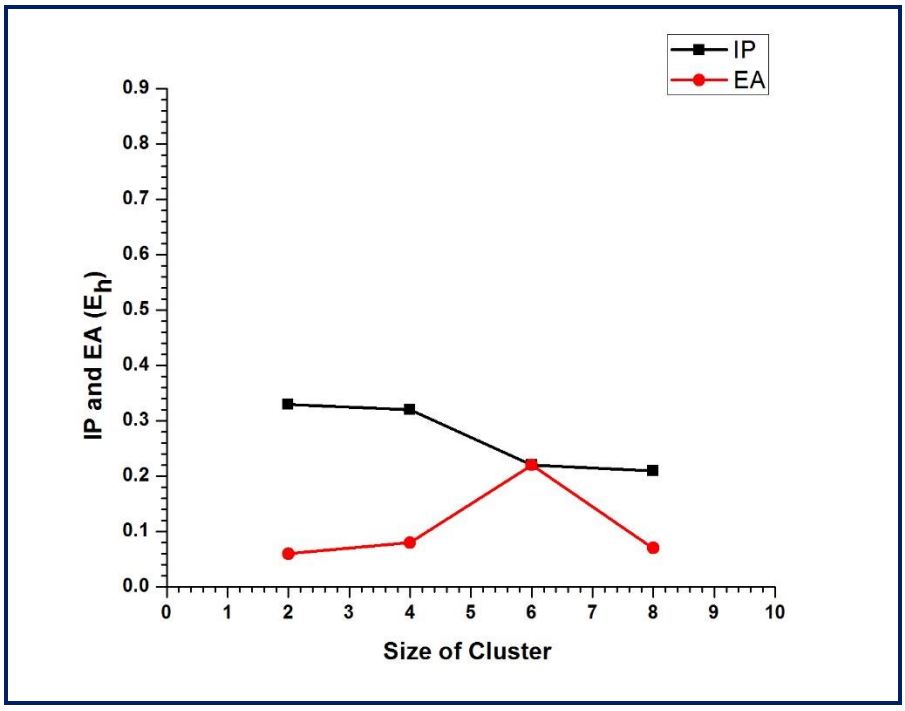

Figure 4.5: Ionization potential and electron affinity gap vs cluster size of most stable Zn_mO_n (m+n = 2-8) nanoclusters**.**

the graph, it is clear that the value of ionization potential is greater than electron affinity. The value of IP is decreasing with the size of the cluster. It is maximum for ZnO linear (0.33 E_h) and minimum for Zn_5O_3 linear (0.21 E_h) structure. The behavior of electron affinity with the size of the cluster is zigzag. The value of EA is increasing from (m+n = 2-6) and after then it is decreasing up to (m+n=8). The maximum and minimum values of EA are 0.22 E_h and 0.06 E_h for (m+n = 6 and 2) nanoclusters, respectively.

4.3.4 Vibrational Analysis

Analysis of vibrational frequencies is a very significant parameter in exploring the local minimum in structures. It is observed that even for a small number of atoms in a cluster there are plenty of possible structures which may represent local minima on the energy hypersurface. In the present investigation, the displacement is found out and the obtained above calculated physical quantities for the most stable nanoclusters are listed in

Table 4.2: The calculated vibrational frequencies (cm^{-1}), infrared intensities (IR Int. in km/mol) and Raman scattering activities (Raman activity in $Å^4$/amu) of most stable Zn_mO_n (m+n = 2-8) nanoclusters.

Nanocluster	Configuration	Properties	Values
ZnO	Linear	Frequency	441.64
		IR Int.	3.63
		Raman activity	61.4472
ZnO_3	$Rhomboidal_1$	Frequency	277.01, 312.00, 401.25, 651.09, 795.47, 856.97
		IR Int.	35.93, 23.34, 4.97, 0.12, 38.68, 139.10
		Raman activity	29.93, 24.31, 6.82, 16.60, 2.59, 4.83
Zn_4O_2	Planer	Frequency	7.89, 71.25, 91.23, 112.76, 115.06, 144.49, 185.13, 210.23, 413.72, 491.33, 595.33, 632.29
		IR Int.	0.02, 7.41, 2.08, 7.30, 7.08, 17.07, 2.48, 1.09, 3.87, 60.78, 35.55, 132.74
		Raman activity	0.95, 143.96, 14.93, 12.77, 43.56, 0.44, 135.20, 1.00, 16.46, 21.98, 337.28, 1629.18
Zn_5O_3	Linear	Frequency	12.05, 17.34, 38.81, 45.29, 66.87, 91.79, 116.72, 121.68, 150.08, 201.93, 210.69, 243.49, 249.76, 331.97, 393.12, 617.29, 746.32, 880.54
		IR Int.	0.68, 0.01, 1.25, 0.36, 17.93, 11.49, 1.57, 8.13, 3.75, 7.12, 33.122, 276.14, 102.41, 3.27, 10.82, 3.93, 21.76, 229.86,
		Raman activity	8.27, 9.55, 16.82, 48.10, 316.44, 62.83, 495.56, 98.46, 9.19, 181.42, 12.58, 5597.79, 3099.41, 2407.19, 127.51, 4570.13, 10653.4546, 36930.5561

table 4.2. The above physical properties have not been reported by any other worker for the considered nanocluster. The above properties are discussed for each most stable nanocluster in the following section: For ZnO, the stretching mode frequency of 441.64 cm^{-1} is obtained which is both IR and Raman active. The values of IR intensity and Raman Activity at this frequency are 3.63 km-mol^{-1} and 61.4472 $Å^4$/amu found. Our IR value is slightly lower than the value 4.74 km/mol [25] reported by Xuelie et al. For ZnO_3 $rhomboidal_1$ structure, the frequencies 277.01 cm^{-1}, 312.00 cm^{-1}, 401.25 cm^{-1}, 651.09 cm^{-1}, 651.09 cm^{-1}, 795.47 cm^{-1} and 856.97 cm^{-1} are obtained, wherein the highest frequency of 856.97 cm^{-1} corresponds to the Zn-O stretching vibration. In this case frequency, 856.97 cm^{-1} is found to highly IR reactive in comparison to others. The value of IR intensity at this frequency is 139.10 km-mol^{-1}. The lowest frequency for this configuration is 7.89 cm^{-1} and the value of IR intensities at this frequency is 0.02 km-mol^{-1}. In the case of Zn_5O_3 linear structure, 18 modes of vibrational frequencies have existed and each mode of frequency is IR and Raman active. The frequencies are 12.05, 17.34, 38.81, 45.29, 66.87, 91.79, 116.72, 121.68, 150.08, 201.93, 210.69, 243.49, 249.76, 331.97, 393.12, 617.29, 746.32, 880.54 cm^{-1} respectively. At the highest frequency, asymmetrical stretching exists between Atom O_2, Zn_3, O_3 and Zn_1. The values of IR and Raman activity at this frequency are 229.86 km-mol^{-1} and 36930.5561 $Å^4$/amu respectively.

4.5 Conclusion

In summary, DFT methods were used for the optimization of the most stable structures of the Zn_mO_n nanoclusters. The calculated properties include bond lengths, multiplicity, point group symmetry, binding energy, HOMO-LUMO energy gap, dipole

moments, ionization potential and electron affinity for the Zn_mO_n nanoclusters. Our results reveal that the existence of the most stable configurations of various Zn_mO_n nanoclusters depends on final binding energy, and the nanocluster Zn_5O_3 (m+n = 8) with linear structure is most stable among all considered nanoclusters. In general, nanoclusters with high BEs have a large number of Zn atoms. It was observed that the value of HOMO-LUMO gap decreases with the increase of cluster size. FBE is increasing with the increasing number of atoms i.e. the size of the cluster. The results of the present study should be useful in modelling and understanding the growth of zinc-based clusters at the nanoscale. We believe that the results provide new insights that would have certainly important implications to advance theoretical and experimental studies of clusters.

References

[1] A. B. Djurišić, A. M. C. Ng, X.Y. Chen, *Progress in Quantum Electronics*, 34, 191 (2010).

[2] A. P. Alivisatos, J. Phys. Chem. 100, 13226 (1996).

[3] C. F. Landes, S. Link, M. B. Mohamed, B. Nikoobakht, M. A. El-Sayed, Pure and Appl. Chem., 74, 1675 (2002).

[4] G. Heiland, E. Mollwo, and F. Stockmann, Solid State Phys., 8, 193 (1959).

[5] J. R. Haynes, Phys. Rev. Lett., 17, 16 (1966).

[6] Y. Xia et al., Adv. Mater. 15, 353 (2003).

[7] B. Wen, R. Melnik, Appl. Phys. Lett., 92, 261911 (2008).

[8] Ü. Özgür, Ya. I. Alivov, C. Liu, A. Teke,b_ M. A. Reshchikov, S. Doğan, V. Avrutin, S. J. Cho, and H. Morkoçd, Jour. of Appl. Phys., 98, 041301 (2005).

[9] L. Ovsiannikova, Acta Phys. Polo. A, 122 1062 (2012).

[10] P. J. Sebastian and M. Ocampo, Sol. Energy Mater. Sol. Cells, 44, 1 (1996).

[11] E. Corcoran, Sci. Am., 263, 74 (1990).

[12] Z. L. Wang, Mater. Today, 7, 26 (2004).

[13] X. Y. Kong, Y. Ding, R. Yang, Z. L. Wang, Science, 303 1348 (2004).

[14] M. H. Zhao, Z. L. Wang, S. X. Mao, Nano Lett., 4, 587 (2004).

[15] U. Ozgur, Y. I. Alivov, C. Liu, A. Teke, M. A. Reshchikov, S. Dogan, V. Avrutin, S. J. Cho, H. Morkoc, J. Appl. Phys., 98, 041301 (2005).

[16] M. J. Spencer, Prog. Mater. Sci., 57 437 (2012).

[17] M. M. Brewster, X. Zhou, M. Y. Lu, S. Gradecak, Nanoscale vol. 4, 1455 (2012).

[18] Y. S. Park, C. W. Litton, T. C. Collins, and D. C. Reynolds, Phys. Rev., 143, 512 (1966).

[19]. L. Ovsiannikova, Acta Phys. Pol. A, 122, 1062 (2012).

[20] X. Wang, B Wang, L Tang, J. Zhao, Phys. Lett. A, 374, 850 (2010).

[21] R. Cusco, E. A-Llado, J. Ibanez, L. Artus, J. Jimenez, B. Wang, M. J. Callahan, Phys. Rev. B, 75, 165202 (2007).

[22] M. Lucas, Z. L. Wang, E. Riedo, Phys. Rev. B, 81, 045415 (2007).

[23] X. Lü, X. Xu, N. Wang, Q. Zhang, M. Ehara, H. Nakatsuji, Chem. Phys. Lett., vol. 291, 445 (1998).

[24] J. M. Matxain, J. E. Fowler, J. M. Ugalde, Phys. Rev. A, 62, 053201 (2000).

[25] J. Joswig, S. Roy, P. Sarkar, M. Springborg, Chem. Phys. Lett., 365, 75 (2002).

[26] M. J. Frisch, G. W. Truck's, et-al, Gaussian, Inc., Wallingford CT, (2009).

[27] N. M. O. Boyle, A. L. Tenderholt, K. M. Langner, J. Comp. Chem., 29, 839 (2008).

[28] A. Jain, V. Kumar, Y. Kawazoe, Comp. Mater. Sci., 36, 258 (2006).

[29] B. L. Wang, S. Nagase, J. J. Zhao, G. H. Wang, J. Phys. Chem. C, 1114956 (2007).

[30] X. Cheng, F. Li, Y. Zhao, J. of Mol. Struct. theoc., 894, 121 (2009).

Chapter-5

A Density Functional Theory Study on Structural Stability and Electronic Properties of Co_xO_y $(x+y=4-12)$ Nanoclusters

Chapter 5

A Density Functional Theory Study on Structural Stability and Electronic Properties of Co_xO_y (x +y = 4−12) Nanoclusters

5.1 Introduction

Transition metals in contact with oxygen atoms have been topic to intensive research in the scientific realm due to their special physical, chemical, electronic, magnetic properties and wide applicability [1-5]. Among these, cobalt oxide (CoO) has engrossed special attention owing to its enormous potential for application in sensing, catalysis, electronics, electrode materials and magnetic materials [6-9]. An oxide of cobalt (CoO) is gray or blue-black powder: possessing three oxidation states [10], named as:

(i) Cobalt monoxide or cobalt [II] oxide (CoO, cubic crystal structure)

(ii) Cobalt [III] oxide (Co_2O_3)

(iii)Cobalt [II, III] oxide (Co_3O_4, cubic crystal structure)

These oxidation states of CoO and nanoscale cobalt systems have attracted substantial attention due to their versatile properties which are most used in gas sensors, electrochromic devices, chemical and ceramic industries, and coloring glass etc. [10]. Generation of H_2 and O_2 gas from water through photocatalytic water splitting utilizing abundant solar energy has received great interest in recent years [11] for converting sunlight into clean and renewable energy**.** In this context, it has been shown that the CO_3O_4 has high activity because of its superb reducibility, richness in oxygen vacancies, and high concentration of electrophilic oxide species such as $O_{ads,}$ O^-, or O_2^- [12]. A number of experimental and theoretical studies have been dedicated to metal oxide in form of clusters and nanoparticles [13-22]. Properties of these

systems have been found to show a strong size-dependence at the nano and sub nanoscale, and are clearly very different from those of their atomic and bulk counterparts [23]. This may offer new possibilities for the development of highly functional structures with desirable physicochemical properties by a bottom up approach with clusters serving as building blocks for materials named as cluster-assembled materials. It has been reported that experimental data on cobalt oxide usually, belong to CoO [24-25]. Xie and coworkers studied the reaction of neutral cobalt oxide cluster Co_mO_n (m = 3–9, n = 3–13) with NO, CO, C_2H_4 and C_2H_2 [26] in a fast flow reactor using time of flight mass spectrometry, and found solid oxidation reaction dependency on cluster size. By performing the flow tube experiment Kapiloff et al. found that the response of smaller clusters of $(Co)^-_n$ (where n = 2-8) with O_2 is maximum [14]. Yin et al. performed an experimental and theoretical investigation of Co_mO_n clusters [27]. Furthermore, they found comparatively high stability in cationic $Co_{11}O_{12}^+$ and $Co_{12}O_{12}^+$ clusters for the $Co_mO_n^+$ clusters. Density functional theory calculations indicated more stability in tower or cage structures of Co_9O_9 and $Co_{12}O_{12}$ in comparison to the bulk NaCl-like cubic structure [27-28]. Dibble et al. observed photo dissociation mass spectra of Co_xO_y which show prominent stoichiometries of x = y [29]. DFT study by Uzunova et al. confirmed that CoO_4 possessed diperoxide $Co(O_2)$ structure and CoO_2 Co-dioxide structure [30]. By means of DFT method, Gutsev et al. has reported geometrical structure and electronic state of anion cobalt oxide cluster (CoO^-) [16]. The stability of CoO clusters has been considered as a most attractive system which is revealed in many size-dependent properties like ionization energies and dissociation energy [26].

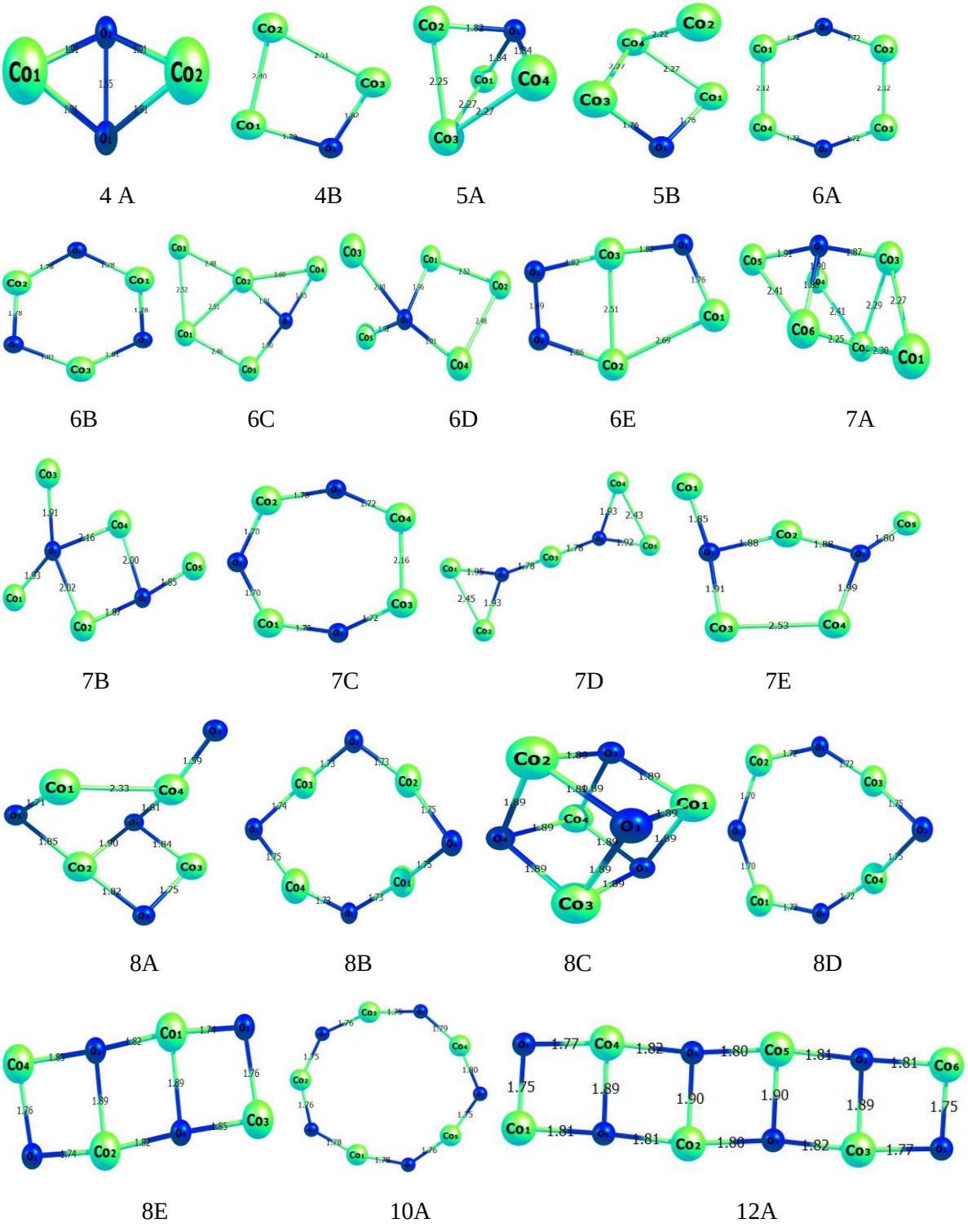

Figure 5.1: B3LYP/LANL2DZ geometrically optimized structures of Co_xO_y (x+y = 4-12) nanoclusters.

In spite of the previous investigations on CoO, it is significant to extend the knowledge about the structure, stability and electronic properties of these clusters for a better understanding of cluster reactivity and its role in sensing and catalysis.

Considering the above fact, it is intended to study the cobalt oxide nanoclusters Co_xO_y (x+y = 4-12), their structural stability and electronic properties by employing density functional theory, and to find the global and local minimum on potential energy surfaces (PES) for further improvement of clusters with modified properties. Moreover, to the best of our knowledge, the cobalt oxide nanoclusters Co_xO_y (x+y = 4-12) excluding (x+y = 11) clusters are explored for the first time within the formalism of density functional theory.

5.2 Computational Details

The geometry optimization, electronic property and structural stability calculations of Co_xO_y (x+y = 4-12) have been performed by a B3LYP method and LANL2DZ basis set within the density functional theory which consists of local and nonlocal relations without imposing any constraint as implemented in Gaussian 09 package [32-35]. Firstly, a number of possible structures for each Co_xO_y nanoclusters were constructed and then each geometrical structure was successfully optimized. Lowest energy for every structure was attained by reducing the atomic locations [36-37]. Some other software like Chemcraft is used for the visualization and analysis of the HOMO-LUMO energy gap [38].

5.3 Results and Discussion

5.3.1 Structure Stability of CoO Nanoclusters

This section mainly focused on the structural stability of Co_xO_y nanoclusters. For stability determination of CoO nanoclusters of different stoichiometry, binding energy (BE) of the nanoclusters have calculated by using the equation given below-

$$BE = [xE(Co) + yE(O) – E(Co_xO_y)]/ x+y \quad \text{…….5.1}$$

Where E(Co), E(O) are considered as the total energy of Co and O respectively, while $E(Co_xO_y)$ is the total energy of Co_xO_y nanocluster and x+y corresponds to the total number of Co and O atoms. Moreover, for exact determination of the binding energy of a system, the ZPE (zero point energy) is subtracted from the previously calculated binding energy values, which is then termed as final binding energy (FBE).

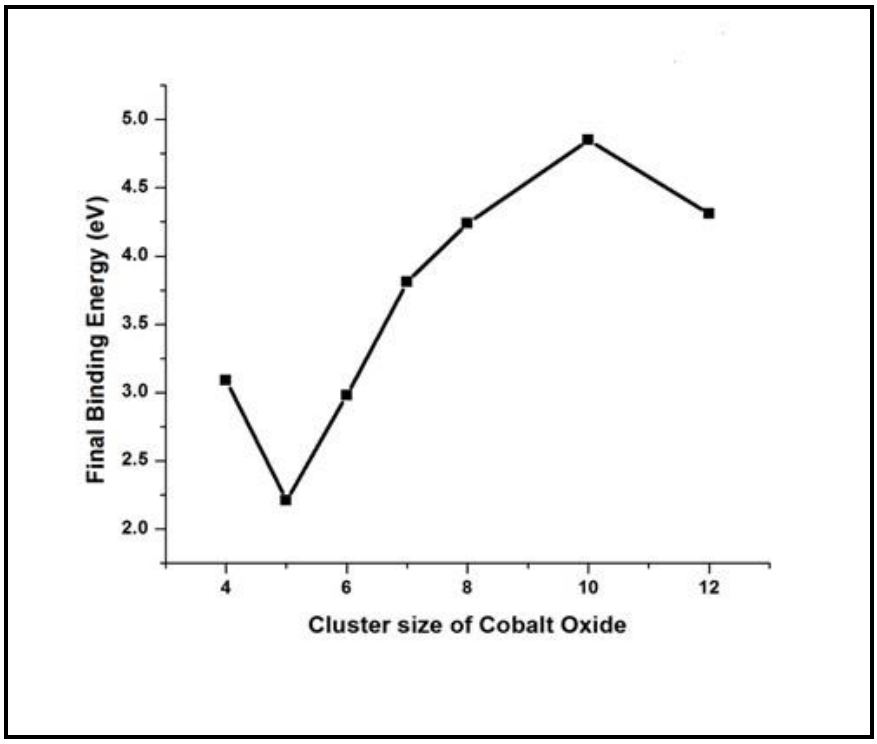

Figure 5.2: Graph between final binding energy and cluster size of Co_xO_y (x+y = 4-12) nanoclusters.

Table 5.1: Point group symmetry, spin multiplicity, final binding energy per atom (FBE), zero point energy (ZPE), dipole moment and HOMO-LUMO energy gap for all the configuration of Co_xO_y (x+y = 4-12) nanoclusters.

S.No.	Structure	Spin Multiplicity	Point Group	FBE per atom (eV)	HOMO-LUMO energy Gap (eV)	Dipole Moment (Debye)	Zero Point Energy (a.u.)
1.	CoO(4A)	Singlet	C_1	2.91	1.86	3.85	0.005
2.	**CoO(4B)**	**Doublet**	C_1	**3.09**	**2.43**	**3.78**	**0.004**
3.	CoO(5A)	Singlet	C_1	2.13	1.77	2.16	0.006
4.	**CoO(5B)**	**Singlet**	C_1	**2.21**	**2.58**	**3.62**	**0.006**
5.	CoO(6A)	Singlet	C1	2.81	2.25	0.005	0.009
6.	**CoO(6B)**	**Doublet**	C_1	**4.74**	**3.60**	**0.39**	**0.010**
7.	CoO(6C)	Doublet	C_1	2.98	1.83	0.61	0.005
8.	CoO(6D)	Doublet	C_1	2.94	1.85	0.71	0.005
9.	CoO(6E)	Doublet	C_1	4.17	2.35	6.47	0.008
10.	CoO(7A)	Singlet	C_1	1.79	1.65	0.62	0.008
11.	CoO(7B)	Doublet	C_1	3.70	2.08	0.76	0.008
12.	CoO(7C)	Singlet	C_1	3.57	2.11	1.31	0.012
13.	CoO(7D)	Doublet	C_1	3.60	2.06	0.51	0.008
14.	**CoO(7E)**	**Doublet**	C_1	**3.81**	**1.89**	**2.87**	**0.008**
15.	CoO(8A)	Singlet	C_1	4.18	2.57	2.28	0.015
16.	CoO(8B)	Singlet	C_1	3.92	2.13	2.48	0.015
17.	**CoO(8C)**	**Singlet**	C_1	**4.24**	**2.04**	**0.006**	**0.015**
18.	CoO (8D)	Singlet	C_1	4.19	2.18	2.77	0.015
19.	CoO(8E)	Singlet	C_1	4.14	1.73	0.03	0.016
20.	**CoO(10A)**	**Singlet**	C_1	**4.85**	**2.69**	**0.46**	**0.018**
21.	**CoO(12A)**	**Singlet**	C_1	**4.31**	**1.32**	**0.001**	**0.025**

Herein, we have used different labeling just for the sake of clarity in description. The calculated value of binding energy, HOMO-LUMO energy gap, spin multiplicity, point group symmetry and dipole moments of CoO nanoclusters are displayed in table 5.1. The optimized geometries of CoO nanoclusters and corresponding bond lengths are shown in figure 5.1. For the discussion of clusters properties and deviation of the chemical bond with the shape and size of the clusters, rigorous determination of equilibrium structures are much essential [36]. The Graph between binding energy of Co_xO_y and size of cobalt oxide nanoclusters is represented by figure 5.2. This section will present the equilibrium structures and stabilities of clusters.

Co_xO_y (x+y = 4): Firstly, those systems were considered, which contain four atoms in the nanocluster. Two types of geometries have been optimized, which are CoO (labeled as 4A) and CoO (labeled as 4B). As shown in figure 5.1, each has binding energy 2.91 eV and 3.09 eV, respectively. It may be seen the CoO (4B) nanocluster has greater final binding energy than 4A, therefore, it is expected to be a more stable configuration which can also be revealed from the table 5.1. The bond lengths between the Co and O are presented in figure 5.1, which ranges from 1.29 Å to 2.51 Å, whereas the dipole moment is found in the range of 3.78 to 3.85 Debye. The HOMO-LUMO energy band gap is 1.86 eV for CoO (4A) and 2.43 eV for CoO (4B). Here, the energy gap of CoO (4B) is greater than CoO (4A), which also confirms the relative stability of CoO (4B).

Co_xO_y (x+y = 5): For five atom cluster configuration, two types geometry of nanoclusters exists, namely as CoO (5A) and CoO (5B) which comprises four Co atoms and one O atom. From table 5.1, it is clear that CoO (5B) is more stable than CoO (5A) because the binding energy of CoO (5B) is slightly more than CoO (5A). In this case, the

bond length between the Co and the O is given in figure 5.1, ranges from 1.76 Å to 2.27 Å. The dipole moments are given as 2.16 Debye to 3.62 Debye for CoO (5A) and CoO (5B) configuration, respectively. Moreover, the HOMO-LUMO gap (1.77eV) for CoO (5A) and 2.58 eV for the CoO (5B) shows that the both the nanoclusters are in the range of semiconductor.

Co_xO_y (x+y = 6): For these structural types, five geometries have been considered which are given in figure 5.1. It is evident that the CoO (6B) configuration is more stable due to having a larger value of its binding energy (4.74 eV) than the other geometries for this configuration. The bond lengths exist between the ranges from 1.72 Å to 2.69 Å. In this configuration, the dipole moment is in the range of 0.005 Debye to 6.47 Debye as shown in table 5.1. HOMO-LUMO energy gap is different for each geometry in the range of 1.83 eV to 3.60 eV. This shows that CoO (6B) is a more stable configuration in this range. From the graph, it can be seen that the binding energy of the clusters in the size range from 4 to 5 drops sharply and shows a minima at n = 5, whereas for the sizes n > 5 the binding energy curve increases up to n = 10 and thereafter decreases slightly for n = 12. This is an indication of relative higher stability of the clusters as compared to configuration at n = 5. Out of all the configurations CoO (10A) is more stable amongst all the configurations because of its highest FBE.

5.3.2 Electronic Properties of CoO Nanoclusters

HOMO-LUMO energy gap of the molecules is a significant quantity that depends upon the chemical reaction between atoms and molecules and structural geometries [34, 35]. Our evaluated HOMO-LUMO energy gap for Co_xO_y (x+y = 4-12) clusters were shown in table 5.1. In order to get insights into the electronic properties, the graph

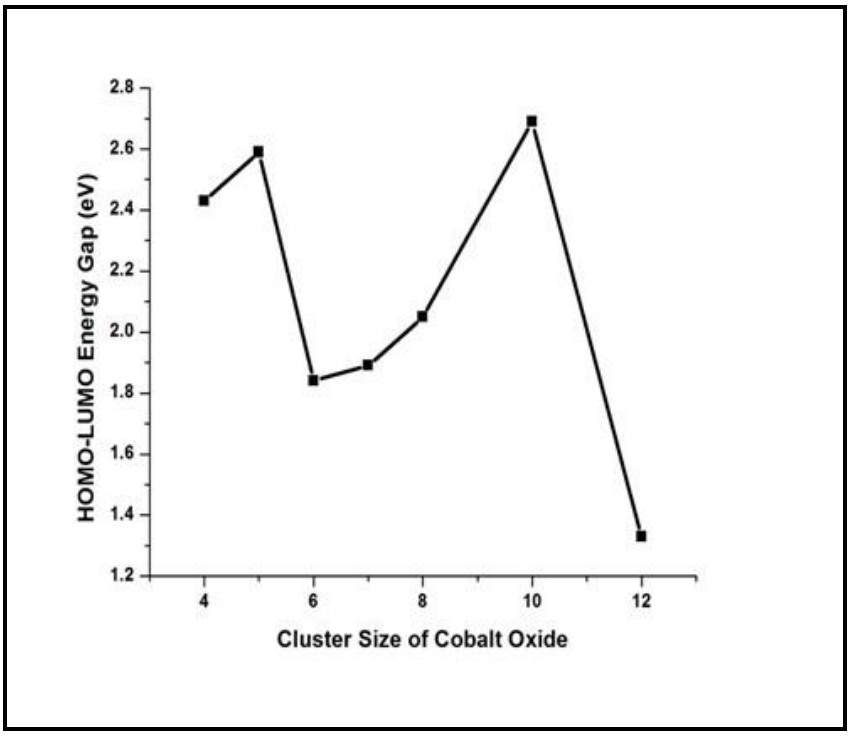

Figure 5.3: Graph between HOMO–LUMO energy gap and size of Co_xO_y (x+y = 4-12) nanoclusters.

between the HOMO-LUMO energy gap and clusters size for the most stable nanoclusters has been plotted in figure 5.3. A perusal of figure 5.3 reveals that the HOMO-LUMO energy gap increases from 4 to 5 no. of atoms and then it decreases from 5 to 6 no. of atoms, after that it further increases from 6 to 10 numbers of atoms and finally it decreases from 10 to 12 numbers of atoms. Zigzag behavior of HOMO-LUMO energy gap with the clusters size may be seen which means that the optimized nanoclusters show different HOMO-LUMO energy band gap for different geometries. The nanocluster for which HOMO-LUMO gap is smaller, does not require higher energy for the movement of electrons from one level to another level of energy, and the nanoclusters which have relatively higher HOMO-LUMO gap require more energy to go from one energy level to another. It means these nanoclusters are more stable than the other but their conductivity

decreases in comparison to those which have smaller energy band gap i.e., exhibiting lesser chemical reactivity. Conclusively, out of all the configurations CoO (10A) is more stable than other nanoclusters because of having a large band gap and highest FBE.

5.4 Conclusion

In the present chapter, properties of cobalt oxide nanoclusters such as the bond lengths, spin multiplicity, point group symmetry, binding energy, dipole moments and HOMO-LUMO energy gap have been calculated. It is observed that different configurations of cobalt oxide nanoclusters exhibit important chemical, physical and electronic properties which are very useful in the field of material science, nanotechnology etc. Our obtained results demonstrate that the presence of the best stable formations of different Co_xO_y nanoclusters depends on FBE and cluster morphology. The HOMO-LUMO energy gaps, as well as binding energy, are highest for CoO (10A). The smallest value of HOMO-LUMO energy band gap was obtained for CoO (12A) configuration which reveals that this structure having large band gap and FBE is more stable and requires sufficiently high energy for breaking it into their components. Moreover, the HOMO-LUMO energy band gap increases by adding the more number of atoms in the clusters. It is expected that our investigation on these properties will be helpful for the further study of such types of nanoclusters and also would aid the experimentalist for designing materials with new or improved applications.

References

[1] C. Lin, J. A. Ritter, B. N. Popov, J. Electrochem. Soc., 145, 4097 (1998).

[2] G. Wang, Y. Chen, K. Konstantinov, M. Lindsay, H. Liu, S. Dou, J. Power Sources 109, 142 (2002).

[3] V. E. Henrich, P. A. Cox, *The Surface Science of Metal Oxides*, (1994).

[4] G. A. Samorjai, *Introduction to Surface Chemistry and Catalysis*, (1994).

[5] P. A. Cox, *Transition Metal Oxides* (1992).

[6] C. N. Rao, B. Raveau, *Transition Metal Oxides* (1998).

[7] W. Eerenstein, N. D. Mathur, J. F. Scott, Nature, London, 442, 759 (2006).

[8] S. M. Borghei, F. Bakhtiyari, Acta Phys. Polon. A, 3, 131 (2017).

[9] N. T. Tung, N. M. Tam, M. T. Nguyen, P. Lievens, and E. Janssens, The Jour. of Chem. Phy., 141, 044311 (2014).

[10] E. L. Uzunova, G. S. Nikolov, H. Mikosch, J. Phys. Chem., A, 106, 4104 (2002).

[11] S.-S. Yi, X.-B. Zhang, B.-R. Wulan, J.-M. Yan, Q. Jiang, Energy Environ. Sci., 11, 3128 (2018).

[12] Q. Liu, L. C. Wang, M. Chen, Y. Cao, H. Y. He, K. N. Fan, J. Catal. 263, 104 (2009).

[13] G. V. Chertihin, A. Citra, L. Andrews, C. W. Bauschlicher, J. Phys. Chem., A, 101, 8793 (1997).

[14] E. Kapiloff, K. M. Ervin, J. Phys. Chem., A, 101, 8460 (1997).

[15] M. R. Castell, S. L. Dudarev, G. A. D. Briggs, A. P. Sutton, Phys. Rev., B, 59, 7342 (1999).

[16] M. A. Langell, M. D. Anderson, G. A. Carson, L. Peng, S. Smith, Phys. Rev., B, 59, 4791 (1999).

[17] G. L. Gutsev, B. K. Rao, P. Jena, J. Phys. Chem., A, 104, 5374 (2000).

[18] A. Pramann, K. Koyasu, A. Nakajima, K. Kaya, *J. Phys. Chem. A*, 106, 4891 (2002).

[19] B. C. Guo, K. P. Kerns, A. W. Castleman, *J. Phys. Chem.* 96, 6931 (1992).

[20] R. J. Van Zee, Y. M. Hamrick, S. Li, W. Weltner, *J. Phys. Chem.* 96, 7247 (1992).

[21] D. J. Clouthier, G. Huang, A. J. Merer, E. J. Friedman-Hill, *J. Chem. Phys.*, 99, 6336 (1993).

[22] M. Andersson, J. L. Persson, A. Rosen, J. Phys. Chem., 100, 12222 (1996).

[23] B. Nia, X. Wang, Chem. Sci., 7, 3978 (2016).

[24] K. P. Huber, G. Herzberg, Constants of Diatomic Molecules; van Nostrand Reinhold, New York, (1979).

[25] A. G. Adam, Y. Azuma, J. A. Barry, G. Huang, M. P. Lyne, A. Merer, Schroder, J. O. J. Chem. Phys., 86, 5231 (1987).

[26] Y. Xie, F. Dong, S. Heinbuch, J. J. Rocca, E. R. Bernstein, Phys. Chem. Chem. Phys., 12, 947 (2010).

[27] S. Yina, W. Xuea, X.-L. Dinga, W.-G. Wang, S.-G. He, M.-F. Ge, Inter. Jour. of Mas. Spectro., 281, 72 (2009).

[28] X. Shi, S. L. Bernasek, A. Selloni, J. Phys. Chem. C, 120, 14892 (2016).

[29] C. J. Dibble, S.T. Akin, S. Ard, C.P. Fowler, M.A. Duncan, J. Phys. Chem., A, 116, 5398 **(**2012).

[30] E. L. Uzunova, G. S. Nikolov, H. Mikosch, Chem. Phys. Chem., 5, 192 (2004).

[31] N. T. Tung, N. M. Tam, M. T. Nguyen, P. Lievens, E. Janssens, The Jour. of Chem. Phy., 141, 044311 (2014).

[32] M. J. Frisch, G. W. Trucks, H .B. Schlegel et al., Gaussian 09, Revision D, 01, Gaussian, Inc., Wallingford, Conn, USA, (2009).

[33] A. D. Becke, J. Chem. Phys., 104, 1040 (1996).

[34] C. Lee, W. Yang, R.G. Parr, Phys. ReV., B, 37, 785 (1988).

[35] B. Miehlich, A. Savin, H. Stoll, H. Preuss, Chem. Phys. Lett., 157, 200 (1989).

[36] R. Shastri, D. Kumar, S. P. Goutam, R. R. Yadav, A. K. Yadav, *Int. J. Adv. Res.*, 3, 787 (2015).

[37] R. Shastri, D. Kumar, D. Kumar, A. K. Yadav, Int. Adv. Res. J. Sci., Eng. Technol., 2, 95 (2015).

[38] Chemcraft 1.8, http://www.chemcraftprog.com

[39] D. Kumar, R. Shastri, D. Kumar, A. K. Yadav, Int. Adv. Res. J. Sci., Eng. Technol., 2, 102 (2015).

[40] R. Shastri, A. K. Yadav, D. Kumar, Eur. Phys. J. Plus, 132, 1 (2017).

Chapter-6

A Comparative Ab Initio Study on Structural Evolution, Stability and Electronic Properties of Undoped and Al-doped Ga_xN_y (x+y=4–25) Clusters

Chapter 6

A Comparative Ab Initio Study on Structural Evolution, Stability and Electronic Properties of Undoped and Al-doped Ga_xN_y (x+y = 4-25) Clusters

6.1 Introduction

The considerable effort has been dedicated on the understanding clusters and predicting the structures of single stable units, which can offer the possibility of developing nanodevices are keys to cluster physics in the last few decades. There is likelihood that a given number of atoms may have many possible structures which are rather close in energy, hence it is very important to evaluate the sensitivity of a given property on structural changes of the cluster. III group nitride based materials are the focal point of many experimental and theoretical studies in recent years because of their peculiar electronic, chemical, optical and biological properties [1-5]. Nevertheless, control over the size, structure, and composition of these nanostructured materials is still the most crucial challenge for the fundamental understanding and practical applications. Among the III group nitride, Gallium nitride (GaN) emerged as extensively studied material with interesting properties such as direct and wide band gap (3.4 eV), high breakdown voltage, thermal conductivity, melting point, and large bulk modulus [6-8] and with plentiful applications [9-13]. Further, with the evolution of nanoscience interest in the properties and capabilities of doped materials has been progressively increasing as doping can improve the photoelectric, electronic and magnetic properties [14-20]. Many authors have focused on the structures, energies, and thermodynamics of GaN clusters using different theoretical approaches. Akasaki et al. have reported that Mg is a simple p-

type doping element [21]. The structure, electronic properties, optical properties and magnetic resonance characteristics of GaN and the polarity reversal of GaN surfaces after Mg doping were investigated experimentally and theoretically [22-26]; and widening of band gap and the emission wavelength areas from the visible light to part of the ultraviolet region in Al-doped GaN film have been reported [27]. Lee et al., [28] studied Al-doped blende GaN compounds with different doping concentrations theoretically and found that the lattice constant linearly decreases with the increase in the doping concentration. Moreover, previous computational studies on ZnO and CdS [29, 30] suggest that the different nanostructures may be built by addition of stable cluster units or by the fragmentation of bulk material; structures achieved with the combining stable cluster units are significantly different and has more stability from the frameworks cut from their bulk structures. These studies motivated for a better understanding of the mechanism of undoped and Al-doped GaN clusters formation by stacking of subunits of a small cube, ring, and sheet; for which there have been no DFT studies so far. To this end, in this chapter, we are focused on how the individual cluster configurations can combine to form extended framework materials; also suitable models to describe and predict the changes of the cluster properties as a function of sizes, such as evolution from small to large clusters and shape. Unfortunately, synthesis of our predicted structures has no experimental evidence; however, this approach is consistent with published theoretical and experimental studies [31-35] on the creation of cluster-assembled materials. One of the specific examples is fulleride crystal comprising of C_{60} clusters as building blocks and the synthesis of III-V semiconducting clusters of the form $(XY)_n$ with mass spectra, where X represents metal or cations, and Y denotes anions [36] and recent experimental

investigation of gallium and nitride [37]. With this background of cluster, we have systematically explored geometric structures, electronic, vibrational properties and stability trend of undoped and doped $Ga_xAl_zN_y$ clusters using the ab initio method based on density functional theory. Additionally, ionization potential (IP), electron affinity (EA), HOMO-LUMO energy gap, the chemical potential (CP), chemical hardness (CH), and dipole moment (DM) have also been calculated.

6.2 Computational Methods

Conventional ab initio methods have been fully justified as a very powerful tool to complement the experiments and to help to a better understanding of unknown phenomena [38]. In this work, all computations have been carried out using first principle calculations within the framework of density functional theory as implemented in the Gaussian 09 program package [39]. For the most precise calculations, the gradient-corrected B3LYP functional form comprising of Becke's three-parameter hybrid exchange functional and Lee, Yang and Parr correlation functional was employed with a larger basis set Los Alamos double-ζ effective core potential LANL2DZ as the basic basis set [40, 41]. Gauss Sum 3.0 [42] and chemcraft [43] software were used for the evaluation of the density of states (DOS) and visualization of molecular orbitals. For the determination of ground and excited state structures of pure GaN clusters, we constructed many structures including small cube, ring, and rhombus; and for each structure, minimum energy is achieved by relaxing the atomic positions without any symmetry constraint. Also, due to spin polarization, each initial configuration was optimized at various possible spin multiplicities. Each structure was further assessed by frequency analysis at the same level of theory to explore for no imaginary frequency. For the

formation of assembled clusters, firstly stable isomers in small size are constructed which act as candidate structure for assembled clusters. Subsequently, different structures of assembled clusters of pure and Al-substituted GaN in two as well as in three dimensions; such as sheets and cube were achieved by sideways and linear stacking, respectively, of m (m = 2-16) stable units of rhombus $(Ga_2N_2)_m$, whereas rings were obtained by linear stacking of m (up to 3) subunits of ring $(Ga_4N_4)_m$. Here Al atoms are substituted at Ga sites and each structure were further optimized. The binding energies (BE) of GaN and Al-GaN clusters were calculated by the equation-

$$BE = [xE(Ga) + yE(N) - E(Ga_xN_y)]/(x+y)] \quad \ldots\ldots\ldots\ldots..\ldots 6.1$$

and

$$BE = [xE(Ga) + zE(Al) + yE(N) - E(Ga_xAl_zN_y)]/(x+z+y)] \quad \ldots 6.2$$

Where, E(Ga), E(N), $E(Ga_xN_y)$ and $E(Ga_xAl_zN_y)$ are the total energy of isolated atoms Ga, N and Ga_xN_y, $Ga_xAl_zN_y$ clusters, respectively, while (x+y) and (x+z+y) are the total numbers of Ga, N, and Ga, Al, N atoms, respectively. For further precise calculations, binding energies are corrected by the consideration of the zero point energy (ZPE). Accordingly, the stability of nanocluster has been considered eventually in terms of final binding energy (FBE). In all fully optimized structures, the convergence of the system energy is obtained up to 10^{-7} eV and the forces of 10^{-3} eV/Å on each atom are achieved.

6.3 Results and Discussion

6.3.1 Geometries and Stability of GaN and Al-substituted GaN clusters

The various optimized geometries of GaN and Al substituted GaN clusters, resulting due to the stacking of basic units of Ga_2N_2, along with the bond lengths are shown in figures 6.1, 6.2, respectively. In table 6.1 and 6.2, symmetries, spin

multiplicities, binding energy, final binding energy (FBE) and the HOMO-LUMO gap that computed are summarized. A perusal of figure 6.1 and table 6.1 reveals that the configuration of Ga_2N_2 corresponds to a symmetric triplet state rhombus geometry in which nitrogen atoms lie opposite to each other at a distance 1.922 Å from Ga atoms. For Ga_4N_4, two different structures, namely, cube-I and planar ring-I are obtained, the most stable structure is the ring form. These structures are similar to the structures proposed by Belbruno et al., [44] Song et al., [45] and Kandalam et al., [46]. Calculated bond lengths for all clusters that range between 1.78 Å to 2.20 Å are comparable to results (1.88Å - 2.06 Å) reported by E. Pournamdari et al., for cube-I [24]. In case of cube-I configuration, predicted Ga-N bond length (2.057 Å) is also in good agreement with previous results of BelBruno et al. (2.032 Å) [44], Song Bin et al., (2.027 Å, 2.048 Å, and 1.926 Å) [45] and Kandalam et al., (2.31 Å and 2.53 Å) [46]. L. Hedin et al. reported that in bulk stoichiometric GaN, the distance between Ga and N is 1.94 Å [47], which is slightly lower than the bond length calculated by us; hence it may be considered that the nature of these Ga-N bonds is similar to the bulk Ga-N bonds. Now, we focus on stacking of starting structures rhombus, cube and ring. For Ga_6N_6, a double cube structure was found, which can be viewed to consist of linear stacking of two layers, namely, a cube formed with Ga_4N_4 and Ga_2N_2. On further stacking of an extra layer of Ga_2N_2 to this structure, an analogous structure cube like nanotube was preferred for Ga_8N_8. It seems that optimized structures are a mere extension of subunit Ga_4N_4. On the other hand, it is noted that the trend is quite different for tube-like structures; Ga_4N_4 octagonal ring stacked on top of each other transform from a planar structure to a tubular configuration. Further stacking of one more planar ring structure to preceding geometry undergoes

similar geometry again. We then considered the sideways stacking of rhombus (4x3), our result predicts the formation of the Ga_6N_6 sheet geometry. On further increasing of subunits up to (4x4), the system continues to maintain the original stable configuration of the sheet. However, for sideways stacking of subunits (5x4), the cluster favors curved geometry, which offers the possibility to obtain nanotube from a sheet of GaN. Here, it is worth mentioning that in all the configurations of GaN cluster, atoms Ga and N are linked to each other in an alternating fashion. An explanation for the preference for the metal-nitrogen bond instead of metal-metal bond or N-N bond could be the existence of the lone pair as only three electrons of pentavalent nitrogen atoms participate in bonding with Ga atom. In order to lower repulsive interaction between the lone-pair electrons, nitrogen atoms tend to sit away from each other. Moreover, rings and rhombus display high-order symmetry, while all other along with stacked configurations possess lower symmetries. This is a natural consequence of their structural types. Also, the appearance of maximum atoms on the surface sites in the above clusters give rise to less surface strain and thereby offering the better probability of doping. A perusal of figure 6.2 reveals that geometry of each Al-substituted GaN cluster keeps the structure similar to the corresponding pure GaN clusters with a slight tilt in cubes. The bond lengths of the Al-N and GaN in Al substituted GaN lies between the 1.76 Å to 1.93 Å and 1.77 Å to 1.98 Å respectively which is in good agreement with the experimental data observed for Al-N (1.90 Å) and Ga-N (1.94 Å) [48]. For each cluster, Al atoms tend to occupy the sites on the peripherals of the clusters, whereas in the planar sheet structures, some of the Al atoms show a tendency to go inside the cluster. The bond length of structures are similar to the bare

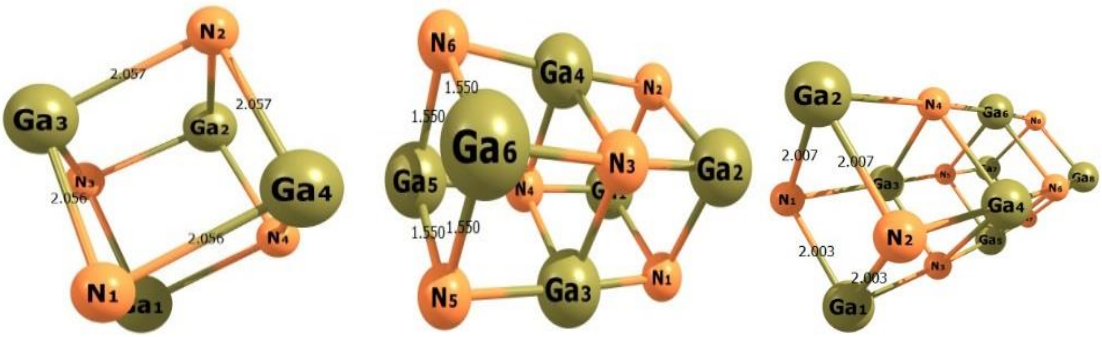

Cube I Cube II Cube III

(a) Structural pattern of cubic GaN clusters.

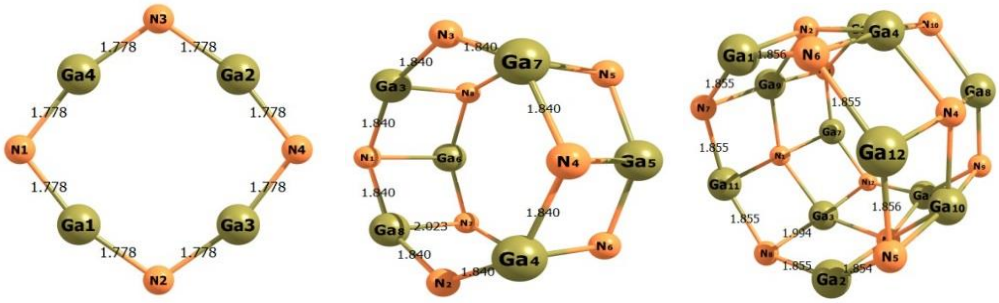

Ring I Ring II Ring III

(b) Structural pattern of ring GaN clusters.

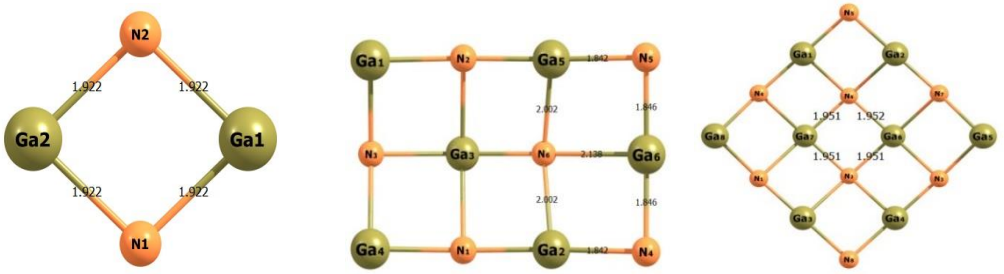

Rhombus Sheet I Sheet II

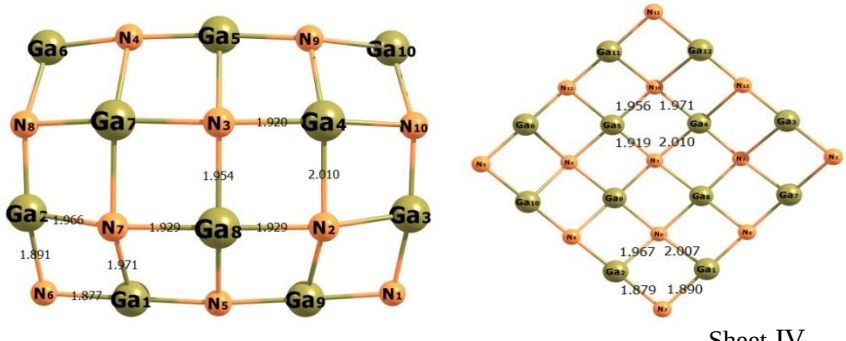

Sheet III Sheet IV

(c) Structural pattern of rhombus GaN clusters

Figure 6.1: B3LYP/LANL2DZ Geometrically optimized structures of GaN Clusters.

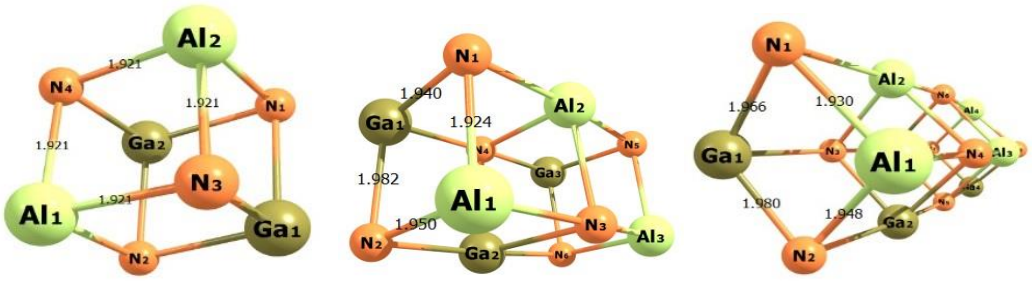

Al-Cube I Al-Cube II Al-Cube III

(d) Structural pattern of cubic Al-doped GaN clusters.

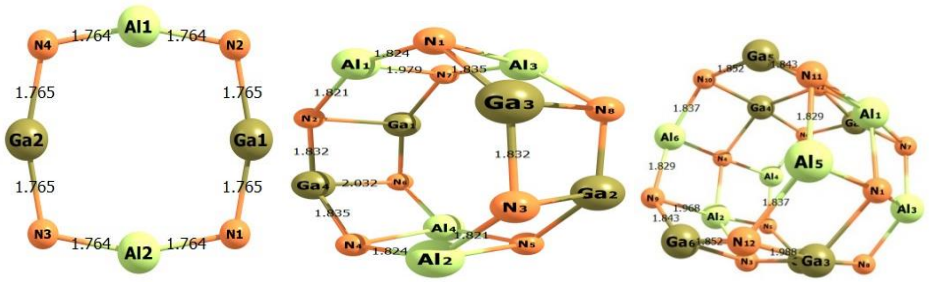

Al-Ring I Al-Ring II Al-Ring III

(e) Structural pattern of ring Al-doped GaN clusters.

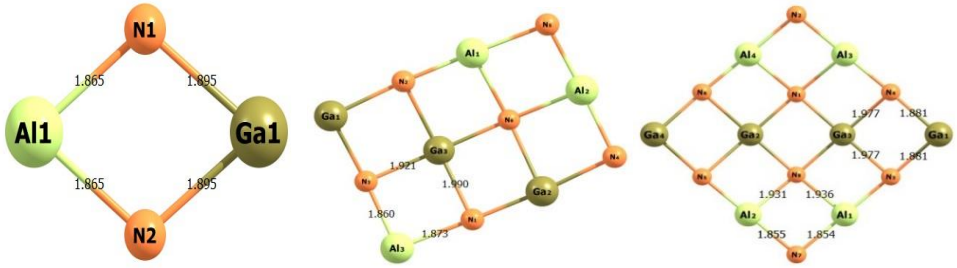

Al-Rhombus Al-Sheet I Al-Sheet II

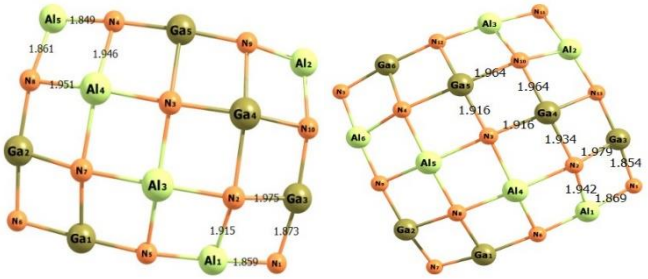

Al_Sheet III Al-Sheet IV

(f) Structural pattern of rhombus Al-doped GaN clusters.

Figure 6.2: B3LYP/LANL2DZ geometrically optimized structures of Al-doped GaN clusters.

Table 6.1: Symmetry, multiplicity of the ground state (GS), binding energy per atom (BE), zero point energy (ZPE), final binding energy (FBE) and HOMO-LUMO gap for all configuration of GaN clusters.

Structures	Configuration	No. of Atom	Symmetry	Multiplicity	BE (eV)	ZEP (eV)	FBE (eV)	HOMO-LUMO Energy Gap (eV)
Ga_4N_4	Cube1	8	C_1	1	3.64	0.42	3.22	1.21
Ga_6N_6	Cube2	12	C_1	3	4.75	0.67	4.08	3.35
Ga_8N_8	Cube3	16	C_1	5	5.00	0.94	4.06	1.77
Ga_4N_4	Ring1	8	D_2H	1	4.10	0.43	3.67	2.09
Ga_8N_8	Ring2	16	C_1	1	4.66	1.07	3.59	1.61
$Ga_{12}N_{12}$	Ring3	24	C_1	1	4.90	1.64	3.26	2.12
Ga_2N_2	Rhombus	4	D_2H	3	3.96	0.15	3.81	5.10
Ga_6N_6	Sheet(4*3)	12	C_1	1	4.02	0.67	3.35	0.95
Ga_8N_8	Sheet (4*4)	16	C_1	3	4.87	0.94	3.93	1.08
$Ga_{10}N_{10}$	Sheet(5*4)	20	C_1	1	4.46	1.29	3.17	2.09
$Ga_{12}N_{13}$	Sheet(5*5)	25	C_1	4	5.02	1.58	3.44	6.02

Table 6.2: Symmetry, Multiplicity of the ground state (GS), Binding energy per atom (BE), Zero point energy (ZPE), Final binding energy (FBE) and HOMO-LUMO gap for all configuration of Al-substituted GaN clusters.

Structures	Configuration	No. of Atom	Symmetry	Multiplicity	BE (eV)	ZEP (eV)	FBE (eV)	HOMO-LUMO Energy Gap (eV)
$Ga_2Al_2N_4$	Al_Cube1	8	C_1	1	3.84	0.47	3.37	1.23
$Ga_3Al_3N_6$	Al_Cube2	12	C_1	3	4.81	0.77	4.04	1.39
$Ga_4Al_4N_8$	Al_Cube3	16	C_1	3	5.00	1.10	3.90	0.91
$Ga_2Al_2N_4$	Al_Ring1	8	D_{2H}	1	4.10	0.48	3.62	2.54
$Ga_4Al_4N_8$	Al_Ring2	16	C_1	1	4.66	1.20	3.46	2.58
$Ga_6Al_6N_{12}$	Al_Ring3	24	C_1	1	4.90	1.84	3.06	2.87
$Ga_1Al_1N_2$	Al_Rhombus	4	C_S	1	3.25	0.17	3.08	1.48
$Ga_3Al_3N_6$	Al_Sheet(4*3)	12	C_1	3	4.81	1.10	3.71	1.68
$Ga_4Al_4N_8$	Al_Sheet (4*4)	16	C_1	3	5.04	1.10	3.94	2.18
$Ga_5Al_5N_{10}$	Al_Sheet(5*4)	20	C_1	1	4.66	1.42	3.24	2.16
$Ga_6Al_6N_{13}$	Al_Sheet(5*5)	25	C_1	4	5.13	1.80	3.33	1.65

GaN clusters with slight deviation; indicating that the bonding characteristics remain the same in the doped clusters [44, 46]. The slight deviation in bond lengths may be attributed to the difference in atomic radius and electronegativity of the atoms. From table 6.1, it is noticed that except of Al-doped ring I and rhombus, the geometry of the clusters have C_1 point group symmetry, which indicates that the substitution of Al atoms to the bare cluster does not induce considerable change in configurational symmetry of most of the structures analyzed, except for ring-I (D_{2h}) and rhombus geometries (C_S). We now turn our attention to the stability of the clusters. The value of final binding energy as shown in figure 3, rises monotonically with increasing size of cubic clusters; the maximum increase is in cube-II signifies particular stability of cube-II, note that the energy difference between the structures is small. Quite a similar trend is observed for doped cubic cluster and is maximum of 4.04 eV for cube-II. Thus, the stability of cubes increases with size and with increasing aluminum content, except for Al-doped cube-III. Unlike cubes, there is a decrease in final binding energy with the size for the ring configurations of doped and undoped clusters; this decrease in the energy may be viewed as an attempt by stacked GaN clusters to transform from the planar configurations to favor tubular structures with the increase in the cluster size. In particular, a planar ring-I structure with maximum FBE (3.67 eV) is found to be the most stable which slightly greater than 3.03 eV [49] and 3.16 eV [46]. The binding energy in the case of GaN cube-I and cube-II are 3.22 eV and 4.08 eV having good agreement with the 3.36 eV and 3.66 eV [49, 46] respectively. The energies calculated for the set of rhombus and sheet configurations namely, I, II, III, and IV of Al-doped and undoped GaN clusters do not follow the above trend, and FBE varies sharply as oscillatory humps or dips. Particular

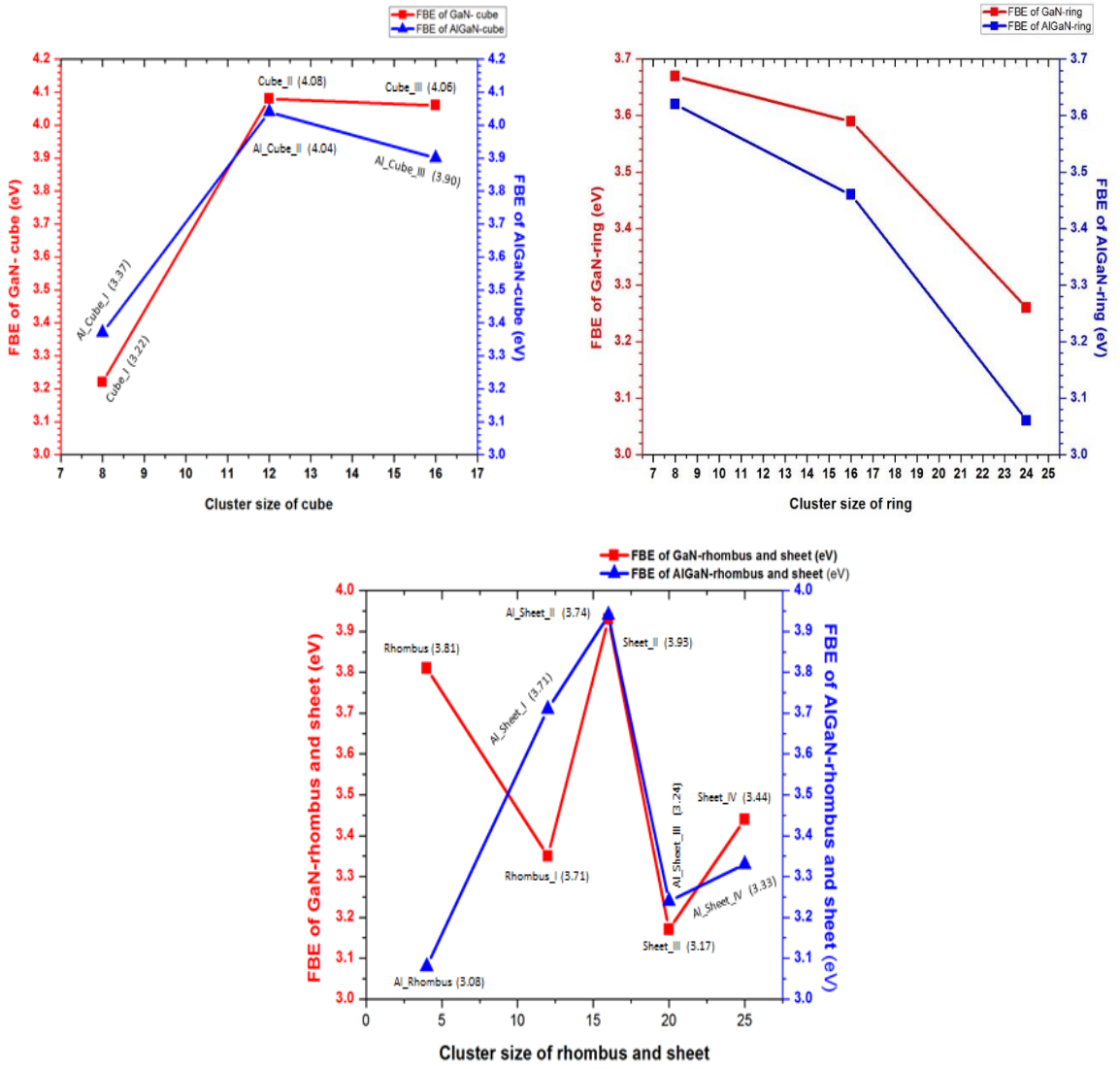

Figure 6.3: Variation of final binding energy (FBE) per atom with cluster size of GaN and Al-GaN clusters.

humps for a specific size of clusters imply their stabilities relative to neighboring clusters. Al-doped sheet configurations are relatively more stable than the pure one due to their more binding energy. Further, the FBE curves show that the binding energies of most of the Al-doped GaN clusters are lower than those of the pure GaN clusters [44, 46]. Indeed, for all compositions and size of clusters, the GaN cube-II is the most stable structural type; the final binding energy for other possible cluster types are lower than that for the GaN cube-II. From the above discussion, it is obvious that for all clusters, even the

numbers of atoms are same, FBE varies with the stacking mode of basic units and either enhancing the number of atoms or increasing Al content. Also because of open configurations of nanoclusters, properties are prominently affected by large surface effects.

6.3.2 Electronic Properties of Al-Substituted GaN Clusters

The electronic properties of undoped and Al-GaN clusters are deliberated in terms of highest occupied molecular orbital (HOMO) and lowest unoccupied molecular orbital (LUMO). The energy gap between HOMO and LUMO is a significant quantity as most

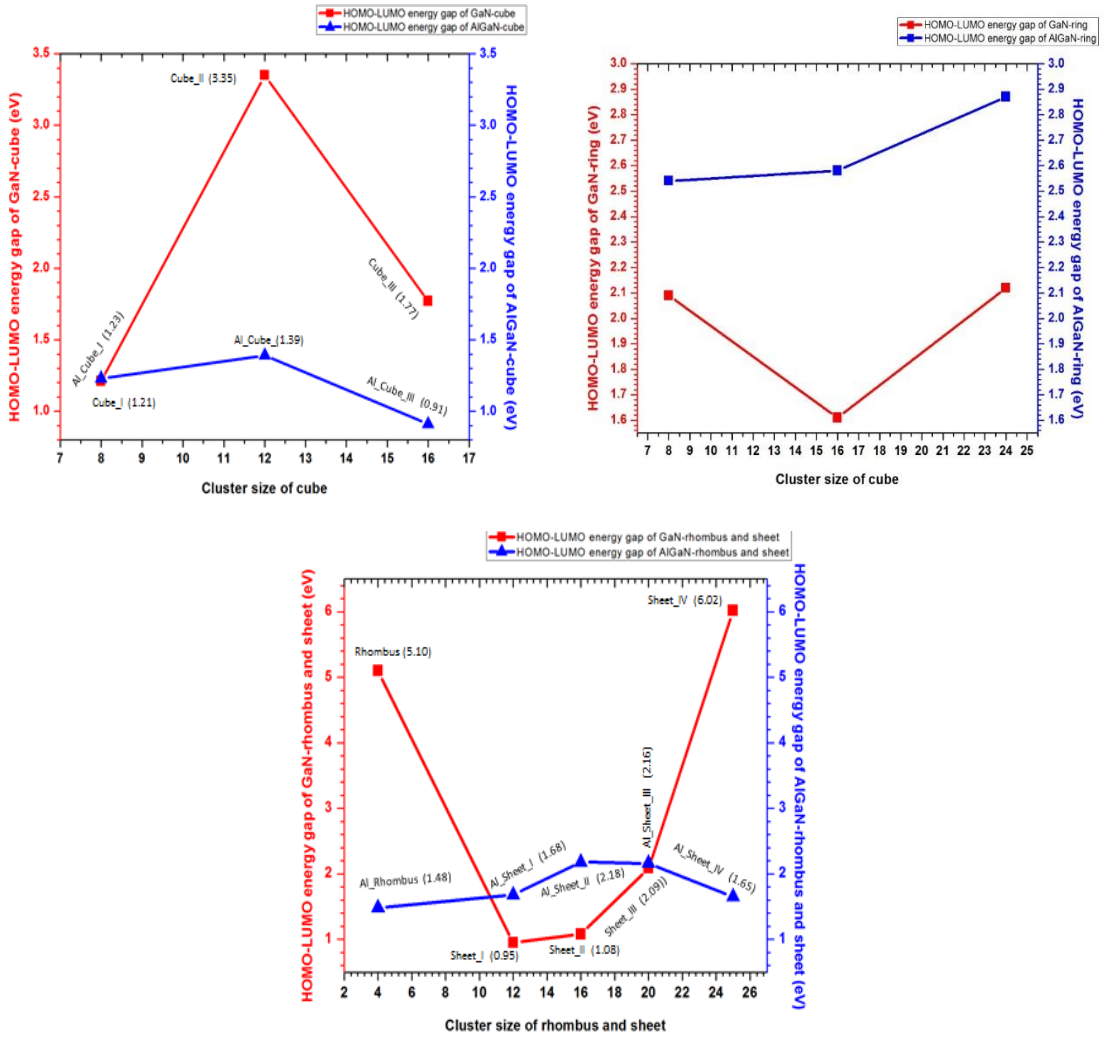

Figure 6.4: Variation of the HOMO-LUMO gap with cluster size of GaN and Al-GaN clusters.

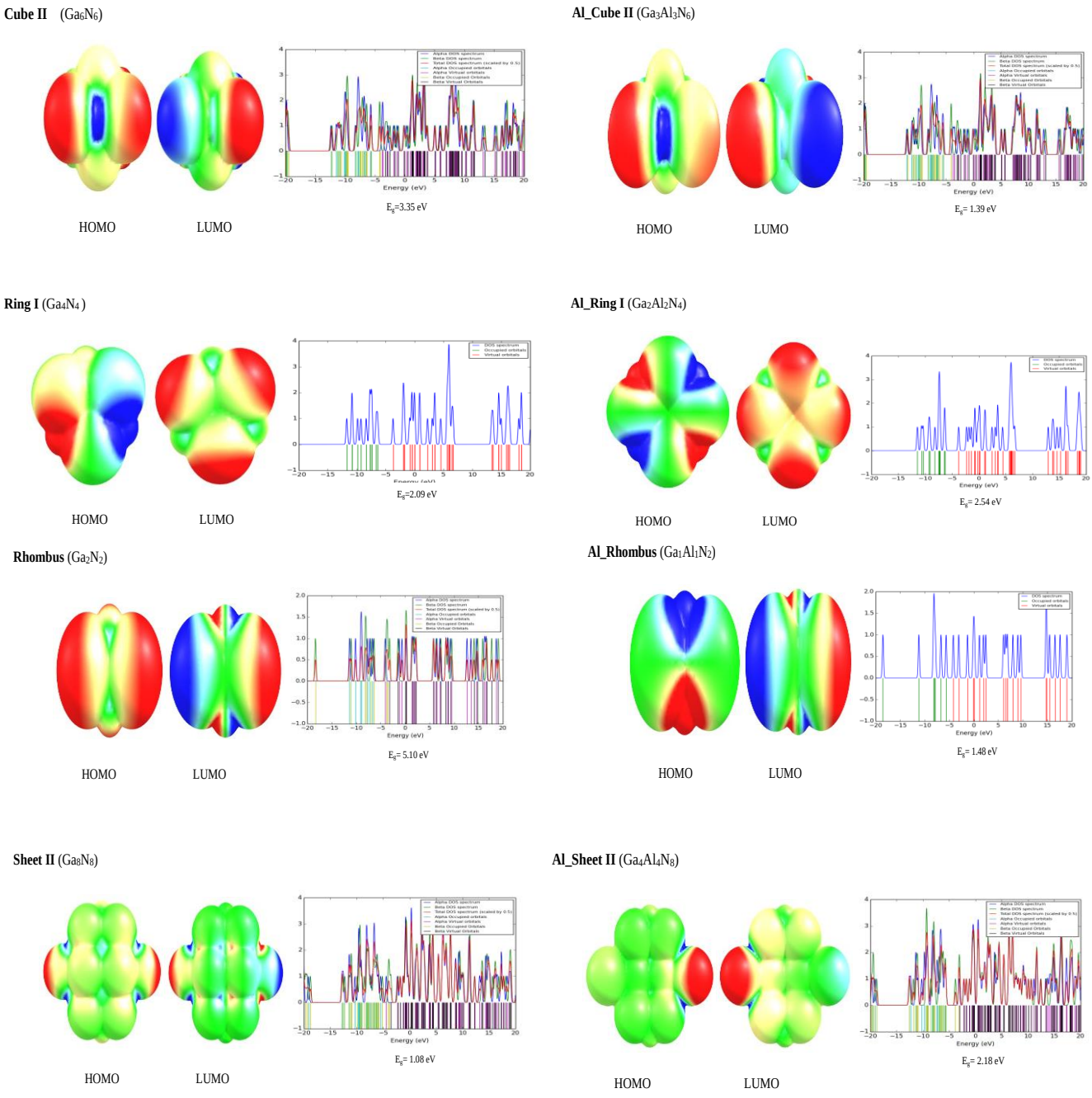

Figure 6.5: DOS, HOMO-LUMO energy diagram for most stable configurations of the cube, ring, rhombus, and sheet of GaN and Al-GaN clusters.

of a material's behavior, such as intrinsic conductivity, optical transitions, or electronic transitions, depend on it. Also, it indicates the ability of electrons to jump from occupied orbital to unoccupied orbital. The calculated values of HOMO-LUMO energy gaps of pure GaN and Al-GaN clusters are shown in table 6.1, 6.2, and the size dependence of

HOMO-LUMO energy gap diagram and DOS for most stable configurations in cube, ring, rhombus and sheet structures are depicted in figure 6.4, 6.5. Table 6.1, 6.2 shows that the magnitude of the gaps for undoped and doped clusters varies from 0.95 to 6.02 eV, 0.91-2.87 eV, respectively and some of these clusters yet exhibit semiconducting properties as for bulk the band gap of GaN is 3.43 eV [50-53]. It is found that the HOMO-LUMO gaps of doped GaN present a similar trend as observed for corresponding pure GaN clusters except for sheet structures (figure 6.4). HOMO-LUMO gap modified greatly in ring structures after the doping as compared to corresponding undoped structure, while it is reduced in cube structures. Also, their relative differences for rings are smaller than the cubes. The HOMO-LUMO gap for GaN ring-I, Cube-I, and Cube-II are 2.09 eV , 1.21 eV, and 3.35 eV respectively, which is close to published result for ring-I 1.67 eV [46], 1.68 eV [49], 2.41 eV [45], cube-I 0.82 eV [49] and cube-II 1.70 eV [49], 2.60 eV [46]. For sheet-like structures, on the other hand, it shows the zigzag behavior with the clusters size. The minimum value of HOMO-LUMO gap is observed for the Al-cube-III (0.91 eV) structure and maximum for the Al-ring-III (2.87 eV). The higher bandgap restricts the movement of an electron from HOMO to LUMO, which will not robustly take part in electrical conduction and chemical reaction. In other words, these clusters presumably have lower chemical stabilities. The clusters having the minimum value of energy gap expected to be more reactive than large energy gap; thus doping in nanocluster could be more advantageous. Figure 6.5 reveals that in both cases, some of the GaN and Al substituted GaN clusters exhibit alpha and a beta band of energy due to the spin of electrons. The study of the higher atomic structure of GaN and Al-GaN clusters reveal the better location of charge near the Fermi level. The proximity of charge

near Fermi level with small HOMO-LUMO gap will enable easier movement of electrons to the valence band. Furthermore, it should be noted that more states are seen in the virtual orbital that may be caused by the introduction of the atom which gives rise to the localization of charge in the virtual orbital.

6.3.3 Ionization Potential and Electron Affinity of Al-doped GaN Clusters

The Ionization potential (IP) is defined as the amount of energy needed to take out one electron from the cluster while the electron affinity (EA) is the amount of energy evolved when an electron is attached to the cluster [54]. The value of ionization potential (IP) and electron affinity (EA) have evaluated, by taking the energy difference between a neutral cluster and cation/anion, respectively as below-

$$IP = \text{Energy of neutral cluster} \sim \text{Energy of cation cluster} \quad \ldots..6.3$$

and the electron affinity -

$$EA = \text{Energy of neutral cluster} \sim \text{Energy of anion cluster} \quad \ldots6.4$$

The variation of IPs and EAs as a function of cluster size [55, 56] for different clusters of GaN and Al-GaN are reported in figure 6.6, and the corresponding data are listed in table 6.3. As can be seen in table 6.3, the structural relaxation upon ionization leads to lowering the IP values. Among GaN cubes and rings, the maximum value of adiabatic (vertical) IP is 8.01(8.11) eV for the ring-I configuration, and the minimum value is 6.01(6.88) eV for cube-I which is very close to vertical IP 8.09 and 7.62 eV [49] respectively. For EA, the higher value is 3.78(3.40) eV close to vertical EA 3.08 eV [49], and the lower value is 1.28(0.77) eV for cube-I and ring-II respectively for bulk it is 3.1 eV [52]. Likewise, in the case of Al-GaN cube and ring configurations, the maximum and minimum IPs 10.18 eV (10.33 eV) and 6.29 eV (6.49 eV) may be seen for Al-GaN ring-I

Table 6.3: Adiabatic, vertical ionization potential (IP) and electron affinity (EA) in eV for all the configurations of GaN and Al-GaN clusters.

Structures	Configuration	Ionization Potential(IP)		Electron Affinity(EA)	
		Adiabatic(eV)	Vertical(eV)	Adiabatic(eV)	Vertical(eV)
Ga_4N_4	Cube1	6.01	6.88	3.78	3.40
Ga_6N_{12}	Cube2	6.83	7.23	2.99	2.92
Ga_8N_8	Cube3	6.37	6.68	2.82	2.80
$Ga_2Al_2N_4$	Al_Cube1	6.38	6.87	3.35	3.23
$Ga_3Al_3N_6$	Al_Cube2	6.84	7.14	4.15	2.67
$Ga_4Al_4N_8$	Al_Cube3	6.29	6.49	3.35	2.55
Ga_4N_4	Ring1	8.01	8.11	2.29	2.11
Ga_8N_8	Ring2	7.34	7.49	1.28	0.77
$Ga_{12}N_{12}$	Ring3	7.05	7.20	2.14	0.84
$Ga_2Al_2N_4$	Al_Ring1	10.18	10.33	2.31	2.20
$Ga_4Al_4N_8$	Al_Ring2	8.34	8.68	2.16	2.09
$Ga_6Al_6N_{12}$	Al_Ring3	8.74	9.46	1.86	1.80
Ga_2N_2	Rhombus	7.81	11.02	2.08	0.94
$Ga_1Al_1N_2$	Al_ Rhombus	7.09	10.19	2.24	1.51
Ga_6N_6	Sheet(4*3)	6.09	6.48	3.83	3.35
Ga_8N_8	Sheet (4*4)	6.33	7.16	3.46	2.72
$Ga_{10}N_{10}$	Sheet(5*4)	8.28	9.81	1.43	0.37
$Ga_{12}N_{13}$	Sheet(5*5)	5.98	7.75	5.76	2.86
$Ga_3Al_3N_6$	Al_Sheet(4*3)	6.64	6.87	2.96	2.62
$Ga_4Al_4N_8$	Al_Sheet (4*4)	6.37	6.57	3.10	2.49
$Ga_5Al_5N_{10}$	Al_Sheet(5*4)	6.01	8.14	2.85	1.06
$Ga_6Al_6N_{13}$	Al_Sheet(5*5)	5.77	6.28	3.17	1.87

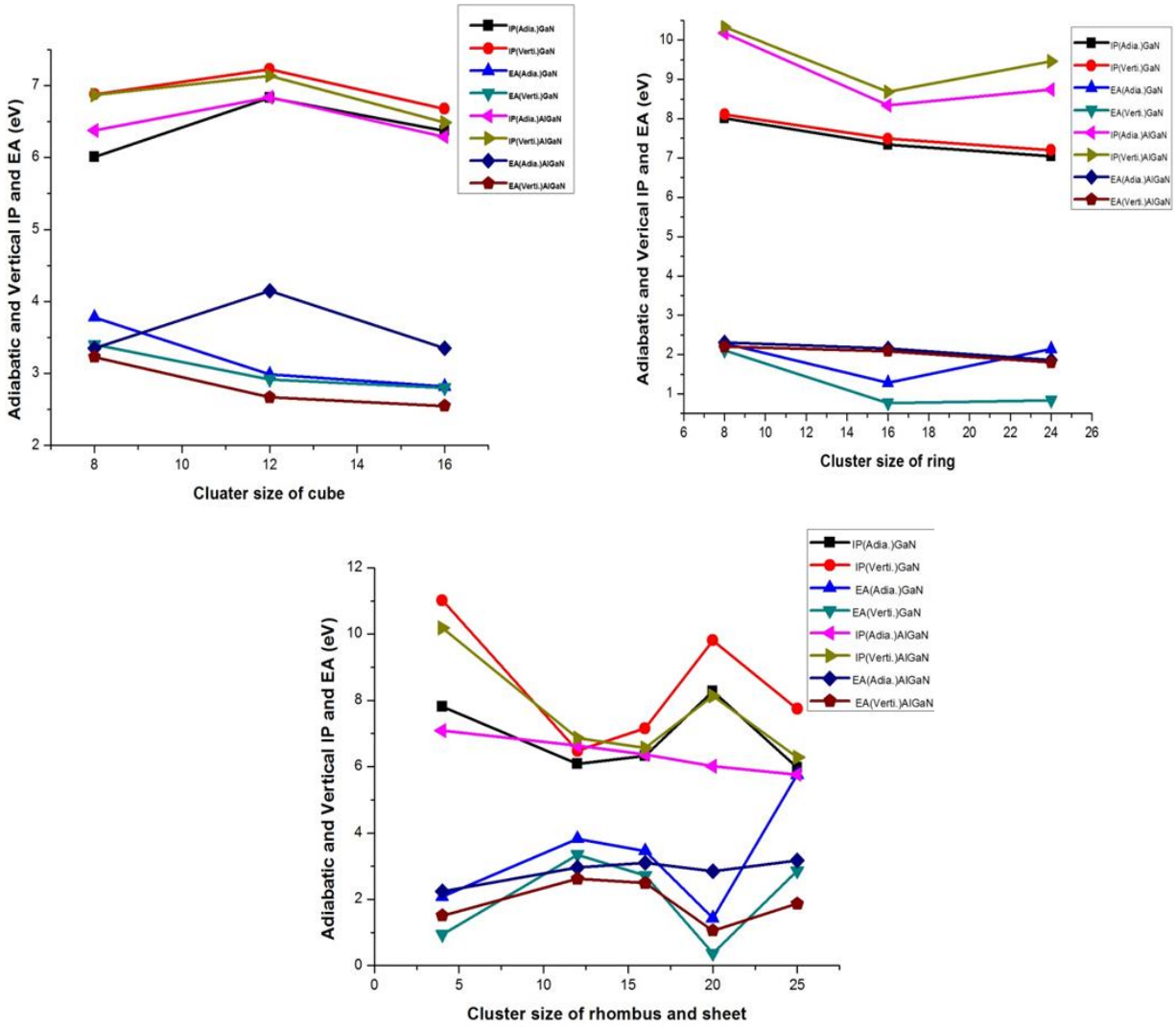

Figure 6.6: Variation of adiabatic, vertical IP and EA with cluster size of GaN and Al-GaN clusters.

and Al-cube-III respectively, whereas the maximum and minimum value of EA are computed to be 4.15(2.67) eV and 1.86(1.80) eV for Al- cube-II and Al-ring-III, respectively. Thus, overall, $Ga_{12}N_{13}$ and $Ga_6Al_6N_{13}$ sheet configuration tends to ionize relatively easier than the other clusters. Moreover, the IP cluster values are much smaller than the IP values of the N atom (14.54 eV) and the N_2 molecule (15.45 eV, experimental value 15.58 eV) [57-59]. Thus, the results further support the association of the ionized

electron to the metallic atoms in the considered nitride clusters. It is noteworthy that replacing Ga atoms in GaN cluster with Al, to give Al-doped clusters, results in the approximate values of VIPs for most clusters except for $Ga_2Al_2N_4$ and $Ga_6Al_6N_{12}$, which have larger VIPs than the corresponding GaN clusters; whereas the $Ga_5Al_5N_{10}$ and$Ga_6Al_6N_{13}$ have smaller VIPs than the corresponding GaN clusters. Figure 6.6 indicates that IPs and EAs of different GaN ring and cube structures vary arbitrarily with increasing the number of the atom. In the case of GaN cube and ring structures, increasing the number of atoms results in a gradual decrease in the IP values. For Al-GaN clusters, the observed maximum adiabatic (vertical) IP for Al-GaN ring-I which is 10.18(10.18) eV, having a number of atoms 8 and the minimum IP is observed as GaN 6.01(6.88) eV having the same number of atoms. The increase in Al atom causes the lower in energy due to the geometry position of atoms. The tendency of IP for GaN and Al-GaN cube and ring clusters possess a zigzag behavior. Among the pure GaN rhombus and sheet configurations, Ga_2N_2 seems to be a magic number cluster with relatively high stability, which is confirmed by its high HOMO-LUMO gap (5.10 eV) and high IP (11.02 eV), as well as low EA (0.94 eV). The high value of EA indicates that the clusters have an active contribution to chemical reactions. Among pure and Al-GaN clusters, Al-GaN cube-II clusters have a high value of EA (4.15 eV), and hence it will be more reactive among all the configurations of GaN; thus Al substituted cubic cluster is suitable for chemical sensors. For the sheets, the maximum and minimum value of adiabatic (vertical) are 5.76(2.86) eV and 1.43(0.37) eV respectively, reflects that GaN sheet IV is also more reactive. On the basis of EA values, it is predicted that structures of ring-II and sheet-III owing to low-value of EA, are an unfavorable structure for chemical sensors.

6.3.4 Chemical Potential and Chemical Hardness of GaN and Al Substituted GaN Clusters

Another useful quantity is the chemical potential and chemical hardness which are computed by using formula as below-

Chemical potential =

- [(Value of Ionization Potential (IP) + value of Electron Affinity (EA)]/ 2 …6.5

and

Chemical hardness =

[(Value of Ionization Potential (IP) - value of Electron Affinity (EA)]/ 2 ….6.6

Chemical hardness has been established as an electronic quantity which is in many cases may be used to characterize the relative stability of molecules and aggregate through the principle of a maximum of hardness. Figure 6.7 shows the variation of chemical potential (CP) chemical hardness (CH) and dipole moment (DP) with a cluster size of cube, ring, rhombus and sheet structures of GaN and Al-GaN. From the above figure 6.7, it is observed that maximum chemical potential for pure GaN cube and ring clusters is 5.13. eV for ring-I, which has 8 atoms and the minimum value is 4.23 eV having 16 atoms for ring-I and ring-II clusters; while in the case of Al-GaN ring and cube clusters higher (6.26 eV) and lower value (4.67 eV) for Al-cube-II, Al-cube-III respectively is seen. On the other hand in case of GaN cube and ring configuration, the maximum and minimum values of chemical hardness are 3.06 eV and 1.86 eV for ring-II and cube-III having 16 atoms. For Al-GaN clusters, cube and ring configurations have the maximum and minimum values of chemical hardness 4 eV and 1.72 eV, respectively for Al-ring-I and Al-cube-III configurations; the highest and lowest value of chemical potential and

Table 6.4: Chemical potential (CP), chemical hardness (CH) and dipole moment (DP) for all the configurations of GaN and Al-GaN clusters.

Structures	Configuration	Chemical Potential (eV)	Chemical Hardness (eV)	Dipole Moment (Debye)
Ga_4N_4	Cube1	5.02	2.85	0.56
Ga_6N_{12}	Cube2	5.00	2.04	1.67
Ga_8N_8	Cube3	4.65	1.86	0.05
$Ga_2Al_2N_4$	Al_Cube1	4.96	1.67	0.01
$Ga_3Al_3N_6$	Al_Cube2	5.20	1.79	1.57
$Ga_4Al_4N_8$	Al_Cube3	4.67	1.72	0.35
Ga_4N_4	Ring1	5.13	2.93	0.00
Ga_8N_8	Ring2	4.23	3.06	0.05
$Ga_{12}N_{12}$	Ring3	4.31	2.82	0.00
$Ga_2Al_2N_4$	Al_Ring1	6.26	4	0.00
$Ga_4Al_4N_8$	Al_Ring2	5.32	3.19	0.00
$Ga_6Al_6N_{12}$	Al_Ring3	5.17	3.64	0.00
Ga_2N_2	Rhombus	5.47	4.00	0.00
$Ga_1Al_1N_2$	Al_ Rhombus	5.26	3.39	0.50
Ga_6N_6	Sheet(4*3)	4.94	1.35	7.21
Ga_8N_8	Sheet (4*4)	4.92	1.83	1.13
$Ga_{10}N_{10}$	Sheet(5*4)	4.96	4.06	7.99
$Ga_{12}N_{13}$	Sheet(5*5)	5.59	1.28	6.10
$Ga_3Al_3N_6$	Al_Sheet(4*3)	4.78	1.99	0.86
$Ga_4Al_4N_8$	Al_Sheet (4*4)	4.64	1.84	0.32
$Ga_5Al_5N_{10}$	Al_Sheet(5*4)	4.52	2.56	0.78
$Ga_6Al_6N_{13}$	Al_Sheet(5*5)	4.28	1.76	7.70

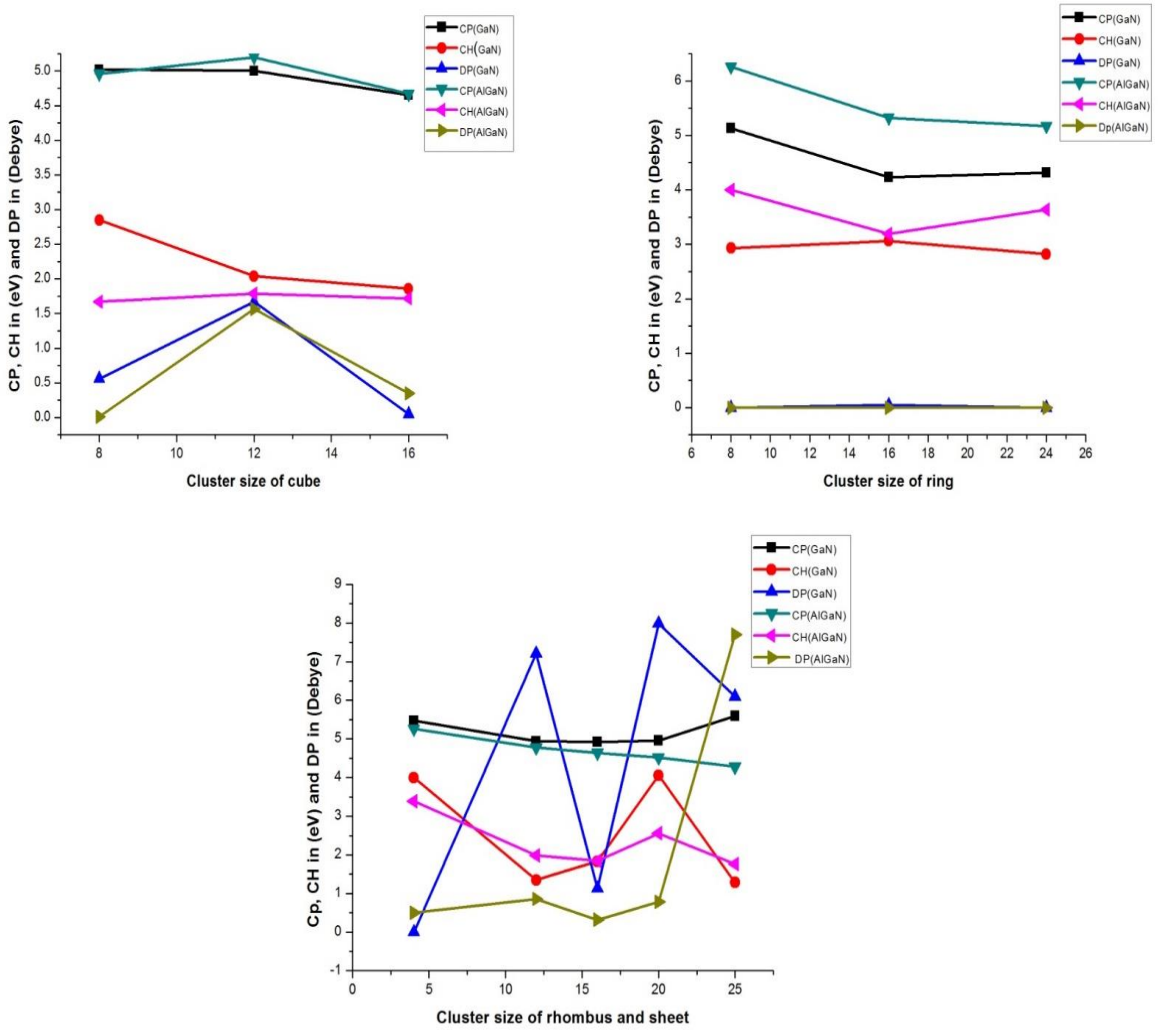

Figure 6.7: Variation of chemical potential (CP) chemical hardness (CH) and dipole moment (DP) with cluster size.

chemical hardness obtained for GaN rhombus and sheets configuration are 5.47 eV, 4.00 eV, and 5.26 eV, 4.92 eV for the sheet IV and sheet II respectively. Our next analysis corresponds to the dipole moment of GaN related clusters. From the calculated value of dipole moments of the cube configurations, the minimum value of dipole moment is 0.01 Debye and the higher value is 1.67 Debye in the Al substituted and simple GaN clusters for the cube-I and cube II, respectively. The low value indicates that the atoms are well

packed and ionic and electronic charges are uniformly distributed. In both cases of ring configurations, the dipole moment is found to be 0.00 Debye. This disappearance shows that their center of gravity of positive and negative charge distributions coincides. Whilst in the case of sheet configurations of GaN clusters, the maximum value of dipole moment 7.90 Debye for sheet-IV is attributed greater asymmetric distribution or larger mismatch of charges present in the cluster and a minimum value of dipole moment is found to be 0.32 Debye for Al-doped sheet-II. In summary, it is observed that values of dipole moment for the Al-substituted clusters are lower than the pure GaN clusters. The obtained value of dipole moment of clusters in different configurations varies with either increasing the number of atoms or substitution of Al atom, which may be due to having different geometrical structures of gallium nitride.

6.3.5 Vibrational Analysis

The vibrational behavior of pure GaN and Al substituted clusters has been analyzed in this section. A complete list of the lowest values of the frequency with corresponding Raman and IR activity is displayed in table 6.5. A possible mode of vibrations of each configuration of GaN and Al-GaN clusters are depicted explicitly as stretching, bending, wagging and twisting, etc. The absence of imaginary frequency in table 6.5 implies that all the configurations have local minima. i.e. they are stable and local minimum energy structures on the potential energy surface. It found that the molecules which are Raman active at frequency ranges from 15 cm^{-1} to 251 cm^{-1} and 22 cm^{-1} to 154 cm^{-1} for GaN and Al-GaN respectively wherein the value (137 cm^{-1}) for GaN-cube-II is close to experimental result for thin film and nanowire 144 cm^{-1} and 145 cm^{-1} [60]. It is worth noting that at most of the frequencies, the clusters have strong Raman activity (weak or

zero IR intensity), while at one frequency, the activity of mode is just reversed. For some frequencies, infrared and Raman activity both are significantly strong; there exists a vibration mode for both undoped and doped ring-I configuration that neither shows IR activity nor Raman, One reason for this may be the significant figure of calculations. As listed in table 6.5, for the cubic configuration of GaN and Al-GaN cluster, Raman activity and IR intensity at the lowest frequency appear due to bending and stretching mode of vibration and are showing increasing behavior with an increase in clusters size. On the other hand, ring configurations of GaN and Al-doped GaN have a number of vibrational frequencies; among them, lowest frequency is 60 and 69 cm^{-1} respectively; and because of centrosymmetric D_{2h} point group, all modes are Raman-active without IR activity, except for undoped ring-II configuration having a non-zero dipole moment. The mode of vibrations is scissoring for the lowest frequency of GaN and Al-GaN. Thus, Raman activity and IR intensities are displaying variations with nanoclusters size, shape and stacking mode. Further, at lowest frequency, out of the structures considered, Raman activity is found to be maximum for cubic-III GaN, which indicates that it is more polarizable than the others; while maximum IR intensity for rhombus Al-GaN results due to large change of the dipole moment, vibrational mode of cluster with no change of dipole moment is infrared inactive. The values of lowest frequencies are decreasing in undoped and doped except GaN cube-II clusters with clusters size; the lowest frequencies being 16 and 22 cm^{-1} for GaN and Al-GaN, belong to bending and twisting mode, which requires less energy than the other modes of vibration. For the undoped and doped cluster displaying the same configuration, lowest vibrational frequency for the undoped cluster is found somewhat smaller than the doped one; in agreement with the lower bond length

Table 6.5: IR intensities, Raman activity and the vibrational mode for the stable clusters of GaN and Al-GaN clusters Frequencies are in cm^{-1}, Raman activities in $Å^4$/amu and intensities are in km/mol.

Structures	Lowest Frequency	Raman Activity	IR Intensity	Vibrational Mode
Ga_4N_4 (Cube I)	91	21.43	4.46	Twisting
Ga_6N_6 (Cube II)	137	14.08	0.68	Twisting
Ga_8N_8 (Cube III)	16	187.96	48.89	Bending
$Ga_2Al_2N_4$ (Al_Cube I)	154	70.93	5.35	Diagonal Stretching
$Ga_3Al_3N_6$ (Al_Cube II)	130	24.90	0.69	Stretching
$Ga_4Al_4N_8$ (Al_Cube III)	111	14.31	0.35	Stretching
Ga_4N_4 (Ring I)	72	0.00	0.00	Rocking
Ga_8N_8 (Ring II)	71	9.78	0.00	Scissoring
$Ga_{12}N_{12}$ (Ring3)	60	6.04	0.00	Scissoring
$Ga_2Al_2N_4$ (Al_Ring I)	89	0.00	0.00	Rocking
$Ga_4Al_4N_8$ (Al_Ring II)	82	10.29	0.04	Scissoring
$Ga_6Al_6N_{12}$ (Al_Ring III)	69	5.41	0.00	Scissoring
Ga_2N_2 Rhombus	251	40.01	0.00	Wagging
$Ga_1Al_1N_2$ (Al_ Rhombus)	124	2.72	106.91	Wagging
Ga_6N_6 (Sheet I)	54	13.98	0.00	Scissoring
Ga_8N_8 (Sheet II)	21	14.90	0.00	Scissoring
$Ga_{10}N_{10}$ (Sheet III)	44	4.93	0.02	Rocking
$Ga_{12}N_{13}$ (Sheet IV)	15	5.07	0.13	Rocking
$Ga_3Al_3N_6$ (Al_Sheet I)	55	4.17	1.54	Wagging
$Ga_4Al_4N_8$ (Al_Sheet II)	43	2.14	0.00	Scissoring

$Ga_5Al_5N_{10}$ (Al_Sheet III)	29	2.25	0.10	Scissoring
$Ga_6Al_6N_{13}$ (Al_Sheet IV)	22	6.14	0.13	Twisting

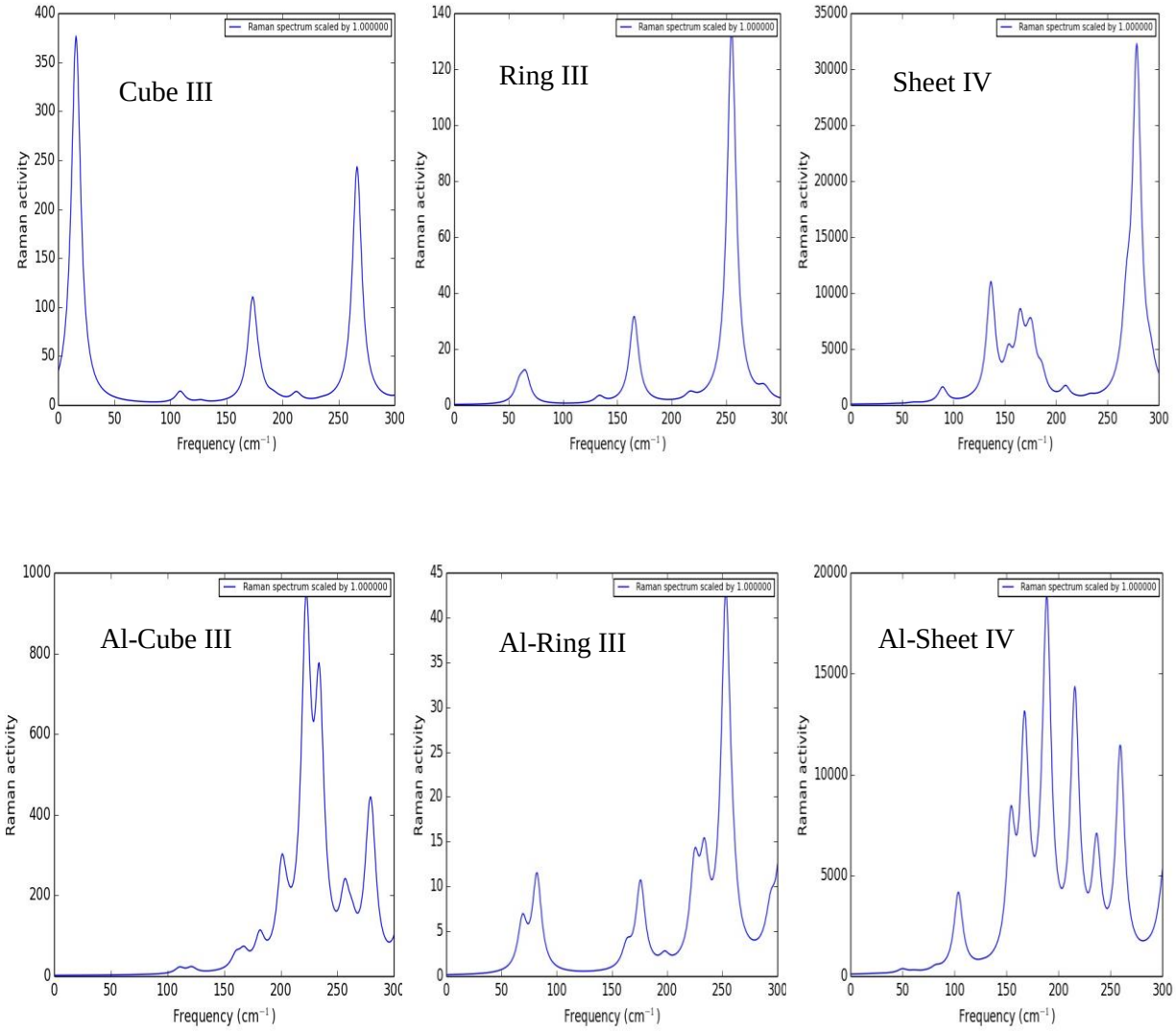

Figure 6.8: Raman Activity for the cube, ring, and sheet of GaN and Al-GaN clusters.

exhibited by the doped clusters. It is a cumbersome and difficult task to find out each of the modes due to vibrational complexity and hence we considered configurations of cube, of Raman and IR activity in Figure 6.8, 6.9 respectively, wherein IR and Raman spectra are spanned through 14 to 300 cm^{-1} and each frequency is related to a specific bending or

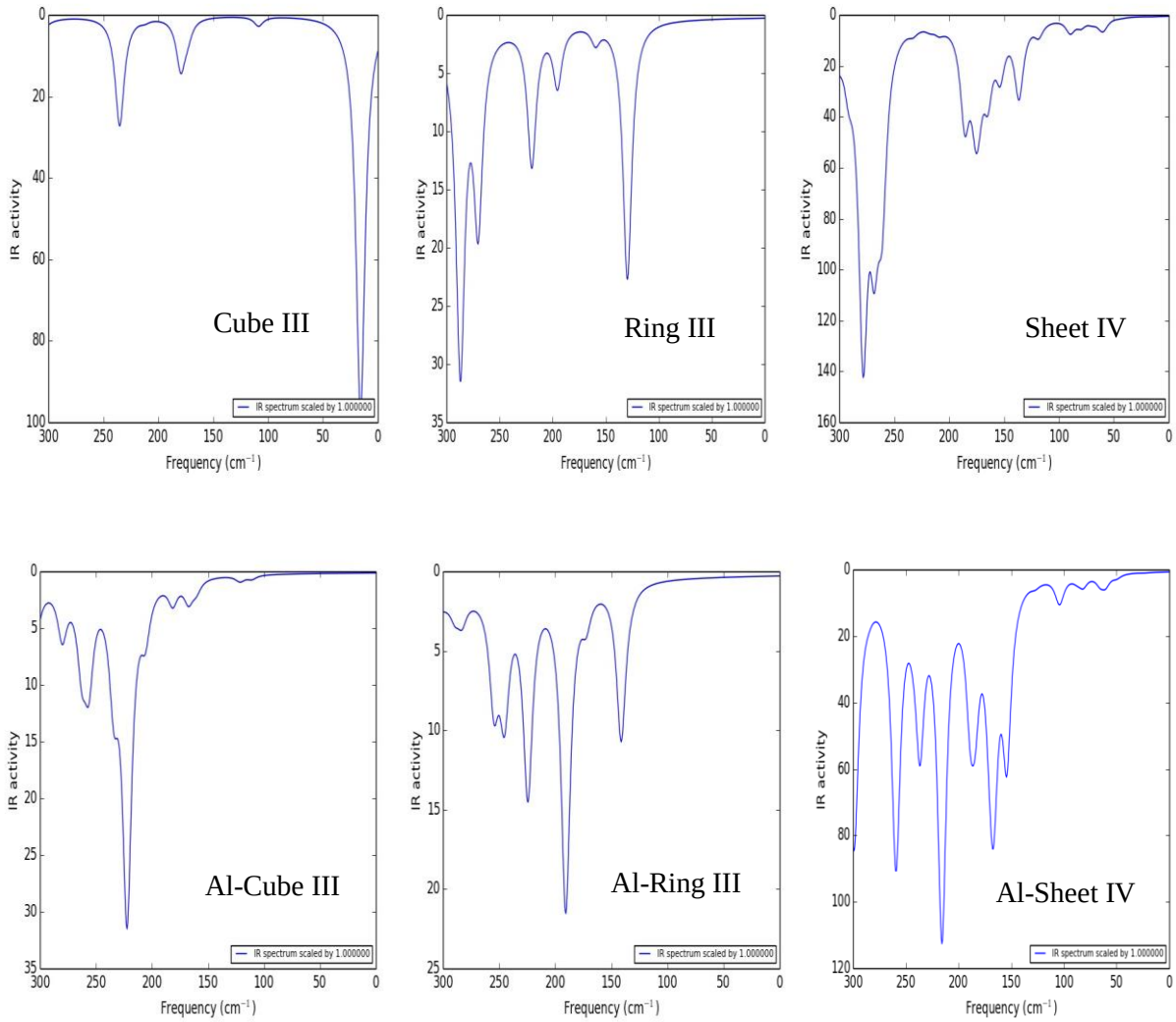

Figure 6.9: IR Activity for the cube, ring, and sheet of GaN and Al-GaN cluster.

stretching mode of vibration. Only a few peaks of absorption appear due to substantial coupling between vibrational modes with an increasing number of atoms/subunits in the clusters. Triple cube configuration of GaN has five distinguished Raman-active vibrational modes with the strongest band at the lowest frequency 16 cm^{-1}, whereas other smaller peaks present towards the high-frequency side. For ring-III (Tubular) structure, six Raman intensity peaks observe, while sheet configuration has 8 peaks; the highest peaks correspond to frequency 254 cm^{-1}, 277 cm^{-1} respectively lying in the mid-IR

region. It is interesting to see that there is an increase in frequency (blue shift) of most intense Raman mode with an increase in the number of atoms and shape of the cluster. Looking at the IR intensity of structures considered, except sheet configuration, equal to a number of Raman peaks are observed in their spectra with the most prominent peaks at 16 cm^{-1}, 288 cm^{-1}, and 279 cm^{-1} respectively. Figure 6.8, 6.9 clearly reflect that in respect of Raman and infrared activity, modes present dependence on the stacking mode and increase in units of cube and rhombus. Also, clusters undergo a distinctive change in their vibrational spectra after substitution of Al atoms to the pure one; the variation of peak positions and intensity along with the appearance of additional bands in the Raman modes and IR spectra may clearly be seen. This may be due to various types of intermolecular interactions and their extent in mixtures with varying Al content. Our calculated Raman spectra can be useful for analytical purposes and contribute significantly to spectral interpretation, vibrational assignments also can provide methodical guidance for future measurement.

6.4 Conclusion

In this work, stacks of a rhombus, rings, and cubes of GaN and Al substituted GaN clusters are constructed and their structural stability, HOMO-LOMO energy gap, ionization potential, electron affinity, chemical potential, and chemical hardness, dipole moment, IR and Raman spectra have been studied by DFT theory. The structures yield some interesting trends, and a strong size, shape and doping dependence of properties has been observed. An analysis of binding energies shows that final binding energy, even the numbers of atoms are same; varies with stacking mode or with an increase in the Al

atoms. For all compositions and size of clusters, the cube type (GaN-cube-II) structure is found as the most stable structure.

A major variation in electronic properties is observed in different structures, few of them exhibit large band gaps and ionization potentials. Dopant Al considerably modifies the HOMO-LUMO energy gap of cubes and sheets. It is observed that values of dipole moment are zero in the case of Al-GaN ring, whereas in different configurations, fluctuates randomly with either increasing the number of atoms or substitution of Al atom. A comparison of ionization potential and electron affinity reveals that Al-doped cube-II clusters is most suitable for chemical sensors due to its high value of EA (4.15 eV). Furthermore, the doping modifies remarkably the vibrational spectra of nanoclusters. An important finding of the present study is that the linear stacking of stable units of the ring may undergo to GaN nanowires. Similarly, sideways stacking of several units of rhombus structure results in nanotube formation. Thus, using the coalescence of GaN nanocluster building blocks, nanomaterials with different dimensionalities can be constructed whose properties may be tailored through the choice of size, composition and doping, thereby providing a viable alternative pathway of creating materials using nanoclusters as building blocks instead of atomic elements.

References

[1] J. T. Hu, T. W. Odom, C. M. Lieber, Acc. Chem. Res., 32, 435 (1999).

[2] Y. H. Li, H. H. Pan, P. S. Xu, Acta Phys. Sin., 54, 317 (2005).

[3] B. Ilan, A. H., S. Zamir, O. Katz, B. Meyler, J. Salzman, Mater. Sci. Eng., A, 14, 302 (2001).

[4] H. P. Zhao, G. Y. Liu, N. Tansu, Appl. Phys. Lett., 97, 131114 (2010).

[5] R. M. Farrell, P. S. Hsu, D. A. Haeger, K. Fujito, S. P. DenBaars, J. S. Speck, S. Nakamura, Appl. Phys. Lett., 96, 231113 (2010).

[6] H. Morkoc, S. Strite, G. B. Gao, M. E. Lin, B. Sverdlov, M. Burns, J. Appl. Phys., 76,1363 (1994).

[7] W. Martiessen, *Condensed Matter and Materials Data*, Springer, Berlin, (2005).

[8] H. Morkoc, S. Strite, G.B. Gao, M.E. Lin, B. Sverdlov, M. Burns, J. Appl. Phys., 76, 1363 (1994).

[9] X. H. Wang, B. K. Chang, Y. J. Du, J. L. Qiao, Appl. Phys. Lett., 99, 042102 (2011).

[10] Y. Zhang, J. Singh, Journal of Appl. Phys., 85, 587 (1999).

[11] S. J. Pearton, J. C. Zolper, R. J. Shul, F. Ren, *GaN: Defect and Device Issues*, (1998).

[12] S. Nakamura, T. Mukai, M. Senoh, Appl. Phys. Lett., 64, 1687 (1994).

[13] P. N. Favennec, H. L. Haridon, M. Salvi, D. Moutonnet, Y. Le Guillou, J. Electron. Lett., 25, 718 (1989).

[14] Y.F. Wu, B.P. Keller, S. Keller, D. Kapolnek, P. Kozodoy, S. Denbaars, U.K. Mishra, J. Appl. Phys. Lett., J, 69, 1438 (1996).

[15] R. J. Trew, M. W. Shin, V. G atto, J. Sol. Stat. Elect., 41, 1561 (1997).

[16] R. Gaska, M. S. Shur, A. D. Bykhovski, A. O. Oriov, G. L. Srider, J. Appl. Phys. Lett., 74, 287 (1999).

[17] E. R. Glaser, M. Murthy, J. A. Freitas, D. F. Storm, L. Zhou, D. J. Smith, Phy., B, 401, 327 (2007)

[18] F. Iskandar, T. Ogi, K. Okuyama, Mat. Lett., 60, 73 (2006).

[19] S. Jantrasee, S. Pinitsoontorn, P. Moontragoon, Jour. of Elec. Mate., 43, 1689 (2014).

[20] P. Moontragoon, N. Vukmirovic, Z. Ikonic, P. Harrison, Microelec. Jour., 40, 483 (2009).

[21] I. Akasaki, H. Amano, Y. Koide, K. Hiramatsu, N. Sawaki, J. Cryst. Growth, 98, 209 (1989).

[22] P. Vennegues, M. Leroux, S. Dalmasso, M. Benaissa, P.D. Mierry, P. Lorenzini, B. Damilano, B. Beaumont, J. Massies, P. Gibart, Phys. Rev., B, 6823, 5214 (2003).

[23] I. Takeshi, Y. Shigeru, I. Yoshifumi, M. Teruaki J. Cryst. Growth **1,** 274 (2005).

[24] E. Pournamdari, M. Khaleghian, Journal of Physical and Theoretical Chem. **8**,199 (2011).

[25] S. Pezzagna, P. Vennegues, N. Grandjean, J. Massies, J. Cryst. Growth **269,** 249 (2004).

[26] Y. J. Du, B. K. Chang, J. J. Zhang, X. H. Wang, B. Li, M. S. Wang, Optoelectron. Adv. Mat., 5, 1050 (2011).

[27] J. Yan-Jun, D. Yu-Jie, W. Mei-Shan, Chin. Phys., B, 22, 117103 (2013).

[28] S. N. Lee, J. K. Son, T. Sakong, W. Lee, H. Paek, E. Yoon, J. Kim, Y. H. Cho, O. Nam, Y.Park, J. Cryst. Growth, 272, 455 (2004).

[29] A. C. Reber, S. N. Khanna, J. S. Hunjan, M. R. Beltran, Eur. Phys. J., D, **43**, 221 (2007).

[30] S. Karthikeyan, E. Deepika, P. Murugan, J. Phys. Chem. C, **116**, 5981 (2012).

[31] K. Holczer, O. Klein, S. Huang, R. B. Kaner, K. Fu, R. L. Whetten, F. Diederich, Science, 252, 1154 (1991).

[32] A. F. Hebard, M. J. Rosseinsky, R. C. Haddon, D. W. Murphy, S. H. Glarum, T. T. M. Palstra, A. P. Ramirez, A. R. Kortan, Nature, 350, 600 (1991).

[33] M. J. Rosseinsky, A. P. Ramirez, S. H. Glarum, D. W. Murphy, R. C. Haddon, A. F. Hebard, T. T. M. Palstra, A. R. Kortan, S. M. Zahurak, A. V. Makhija, Phys. Rev., Lett., 66, 2830 (1991).

[34] P. Jena, S. N. Khanna, B. K. Rao, Materials Science Forum, 232, 1 (1996).

[35] A.W. Castleman, Jr., S.N. Khanna, J. Phys. Chem., C, 113, 2664 (2009).

[36] C.R.A. Catlow, S. T. Bromley, S. Hamad, M. Mora-Fonz, A. A. Sokol, S. M. Woodley, Phy. Chem. Phy., 12, 786 (2010).

[37] J. Kioseoglou, M. Katsikini, K. Termentzidis, I. Karakostas, E. C. Palour, J. App. Phy., 121, 054301 (2017).

[38] A. Szabo, N.S. Ostlund, *Modern Quantum Chemistry*, Dover Publications, New York (1996).

[39] M. J. Frisch, G. W. Trucks, H .B. Schlegel et al., Gaussian 09, Revision D, 01, Gaussian, Inc., Wallingford, Conn, USA, (2009).

[40] C. Lee, W. Yang, R. G. Parr, Phys. Rev., B, **37**, 785 (1988).

[41] A. D. Becke, J. Chem. Phys., 98, 5658 (1993).

[42] N. M. O'Boyle, A. L. Tenderholt, K. M. Langner, J. Comp. Chem., 29839 (2008).

[43] Chemcraft 1.8, http://www.chemcraftprog.com

[44] J. J. BelBruno, Heteroatom Chem., 11, 281 (2000).

[45] S. Bin, C. Pei-Lin, Chin. Phy. Lett., 9, 1488 (2003).

[46] A. K. Kandalam, M. A. Blanco, R. Pandey, J. Phy. Chem., B, 106, 1945 (2002).

[47] L. Hedin, I. B. Lundqvist, J. Phy. C: Solid State Phy., 4, 2064 (1971).

[48] T. Mattila, A. Zunger, Journal of App. Phys., 85, 160 (1999).

[49] J. Zhao, B. Wang, X. Zhou, X. Chen, Wei Lu, Chem. Phy. Lett., 422, 170 (2006).

[50] H. P. Maruska, J. J. Tietjen, App. Phys. Lett., 15, 327 (1969).

[51] W. Shan, J. W. Ager III, K. M. Yu, and W. Walukiewicz, Jour. of App. Phy., 85, 8505 (1999).

[52] B. S. Eller, Jialing Yang, R. J. Nemanich, J. Vac. Sci. Technol., A, 31, 050807 (2013).

[53] S. P. Grabowski, M. Schneider, H. Nienhaus, W. Monch, R. Dimitrov, O. Ambacher, M. Stutzmann, App. Phys. Lett., 78, 2503 (2001).

[54] R. K. Shastri, D. Kumar, S. P. Goutam, R. R. Yadav, A. K. Yadav, Inter. Jour. of Adv. Res., 3, 787 (2015).

[55] R. K. Shastri, D. Kumar, D. Kumar A. K. Yadav, Inter. Adv. Rese. J. in Sci., Eng., and Tech., 2, 95 (2015).

[56] X. Liao, X. Kuang, Eur. Phys. J. Plus, 26, 130 (2015).

[57] D. Dundas, J. M. Rost, Phy. Rev., A, 71, 013421 (2005).

[58] K. P. Huber, G. Herzberg, in NIST Chemistry Web Book, edited by P. J. Lindstrom, W. G. Mallard NIST Vol., 69, (2003).

[59] Y. K. Kim, Phy. Rev., A**,** 66, 012708 (2002).

[60] M. Gopalakrishnan , V. Purushothaman, P. S. Venkatesh, V. Ramakrishnan, K. Jeganathan, Mate. Rese. Bulle., 47, 3323 (2012).

Chapter-7
Conclusions

Chapter 7

Conclusions

This chapter is focused on the main conclusions of the results and discussions that can be drawn from the investigations carried out on CdS, ZnO, CoO and Al-doped GaN clusters in this thesis. This chapter also provides the strategies for further research work in the field of nanoscale materials in form of clusters. First chapter presents a general introduction to materials, functional materials, and literature survey on clusters, scope and objectives of the thesis. The necessity, importance and applications of clusters were also highlighted. Second chapter describes the brief introduction to different computational approaches, particularly density functional theory. In summary, following concluding points and recommendation are made:

1. Density Functional Theory (DFT) is one of the accurate methods for theoretical studies of advanced materials in form small clusters and provide good results very quickly, which are very helpful to understand and explain the new phenomenon. The properties of materials in form of clusters are very significant for the development of new science.
2. The properties of small clusters are a function of their size because when the size of clusters change the properties of the clusters change significantly. The nonlinear structures of Cd_mS_n nanoclusters are more stable in comparison with linear depending on final binding energy (FBE). In general, nanoclusters with high FBEs have a large number of S atoms. It was observed that the value of HOMO-LUMO gap decreases with a number of S atoms.

3. Our results reveal that the existence of the most stable configurations of various Zn_mO_n and Co_xO_y nanoclusters depend on final FBEs. In general, nanoclusters with high BEs have a large number of Zn atoms. It was observed that the value of HOMO-LUMO gap decreases with an increase of cluster size. FBE is increasing with the increasing number of atoms i.e. the size of the cluster.
4. An analysis of binding energies shows that final binding energy, even the numbers of atoms are same; varies with stacking mode or with an increase in the Al-doped atoms. A major variation in electronic properties is observed in different structures, few of them exhibit large band gaps and ionization potentials.
5. The doping modifies remarkably the vibrational spectra of nanoclusters. Dopant Al considerably modifies the HOMO-LUMO energy gap of cubes and sheets. It was observed that values of dipole moment are zero in the case of Al-GaN ring, whereas in different configurations, fluctuates randomly with either increasing the number of atoms or substitution of Al atom. A comparison of ionization potential and electron affinity reveals that Al-doped cube-II clusters is most suitable for chemical sensors due to its high value of electron affinity.
6. An important finding of the present study is that the linear stacking of stable units of the ring may undergo to GaN nanowires. Similarly, sideways stacking of several units of rhombus structure may results in nanotube formation.
7. Variation in HOMO-LUMO gap in different sized clusters considered in the thesis could be useful for devise applications.

Overall, studies on functional materials in form of small clusters obtained new properties, which are significantly associated with clusters size and very useful to understand and explain new phenomenon from the experimental point of view.

List of Publications

List of Publications

Published Research Papers

1. **Rajkamal Shastri,** Anil Kumar Yadav, Devesh Kumar, "*A comparative ab intio study on structural evolution, stability and electronic properties of undoped and Al-doped Ga_xN_y (x + y = 4-25) clusters"* Eur. Phys. J. Plus, 132, 1 (2017).
2. **Rajkamal Shastri,** Devesh Kumar, Surya Pratap Goutam, Raja Ram Yadav, Anil Kumar Yadav, *"Size dependent structural, electronic and vibrational properties of Cd_mS_n (m+n=2-6) nanoclusters: a DFT study"* International Journal of Advanced Research, 3, 787 (2015).
3. **Rajkamal Shastri**, Deep Kumar, Devesh Kumar Anil Kumar Yadav, "*Quantum Chemical Studies on Zn_mO_n (m+n=2-8) Even Nanocluster's Stability"* International Advanced Research Journal in Science, Engineering and Technology, 2, 94 (2015).
4. Deep Kumar, **Rajkamal Shastri**, Devesh Kumar, Anil Kumar Yadav, *"Structures Stabilities and Electronic Properties of GaAs Condensed Clusters"* International Advanced Research Journal in Science, Engineering and Technology, 2, 102 (2015).
5. **Rajkamal Shastri**, Nidhi Awasthi, Devesh Kumar, Anil Kumar Yadav, Diptarka Roy, S. P. Goutam, Anwesh Pandey, *"A Density Functional Theory Study on Structural Stability and Electronic Properties of Co_xO_y (x+y=4-12) Nanoclusters"* Advanced Science, Engineering and Medicine, 10, 1 (2018).

6. Surya Pratap Goutam, Sarvesh Kumar Avinashi, Manju Yadav, Diptarka Roy, **Rajkamal Shastri,** *"Green Synthesis and Characterization of Aluminum Oxide Nanoparticles Using Leaf Extract of Rosa*" Advanced Science, Engineering and Medicine, 10, 1 (2018).

Conference (Oral/Poster) Presentation

1. International E Workshop/Conference on *Computational Condensed Matter Physics and Material Science*, November 25-30, 2014, organized by Advance Materials Research group, CNT Laboratory ABV-IIITM, Gwalior, M.P., India
2. International Conference on *Contemporary Advances of Science and Technology*, August 7-9, 2015, organized by BHU, Varanasi, U.P., India
3. 2nd International conference on *Recent Advances in Nanoscience & Nanotechnology*, December 19-20, 2016, organized by JNU, New Delhi, India
4. International Conference on *Structure and dynamics of biomolecules,* January 27-28, 2017, organized by DDU Gorakhpur University, Gorakhpur, U.P., India
5. 3dr Lucknow science congress and national conference on *Science for society: an interdisciplinary approach*, 31 October to 2 November 2015, organised by Babasaheb Bhimrao Ambedkar University, Lucknow, U.P., India
6. 103rd Indian science congress held at University of Mysore from January 3-4, 2016.

Eur. Phys. J. Plus (2017) **132**: 313
DOI 10.1140/epjp/i2017-11584-7

THE EUROPEAN PHYSICAL JOURNAL PLUS

Regular Article

A comparative ab intio study on structural evolution, stability and electronic properties of undoped and Al-doped Ga_xN_y $(x + y = 4–25)$ clusters

Rajkamal Shastri[a], Anil Kumar Yadav[b], and Devesh Kumar

Department of Applied Physics, Babasaheb Bhimrao Ambedkar University, Lucknow - 226025, U.P., India

Received: 19 March 2017 / Revised: 25 May 2017
Published online: 20 July 2017 –

Abstract. We present a comparative study on structure evolution, binding energies, relative stabilities, electronic and vibrational properties of size-selected GaN and Al-doped GaN clusters by employing B3LYP exchange-correlation function with double-ξ basis set LANL2DZ via the density functional theory (DFT) method. Cube, ring, and rhombus stacks are constructed, and the optimization results suggest that the evolution of basic structural entities of different morphologies from planer rings to nanotubes may be realized by taking into account the stacking mode of stable clusters. We also find that the geometry of each Al-substituted GaN cluster keeps a structure similar to that of the corresponding pure GaN clusters. The stability, IR and Raman activity vary with the growth of units and the stacking mode. The energetic analysis shows that the most stable structure is the 3-dimensional cubic structure. A blue shift in the vibrational frequency of the most intense Raman activity has been observed with variation in size and structure. Moreover, the vibrational properties are significantly affected by the introduction of Al dopants. We also consider parameters, such as HOMO-LUMO gap, ionization potential (IP), electron affinity (EA), dipole moment (DM), chemical potential (CP), chemical hardness (CH), and results were compared and critically discussed for interpretation of the enhanced stability and to extract useful information for their applications.

1 Introduction

In the last few decades, considerable effort has been devoted to the understanding of clusters; and predicting the structures of single stable units, which can offer the possibility of developing nanodevices, is the key to cluster physics. It might be possible that a given number of atoms have various possible structures which are rather close in energy. It is therefore important to evaluate the sensitivity of a given property on structural changes of the cluster. Group III-nitride–based materials have been the focal point of many experimental and theoretical studies in recent years because of their peculiar electronic, chemical, optical and biological properties [1–5]. Nevertheless, control over the size, structure and composition of these nanostructured materials is still the most crucial challenge for their fundamental understanding and practical applications. Among the group III-nitrides, gallium nitride (GaN) emerged as an extensively studied material with interesting properties, such as direct and wide band gap (3.4 eV), high breakdown voltage, thermal conductivity, melting point, and large bulk modulus [6–8] and with plentiful applications [9–13]. Furthermore, with the evolution of nanoscience, interest in the properties and capabilities of doped materials has been progressively increasing as doping can improve photoelectric, electronic and magnetic properties [14–20]. Many authors have focused on the structures, energies, and thermodynamics of GaN clusters using different theoretical approaches. Akasaki *et al.* have reported that Mg is a simple *p*-type doping element [21]. Subsequently, structure, electronic properties, optical properties and magnetic resonance characteristics of GaN and the polarity reversal of GaN surfaces after Mg doping were investigated experimentally and theoretically [22–26], and widening of band gap and the emission wavelength areas from visible light to part of the ultraviolet region in a Al-doped GaN film have been reported [27]. Lee *et al.* [28] studied Al-doped blende GaN compounds with different doping concentrations theoretically and found that the lattice

[a] e-mail: rajshastri4@gmail.com
[b] e-mail: akyadavbbau@gmail.com (corresponding author)

constant linearly decreases with the increase in the doping concentration. Moreover, previous computational studies on ZnO and CdS [29,30] suggest that different nanostructures may be built by addition of stable cluster units or by fragmentation of the bulk material; structures achieved with the combining stable cluster units are significantly different and have a greater stability from the frameworks cut than their bulk structures. These studies motivated us for a better understanding of the mechanism of undoped and Al-doped GaN clusters formation by stacking of subunits of a small cube, ring, and sheet, about which there have been neither DFT nor experimental studies so far. In this paper, we have focused on how individual cluster configurations can combine to form extended framework materials and also on suitable models to describe and predict the changes of the cluster properties as a function of size, such as evolution from small to large clusters and shape. Unfortunately, the synthesis of our predicted structures has no experimental evidence; however this approach is consistent with published theoretical and experimental studies [31–35] on the creation of cluster-assembled materials; one specific example is the fulleride crystal comprising C_{60} clusters as building blocks, and the synthesis of III-V semiconducting clusters of the form $(XY)_n$ with mass spectra, where X represents metals or cations, and Y denotes anions [36] and recent experimental invesitigation of the formation of a wurtzite GaN nanocluster in a silica matrix by rapid thermal annealing and ion implantation of gallium and nitrogen [37]. To this end, we have explored geometric structures, electronic, vibrational properties and stability trend of undoped and doped $Ga_xAl_zN_y$ clusters using the *ab initio* method based on the density functional theory. Additionally, ionization potential (IP), electron affinity (EA), HOMO-LUMO energy gap, chemical potential (CP), chemical hardness (CH), and dipole moment (DM) have also been calculated.

2 Methods and computational details

Conventional *ab initio* methods have been fully justified as a very powerful tool to complement the experiments and to lead to a better understanding of unknown phenomena [38]. In this work, all computations have been carried out using first-principle calculations within the framework of density functional theory as implemented in the `Gaussian 09` program package [39]. For most precise calculations, the gradient-corrected B3LYP functional form comprising Becke's three-parameter hybrid exchange functional and Lee, Yang and Parr correlation functional was employed with the larger basis set Los Alamos double-ζ effective core potential LANL2DZ as the basic basis set [40,41]. `Gauss Sum 3.0` [42] and `chemcraft` [43] softwares were used for the evaluation of the density of states (DOS) and visualization of molecular orbitals. For the determination of ground- and excited-state structures of pure GaN clusters, we constructed many structures including small cube, ring and rhombus, and, for each structure, minimum energy is achieved by relaxing the atomic positions without any symmetry constraint. Also, due to spin polarization, each initial configuration was optimized at various possible spin multiplicities. Each structure was further assessed by frequency analysis at the same level of theory to explore for no imaginary frequency. For the formation of assembled clusters, firstly, stable isomers in small size are constructed which act as the candidate structure for assembled clusters. Subsequently, different structures of assembled clusters of pure and Al-substituted GaN in two as well as in three dimensions, such as sheets and cube, were achieved by sideways and linear stacking, respectively, of m ($m = 2$–16) stable units of rhombus $(Ga_2N_2)_m$, whereas rings were obtained by linear stacking of m (up to 3) subunits of ring $(Ga_4N_4)_m$. The Al atoms were substituted at Ga sites and each structure was further optimized. The binding energies (BE) of GaN and Al-GaN clusters were calculated by the equation

$$BE = [xE(\mathrm{Ga}) + yE(\mathrm{N}) - E(\mathrm{Ga}_x\mathrm{N}_y)]/(x + y)$$

and

$$BE = [xE(\mathrm{Ga}) + zE(\mathrm{Al}) + yE(\mathrm{N}) - E(\mathrm{Ga}_x\mathrm{Al}_z\mathrm{N}_y)]/(x + z + y),$$

where $E(\mathrm{Ga})$, $E(\mathrm{N})$, $E(\mathrm{Ga}_x\mathrm{N}_y)$ and $E(\mathrm{Ga}_x\mathrm{Al}_z\mathrm{N}_y)$ are the total energy of the isolated atoms Ga, N and Ga_xN_y, $Ga_xAl_zN_y$ clusters, respectively, while $x + y$ and $x + z + y$ are the total numbers of Ga, N, and Ga, Al, N atoms, respectively. For further precise calculations, binding energies are corrected by considering the zero point energy (ZPE). Accordingly, the stability of the nanocluster has been considered, eventually, in terms of final binding energy (FBE). In all fully optimized structures, the convergence of the system energy is obtained up to 10^{-7} eV and forces of 10^{-3} eV/Å on each atom were achieved.

3 Results and discussion

3.1 Geometries of assembled GaN and Al substituted GaN clusters and their stability

The various optimized geometries of GaN and Al-substituted GaN clusters, resulting due to the stacking of basic units of Ga_2N_2, along with the bond lengths are shown in figs. 1 and 2, respectively. In tables 1 and 2, symmetries, spin multiplicities, binding energy, final binding energy (FBE) and the HOMO-LUMO gap that we computed are summarized.

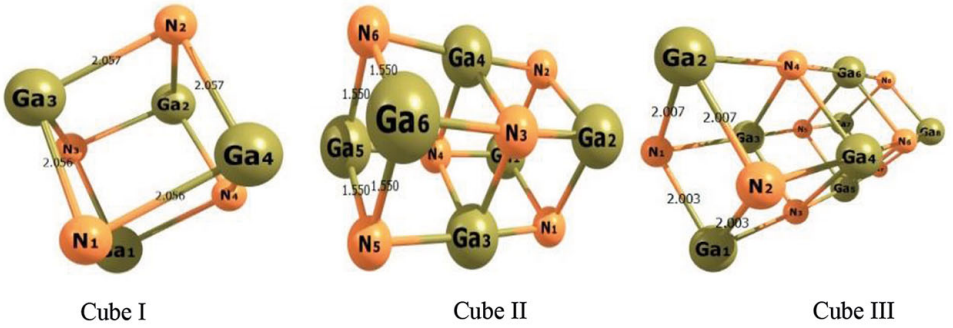

(a)

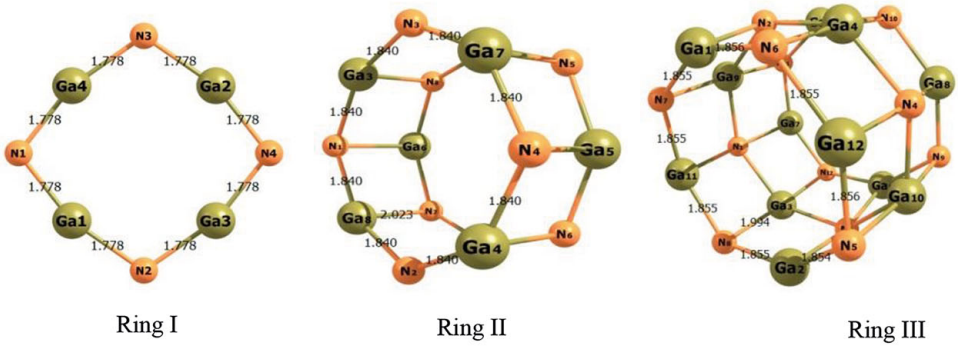

(b)

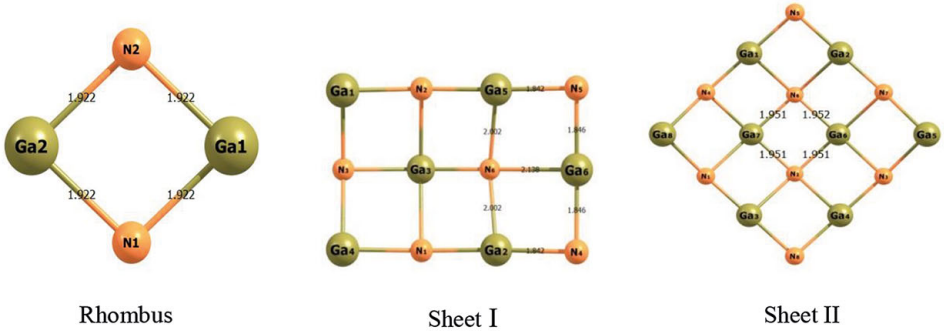

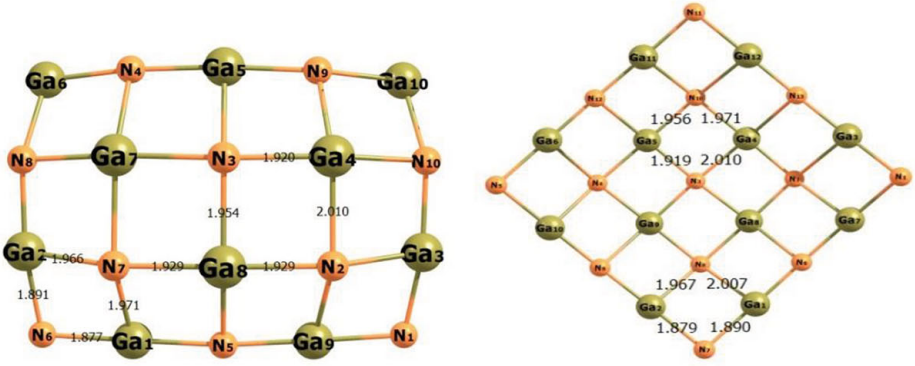

(c)

Fig. 1. B3LYP/LANL2DZ geometrically optimized structures of GaN clusters. (a) Structural pattern of cubic GaN clusters. (b) Structural pattern of ring GaN clusters. (c) Structural pattern of rhombus GaN clusters.

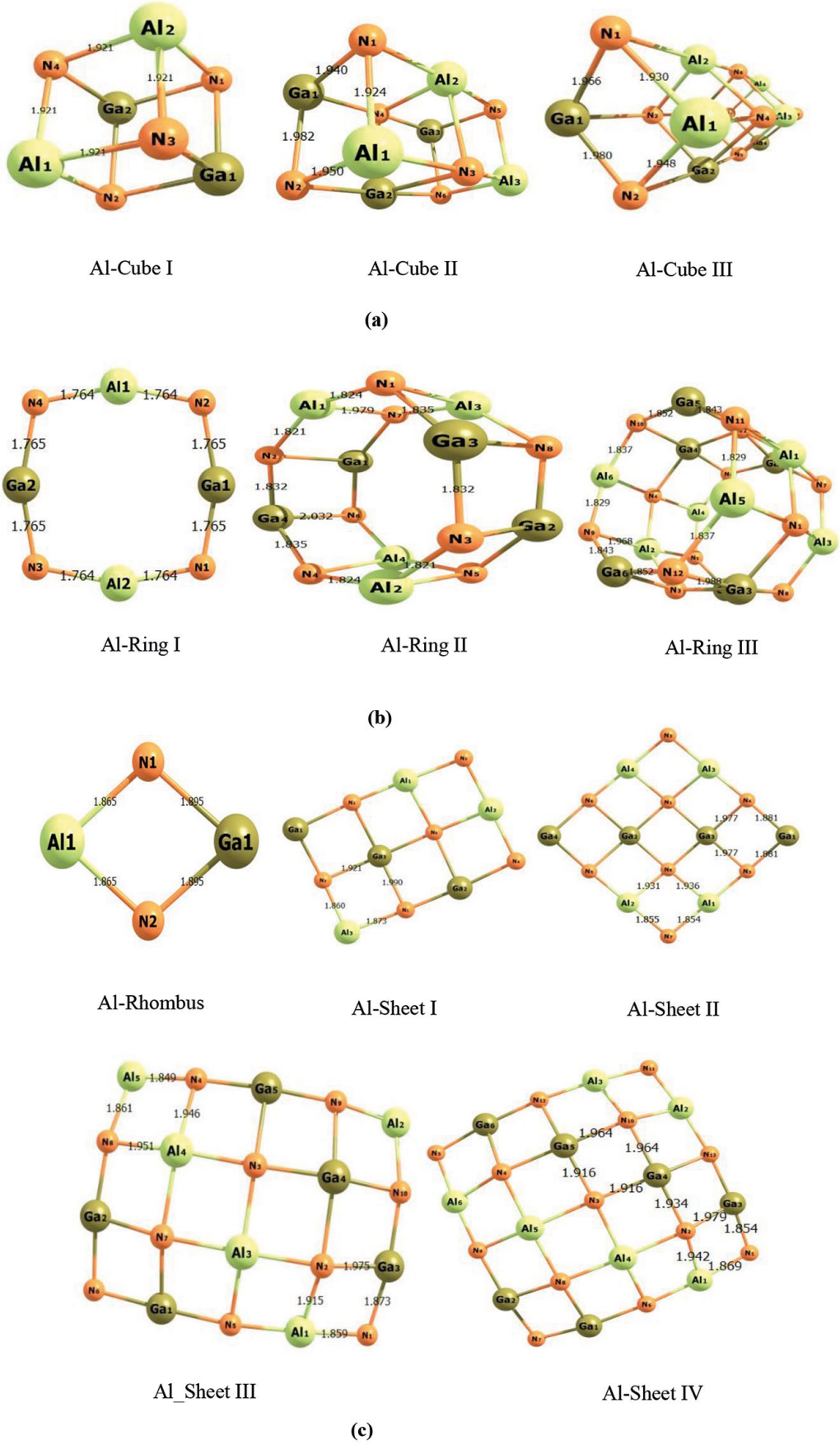

Fig. 2. B3LYP/LANL2DZ geometrically optimized structures of Al-doped GaN clusters. (a) Structural pattern of cubic Al-doped GaN clusters. (b) Structural pattern of ring Al-doped GaN clusters. (c) Structural pattern of rhombus Al-doped GaN clusters.

Table 1. Symmetry, multiplicity of the ground state (GS), binding energy (BE) per atom, zero point energy (ZPE), final binding energy (FBE) and HOMO-LUMO gap for all configurations of GaN clusters.

Structures	Configuration	No. of atoms	Symmetry	Multiplicity	BE (eV)	ZPE (eV)	FBE (eV)	HOMO-LUMO energy gap (E_g) (eV)
Ga_4N_4	Cube I	8	C_1	1	3.64	0.42	3.22	1.21
Ga_6N_6	Cube II	12	C_1	3	4.75	0.67	4.08	3.35
Ga_8N_8	Cube III	16	C_1	5	5.00	0.94	4.06	1.77
Ga_4N_4	Ring I	8	D_2H	1	4.10	0.43	3.67	2.09
Ga_8N_8	Ring II	16	C_1	1	4.66	1.07	3.59	1.61
$Ga_{12}N_{12}$	Ring III	24	C_1	1	4.90	1.64	3.26	2.12
Ga_2N_2	Rhombus	4	D_2H	3	3.96	0.15	3.81	5.10
Ga_6N_6	Sheet I	12	C_1	1	4.02	0.67	3.35	0.95
Ga_8N_8	Sheet II	16	C_1	3	4.87	0.94	3.93	1.08
$Ga_{10}N_{10}$	Sheet III	20	C_1	1	4.46	1.29	3.17	2.09
$Ga_{12}N_{13}$	Sheet IV	25	C_1	4	5.02	1.58	3.44	6.02

Table 2. Symmetry, multiplicity of the ground state (GS), binding energy (BE) per atom, zero point energy (ZPE), final binding energy (FBE) and HOMO-LUMO gap for all configuration of Al-substituted GaN clusters.

Structures	Configuration	No. of atoms	Symmetry	Multiplicity	BE (eV)	ZPE (eV)	FBE (eV)	HOMO-LUMO energy gap (E_g) (eV)
$Ga_2Al_2N_4$	Al_Cube I	8	C_1	1	3.84	0.47	3.37	1.23
$Ga_3Al_3N_6$	Al_Cube II	12	C_1	3	4.81	0.77	4.04	1.39
$Ga_4Al_4N_8$	Al_Cube III	16	C_1	3	5.00	1.10	3.90	0.91
$Ga_2Al_2N_4$	Al_Ring I	8	D_{2H}	1	4.10	0.48	3.62	2.54
$Ga_4Al_4N_8$	Al_Ring II	16	C_1	1	4.66	1.20	3.46	2.58
$Ga_6Al_6N_{12}$	Al_Ring III	24	C_1	1	4.90	1.84	3.06	2.87
$Ga_1Al_1N_2$	Al_Rhombus	4	C_S	1	3.25	0.17	3.08	1.48
$Ga_3Al_3N_6$	Al_Sheet I	12	C_1	3	4.81	1.10	3.71	1.68
$Ga_4Al_4N_8$	Al_Sheet II	16	C_1	3	5.04	1.10	3.94	2.18
$Ga_5Al_5N_{10}$	Al_Sheet III	20	C_1	1	4.66	1.42	3.24	2.16
$Ga_6Al_6N_{13}$	Al_Sheet IV	25	C_1	4	5.13	1.80	3.33	1.65

Analysis of fig. 1 and table 1 reveals that the configuration of Ga_2N_2 corresponds to a symmetric triplet state rhombus geometry, in which nitrogen atoms lie opposite to each other at a distance 1.922 Å from Ga atoms. For Ga_4N_4, two different structures, namely, cube-I and planer ring-I, are obtained, and the most stable structure is the ring form. These are similar to the structures proposed by Belbruno *et al.* [44], Song *et al.* [45], and Kandalam *et al.* [46]. Calculated bond lengths for all clusters that range between 1.78 Å and 2.20 Å are comparable to the results (1.88 Å–2.06 Å), reported by Pournamdari *et al.*, for cube-I [24]. In the case of the cube-I configuration, the predicted Ga-N bond length (2.057 Å) is also in good agreement with previous results of Belbruno (2.032 Å) [44], Song Bin *et al.* (2.027, 2.048, and 1.926 Å) [45] and Kandalam *et al.* (2.31 and 2.53 Å) [46]. Hedin *et al.* reported that in bulk stoichiometric GaN, the distance between Ga and N is 1.94 Å [47], which is slightly lower than the bond length calculated by us; hence it may be considered that the nature of these Ga-N bonds is similar to the bulk Ga-N bonds. Now, we focus on stacking of starting structures: rhombus, cube and ring. For Ga_6N_6, a double-cube structure was found, which can be seen to consist of a linear stacking of two layers, namely, a cube formed with Ga_4N_4 and Ga_2N_2. On further stacking an extra layer of Ga_2N_2 to this structure, an analogous cube-like nanotube structure was preferred for Ga_8N_8. It seems that optimized structures are a mere extension of subunit Ga_4N_4. On the other hand, we note that the trend

is quite different for tube-like structures: the Ga_4N_4 octagonal ring stacked on top of each other transform from a planar structure to a tubular configuration. Further stacking one more planer ring structure to the preceding geometry undergoes a similar geometry, again. We then consider the sideways stacking of rhombus (4×3); our result predicts the formation of a Ga_6N_6 sheet geometry. On further increasing subunits up to (4×4), the system continues to maintain the original stable configuration of the sheet. However, for sideways stacking of subunits (5×4), the cluster favors a curved geometry, which offers the possibility to obtain a nanotube from a sheet of GaN. Here, it is worth mentioning that in all configurations of the GaN cluster, Ga and N atoms are linked to each other in an alternating fashion. An explanation for the tendency for the metal-nitrogen bond instead of the Ga–Ga bond or N–N bond could be the existence of a lone pair on nitrogen atoms as only three electrons of pentavalent nitrogen atoms participate in bonding with the Ga atom. In order to lower repulsive interaction between the lone-pair electrons, nitrogen atoms tend to sit away from each other. Moreover, rings and rhombus display a high-order symmetry, while all others, along with stacked configurations, possess lower symmetries. This is a natural consequence of their structural types.

Also, the appearance of maximum atoms on the surface sites in the above clusters gives rise to less surface strain and thereby offers a better probability of doping. Analysis of fig. 2 reveals that the geometry of each Al-substituted GaN cluster keeps a structure similar to the corresponding pure GaN clusters with a slight tilt in cubes. The bond length of the Al-N and GaN in Al-substituted GaN lies in the range 1.76 Å to 1.93 Å and 1.77 Å to 1.98 Å, respectively, which is in good agreement with the experimentally observed distance for Al-N (1.90 Å) and Ga-N (1.94 Å) [48]. For each cluster, Al atoms tend to occupy the sites on the peripherals of the clusters, whereas in the planar sheet structures, some of the Al atoms show a tendency to go inside the cluster. The bond lengths of doped structures are similar to the bare GaN clusters with a slight deviation, indicating that the bonding characteristics remain the same in the doped clusters [44,46]. The slight deviation in bond lengths may be attributed to the difference in atomic radius and electronegativity of the atoms.

From table 1, we see that except for the undoped ring I and rhombus, the geometry of the clusters have C_1 point group symmetry, which indicates that the substitution of Al atoms to the bare cluster does not induce considerable change in the configurational symmetry of most of the analyzed structures, except for ring-I (D_{2h}) and rhombus geometries (C_S).

We now turn our attention to the stability of the clusters. The value of the final binding energy, as shown in fig. 3, rises monotonically with increasing the size of cubic clusters; the maximum increase in cube-II signifies a particular stability of cube-II; note that the energy difference between the structures is small. A quite similar trend is observed for the doped cubic cluster and is maximum (4.04 eV) for cube-II.

Thus, the stability of cubes increases with size and with increasing aluminum content, except for the Al-doped cube-III. Unlike cubes, there is a decrease in the final binding energy with the size for the ring configurations of doped and undoped clusters; this decrease in the energy may be viewed as an attempt by the stacked GaN clusters to transform from the planar configurations to favor tubular structures with the increase in the cluster size. In particular, the planer ring-I structure with maximum FBE (3.67 eV) is found to be the most stable one, which is slightly greater than the values calculated by others, 3.03 eV [49] and 3.16 eV [46]. The binding energies in the case of GaN cube-I and cube-II are 3.22 eV and 4.08 eV, and are comparable with the 3.36 eV and 3.66 eV [49,46], respectively. The energies calculated for the set of rhombus and sheet configurations, namely I, II, III and IV, of Al-doped and undoped GaN clusters do not follow the above trend, and FBE varies sharply as oscillatory humps or dips. Particular humps for a specific size of clusters imply their stabilities relative to neighboring clusters. Al-doped sheet configurations are relatively more stable than the pure one due to their higher binding energy. Furthermore, the FBE curves show that the binding energies of the most of the Al-doped GaN clusters are lower than those of the pure GaN clusters [44,46]. Indeed, for all compositions and size of clusters, the GaN cube-II is the most stable structural type; the final binding energy for other possible cluster types is lower than that for the GaN cube-II. From the above discussion, it is obvious that for all clusters even the number of atoms is the same, FBE varies with the stacking mode of basic units and either enhancing the number of atoms or increasing Al content. Also because of open configurations of nanoclusters, properties are prominently affected by large surface effects.

3.2 Electronic properties of Al substituted GaN clusters

The electronic properties of undoped and Al-GaN clusters are deliberated in terms of highest occupied molecular orbital (HOMO) and lowest unoccupied molecular orbital (LUMO). The energy gap between HOMO and LUMO is a significant quantity as most of the material's behaviors, such as intrinsic conductivity, optical transitions, or electronic transitions, depend on it. Also, it indicates the ability of electrons to jump from occupied orbital to unoccupied orbital. The calculated values of HOMO-LUMO energy gaps of pure GaN and Al-GaN clusters are shown in tables 1 and 2, and the size dependence of the HOMO-LUMO energy gap diagram and the DOS for most stable configurations in cube, ring, rhombus and sheet structures are depicted in figs. 4 and 5. As can be seen from tables 1 and 2, the gaps for undoped and doped clusters vary from 0.95 to 6.02 eV, 0.91–2.87 eV, respectively. Some of these clusters yet exhibit semiconducting properties as for bulk GaN band gap being 3.43 eV [50–53]. Our calculated values of the HOMO-LUMO

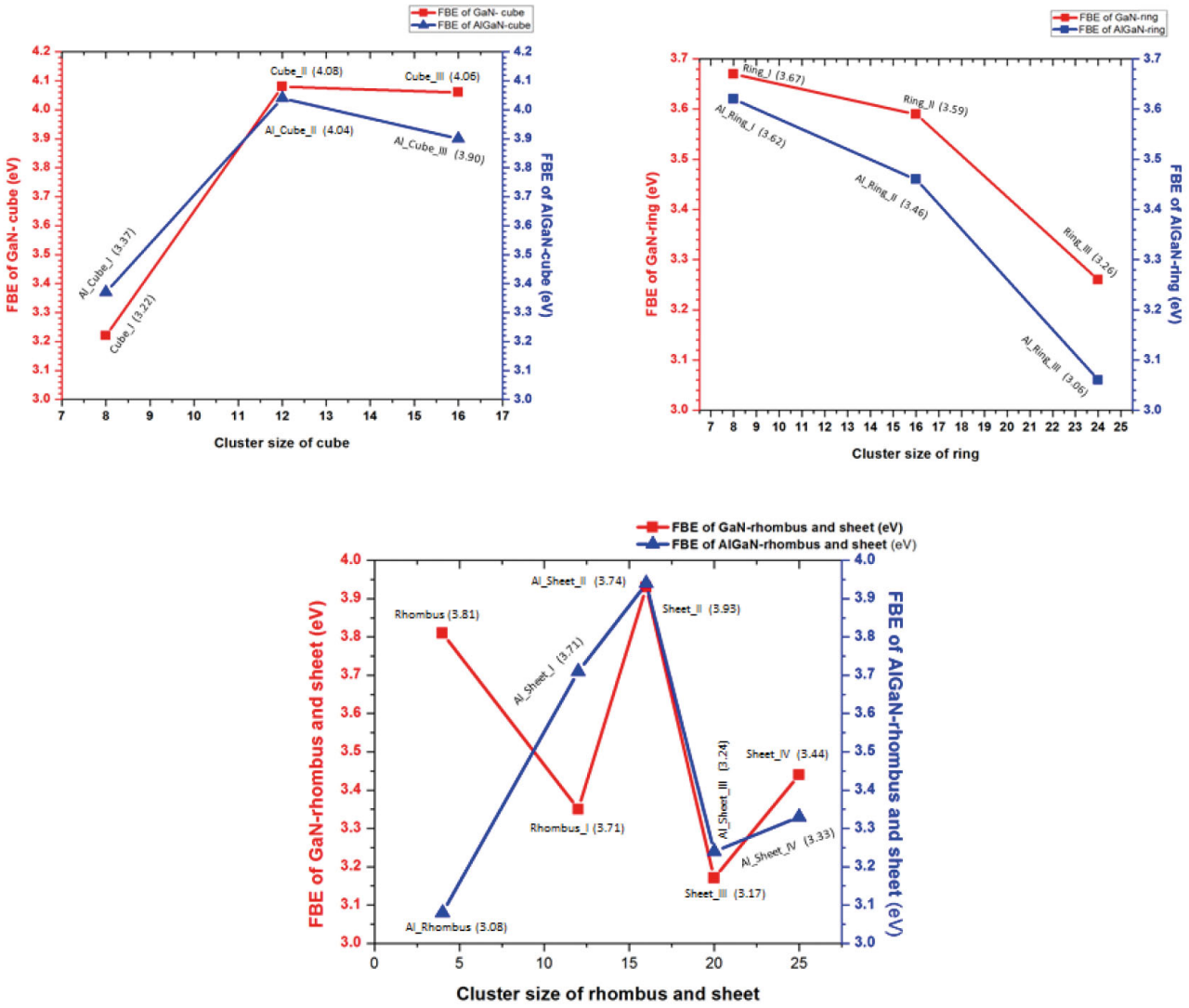

Fig. 3. Variation of final binding energy (FBE) per atom with a cluster size of GaN and Al-GaN.

gap for GaN ring-I, cube-I, and cube-II are 2.09, 1.21, and 3.35 eV, respectively, which is close to the published result for ring-I 1.67 eV [46], 1.68 eV [49], 2.41 eV [45], cube-I 0.82 eV [49] and cube-II 1.70 eV [49], 2.60 eV [46]. We further see that the HOMO-LUMO gaps for doped GaN present a similar trend to that observed for corresponding pure GaN clusters, except for sheet structures (fig. 4). The gap modified greatly in ring structures after doping as compared to the corresponding undoped structure, while it is reduced in cube structures. Also, their relative differences for rings are smaller than those for cubes. For sheet-like structures, on the other hand, it shows a zig-zag behavior with the clusters size. The minimum value of the HOMO-LUMO gap is observed for the Al-cube-III (0.91 eV) structure and maximum for the Al-ring-III (2.87 eV). The higher band gap restricts the movement of the electron from HOMO to LUMO, which will not robustly take part in electrical conduction and chemical reaction. In other words, these clusters

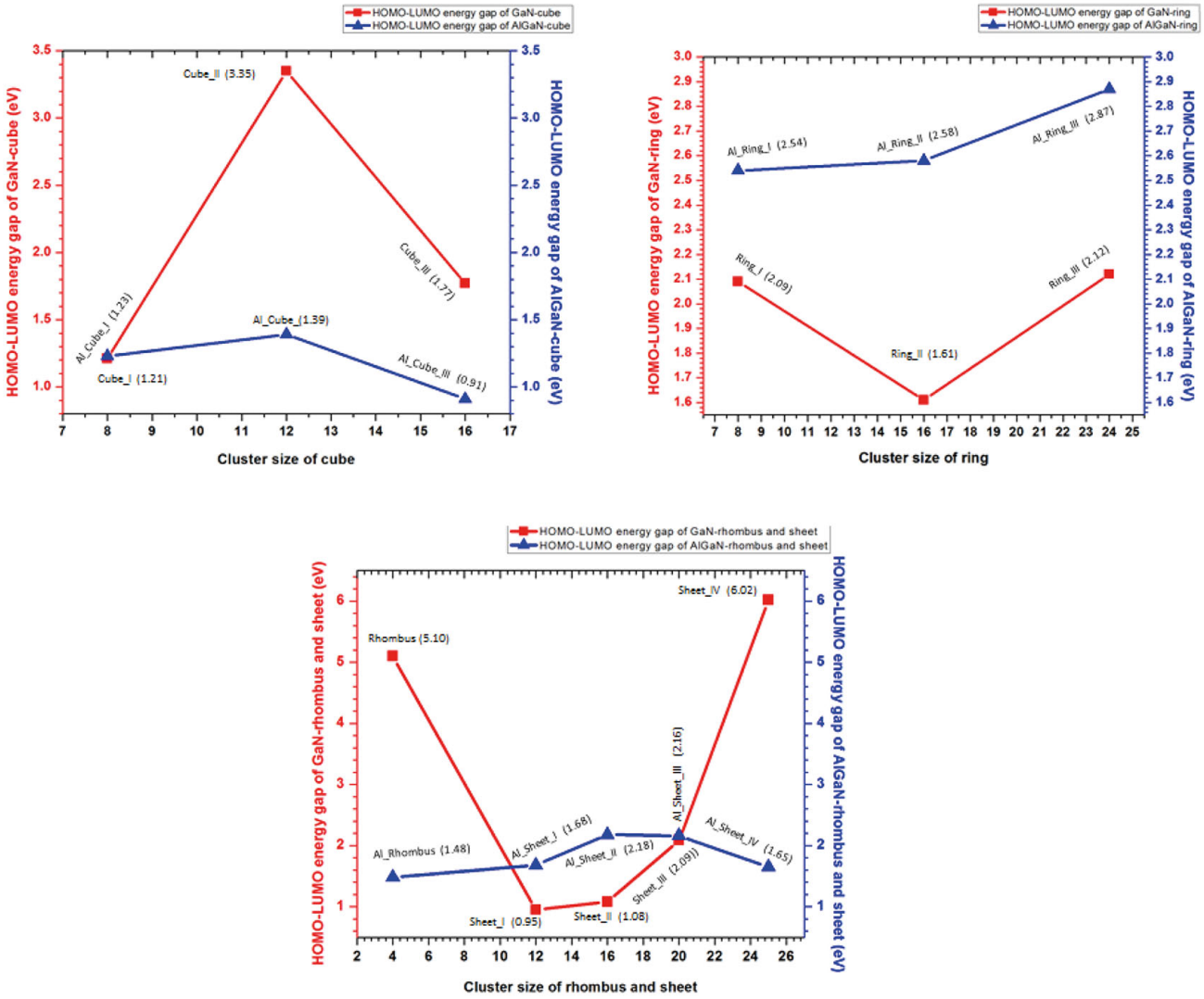

Fig. 4. Variation of the HOMO-LUMO gap with cluster size of GaN and Al-GaN.

presumably have lower chemical stabilities. The clusters having minimum value of energy gap are expected to be more reactive than those with large energy gap; thus doping in nanocluster could be more advantageous. Figure 5 reveals that in both cases, some of the GaN and Al-substituted GaN clusters exhibit an alpha and a beta band of energy due to the spin of electrons. The study of the higher atomic structure of GaN and Al-GaN clusters reveal a better location of charge near the Fermi level. The proximity of charge near the Fermi level with small HOMO-LUMO gap will enable easier movement of electrons to the valence band. Furthermore, it should be noted that more states are seen in the virtual orbital that may be caused by the introduction of the atom which gives rise to localization of charge in the virtual orbital.

Cube II (Ga_6N_6)

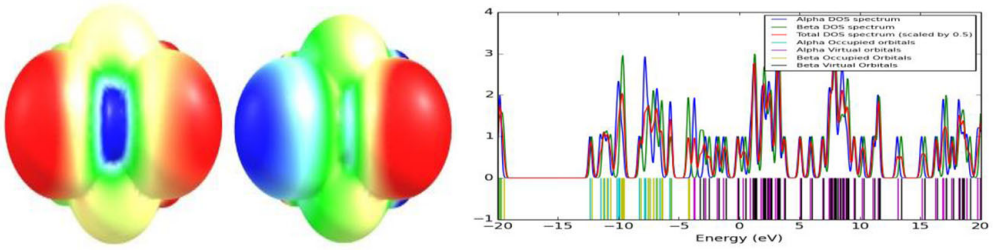

HOMO LUMO

E_g=3.35 eV

Al_Cube II ($Ga_3Al_3N_6$)

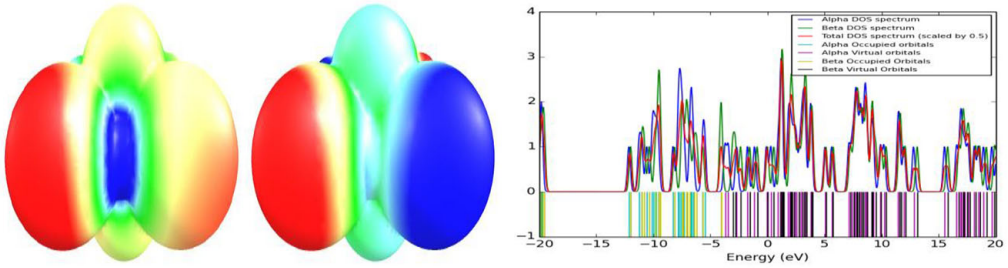

HOMO LUMO

E_g= 1.39 eV

Ring I (Ga_4N_4)

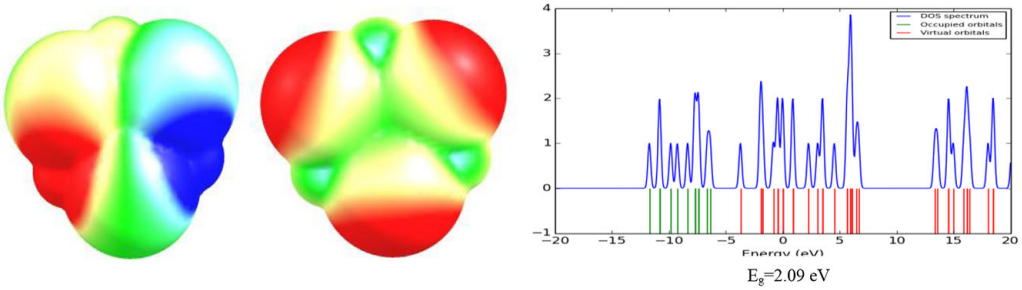

HOMO LUMO

E_g=2.09 eV

Al_Ring I ($Ga_2Al_2N_4$)

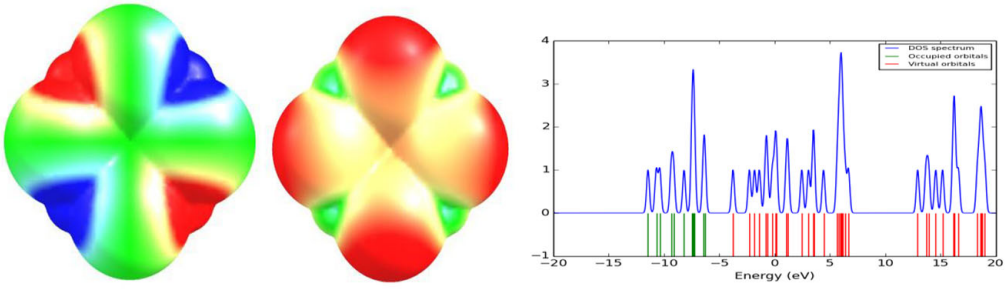

HOMO LUMO

E_g= 2.54 eV

Fig. 5. DOS, HOMO_LUMO energy diagram for most stable configurations of the cube, ring, rhombus and sheet of GaN and Al-GaN clusters.

Rhombus (Ga_2N_2)

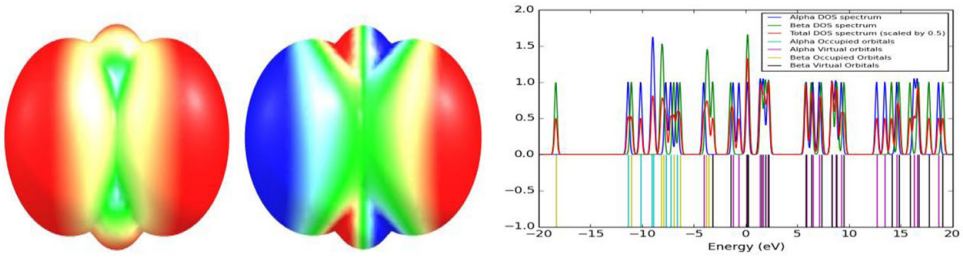

HOMO LUMO

E_g= 5.10 eV

Al_Rhombus ($Ga_1Al_1N_2$)

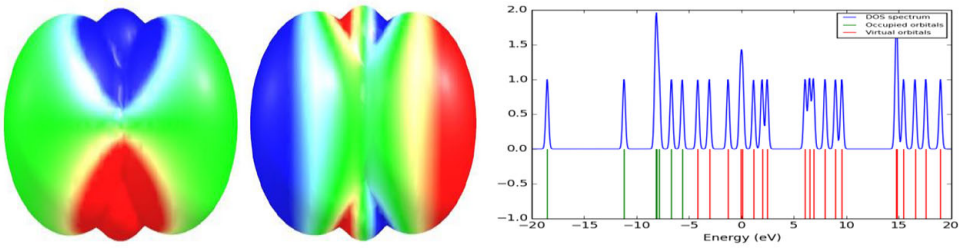

HOMO LUMO

E_g= 1.48 eV

Sheet II (Ga_8N_8)

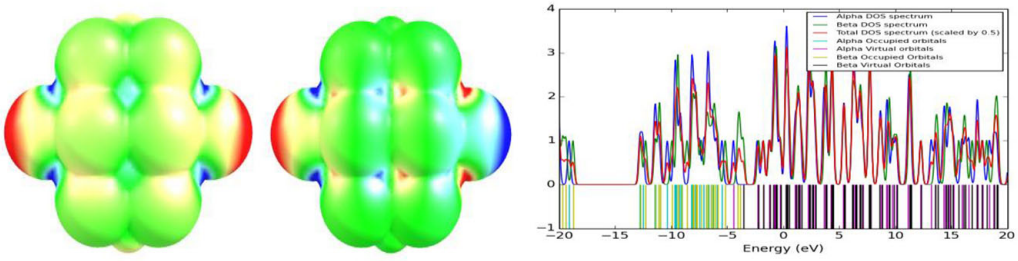

HOMO LUMO

E_g= 1.08 eV

Al_Sheet II ($Ga_4Al_4N_8$)

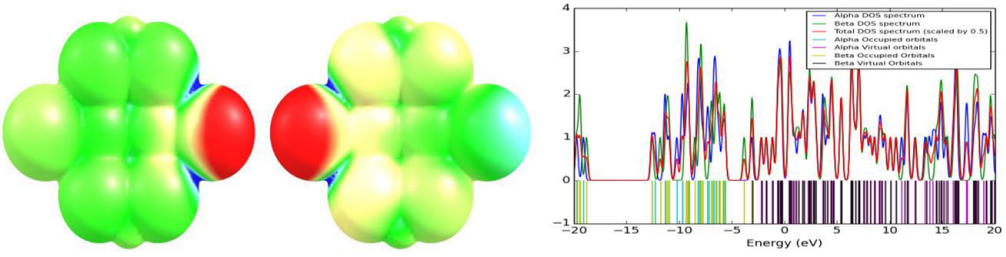

HOMO LUMO

E_g= 2.18 eV

Fig. 5. Continued.

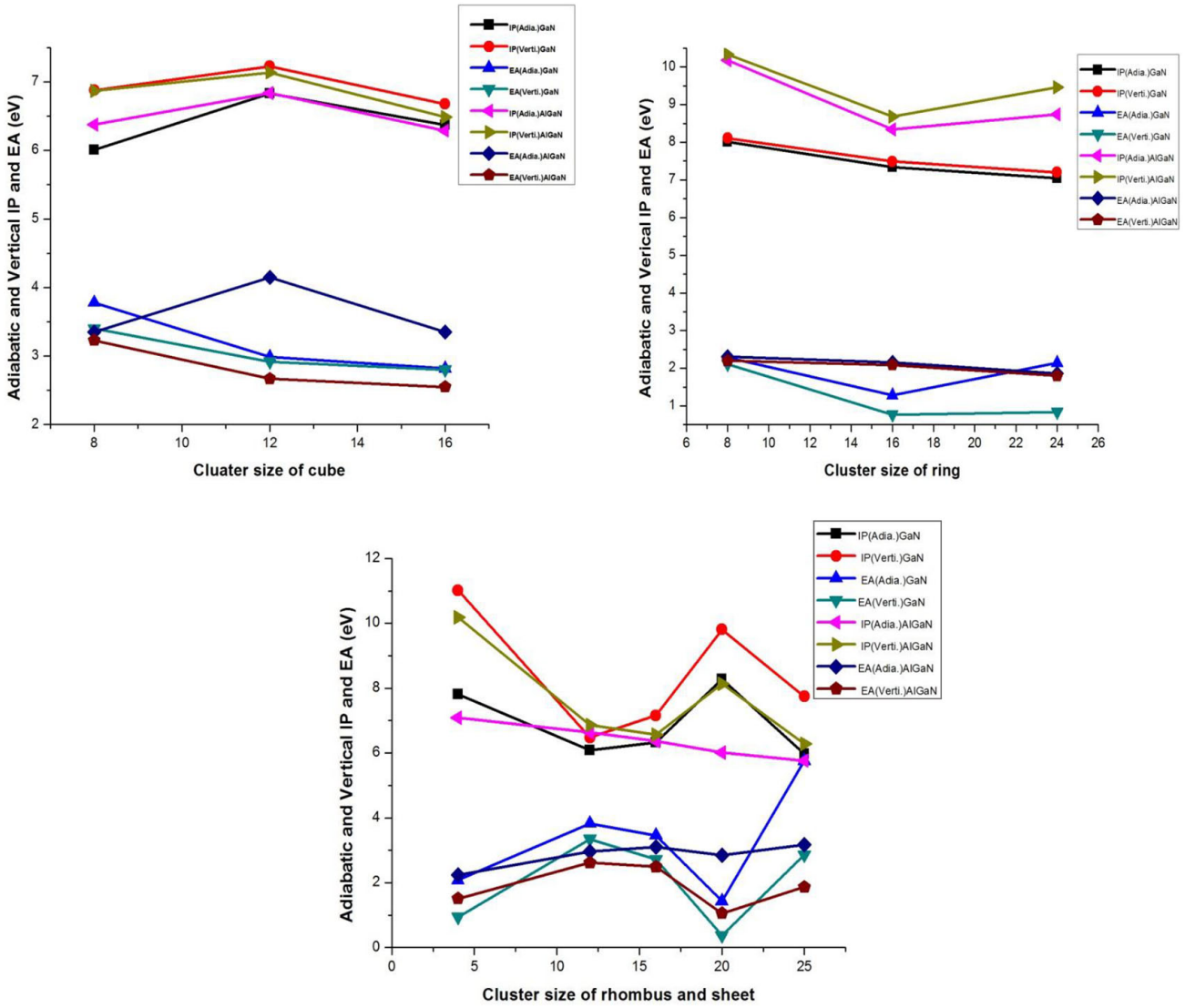

Fig. 6. Variation of adiabatic, vertical IP and EA with cluster size of GaN and Al-GaN clusters.

3.3 Ionization potential and electron affinity of Al-doped GaN clusters

The ionization potential (IP) is defined as the amount of energy needed to take out one electron from the cluster while the electron affinity (EA) is the amount of energy released when an electron is attached to the cluster [54]. We have evaluated the value of ionization potential (IP) and electron affinity (EA), as the energy difference between neutral cluster and cation/anion, respectively, as

$$\text{IP} = \text{Energy of neutral cluster} - \text{Energy of cation cluster}$$

and

$$\text{EA} = \text{Energy of neutral cluster} - \text{Energy of anion cluster.}$$

The variation of IPs and EAs as a function of the cluster size [55,56] for different clusters of GaN and Al-GaN is reported in fig. 6, and the corresponding data are shown in fig. 6. As can be seen in fig. 6, the structural relaxation upon ionization leads to lowering the IP values. Among GaN cubes and rings, the maximum value of adiabatic (vertical) IP is 8.01(8.11) eV for the ring-I configuration, and the minimum value is 6.01(6.88) for cube-I, which is very close to vertical IP 8.09 and 7.62 eV [49], respectively. Our computed EA 3.78(3.40) and 1.28(0.77) eV are close to previous reports on vertical EA 3.08 eV [49] for cube-I and ring-II and for the bulk 3.1 eV [52]. Likewise, in the case of Al-GaN cube and ring configurations, the maximum and minimum IPs 10.18(10.33) and 6.29(6.49) may be seen for Al-GaN ring-I and Al-cube-III, respectively, whereas the maximum and minimum values of EA are computed to be 4.15(2.67) and 1.86(1.80) for Al-cube-II and Al-ring-III, respectively. Thus, overall, $Ga_{12}N_{13}$ and $Ga_6Al_6N_{13}$ sheet configurations

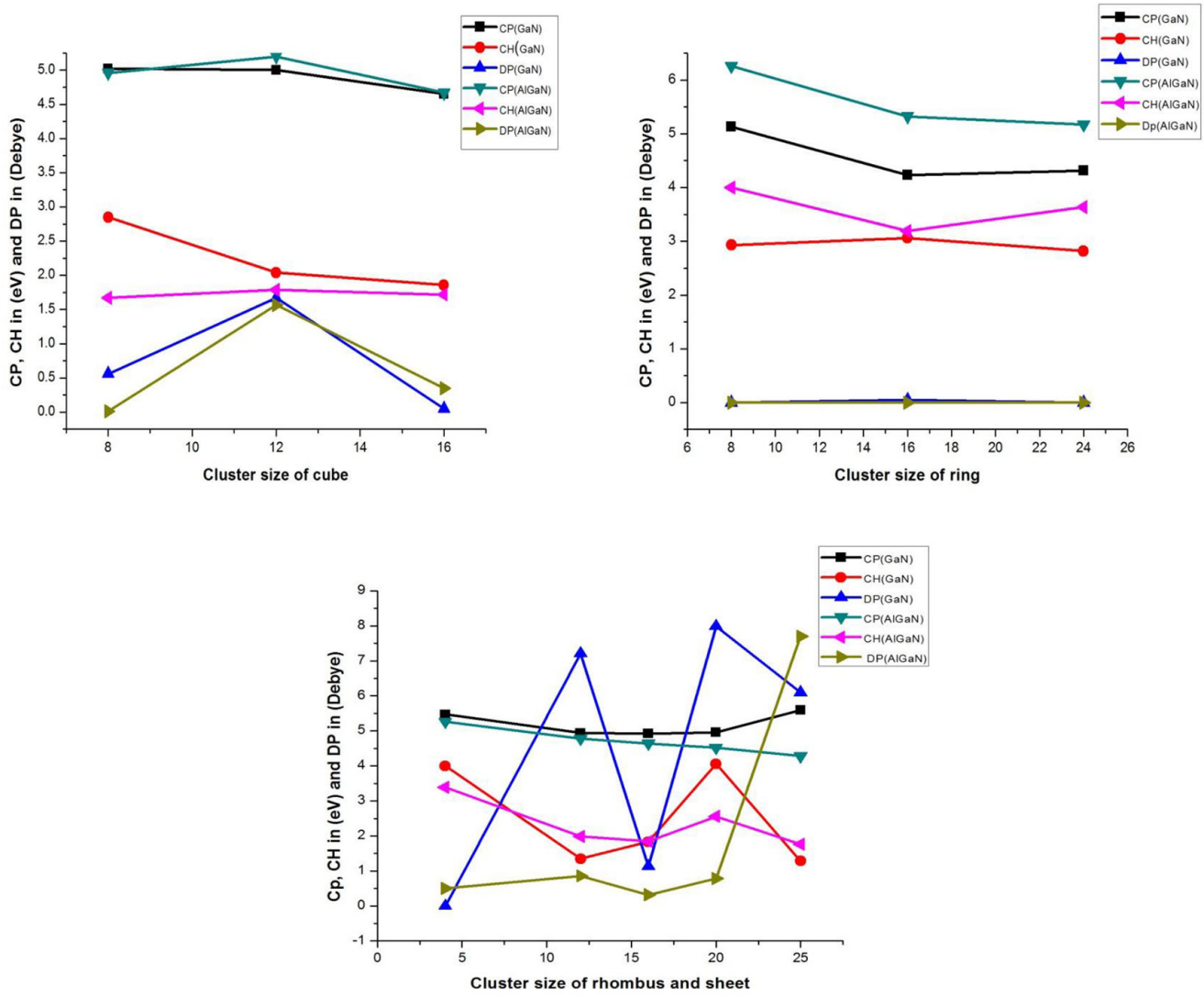

Fig. 7. Variation of chemical potential (CP), chemical hardness (CH) and dipole moment (DP) with cluster size.

tend to ionize relatively easier than the other clusters. Moreover, the IP cluster values are much smaller than the IP values of the N atom (14.54 eV) and the N_2 molecule (15.45 eV, experimental value 15.58 eV) [57–59]. Thus, the results further support the association of the ionized electron to the metallic atoms in the considered nitride clusters. It is noteworthy that replacing Ga atoms in the GaN cluster with Al, to give Al-doped clusters, results in the approximate values of VIPs for most clusters except for $Ga_2Al_2N_4$ and $Ga_6Al_6N_{12}$, which have larger VIPs than the corresponding GaN clusters; whereas the $Ga_5Al_5N_{10}$ and $Ga_6Al_6N_{13}$ have smaller VIPs than the corresponding GaN clusters.

Figure 6 shows that IPs and EAs of different GaN ring and cube structures vary arbitrarily with increasing the number of the atom. In the case of GaN cube and ring structures, increasing the number of atoms results in a gradual decrease in the IP values. For Al-GaN clusters, the observed maximum adiabatic (vertical) IP for Al-GaN ring-I, which is 10.18(10.18) eV, has number of atoms 8 and the minimum IP, observed as GaN 6.01(6.88) eV, has the same number of atoms. The increase in the Al atom causes a decrease in energy due to the geometry position of atoms. The behaviour of IP for GaN and Al-GaN cube and ring clusters is a zigzag one. Among the pure GaN rhombus and sheet configurations, Ga_2N_2 seems to be a magic number cluster with relatively high stability, which is confirmed by its high HOMO-LUMO gap (5.10 eV) and high IP (11.02 eV), as well as low EA (0.94 eV).

The high value of EA indicates that the clusters have an active contribution in chemical reactions. Among pure and Al-GaN clusters, Al-GaN cube-II clusters have a high value of EA (4.15 eV), and hence they will be more reactive among all the configurations of GaN; thus the Al-substituted cubic cluster is suitable for chemical sensors. For the sheets, the maximum and minimum adiabatic (vertical) values are 5.76(2.86) and 1.43(0.37), respectively, reflecting that the GaN sheet IV is also more reactive. On the basis of EA values, it is predicted that ring-II and sheet-III structures, owing to low-value EA, are an unfavorable structure for chemical sensors.

3.4 Chemical potential and chemical hardness of GaN and Al-substituted GaN clusters

Another useful quantity is the chemical potential and chemical hardness which are computed by using the formulas below:

$$\text{Chemical potential} = -[\text{IP value} + \text{EA value}]/2$$

and

$$\text{Chemical hardness} = [\text{IP value} - \text{EA value}]/2.$$

Chemical hardness has been established as an electronic quantity, which in many cases may be used to characterize the relative stability of molecules and aggregate through the principle of maximum hardness. Figure 7 shows the variation of chemical potential (CP), chemical hardness (CH) and dipole moment (DP) with cluster size of cube, ring, rhombus and sheet structures of GaN and Al-GaN.

From fig. 7, it can be seen that the maximum chemical potential for pure GaN cube and ring clusters is 5.13 eV for ring-I, which has 8 atoms and the minimum value is 4.23 eV, and has 16 atoms for ring-I and ring-II clusters; in the case of Al-GaN ring and cube clusters, a higher (6.26 eV) and a lower value (4.67 eV) for Al-cube-II, Al-cube-III, respectively is seen. On the other hand, in the case of GaN cube and ring configuration, the maximum and minimum values of chemical hardness are 3.06 eV and 1.86 eV, for ring-II and cube-III, having 16 atoms. For Al-GaN clusters, cube and ring configurations have the maximum and minimum values of chemical hardness 4 eV and 1.72 eV, respectively, for Al-ring-I and Al-cube-III configurations. The highest and lowest values of chemical potential and chemical hardness obtained for GaN rhombus and sheets configuration are 5.47 eV, 4.00 eV, and 5.26 eV, 4.92 eV for the sheet IV and sheet II, respectively. Our next analysis corresponds to the dipole moment of GaN-related clusters. From the calculated value of dipole moments of the cube configurations, the minimum value of dipole moment is 0.01 Debye and the higher value is 1.67 Debye in the Al-substituted and simple GaN clusters for the cube-I and cube II, respectively. The low value indicates that the atoms are well packed and ionic and electronic charges are uniformly distributed. In both cases of ring configurations, the dipole moment is found to be 0.00 Debye. This disappearance shows that their center of gravity of positive and negative charge distributions coincide. In the case of sheet configurations of GaN clusters, the maximum value of dipole moment 7.90 Debye for sheet-IV is attributed greater asymmetric distribution or larger mismatch of charges present in the cluster and a minimum value of dipole moment is found to be 0.32 Debye for Al-doped sheet-II. In summary, we observed that values of dipole moment for the Al-substituted clusters are lower than the pure GaN clusters. The obtained value of dipole moment of clusters in different configurations varies with either increasing the number of atoms or substitution of Al atom, which may be due to having different geometrical structures of gallium nitride.

3.5 Vibrational analysis

The vibrational behavior of pure GaN and Al-substituted clusters is analyzed in this section. A complete list of the lowest values of frequency with corresponding Raman and IR activity is displayed in table 3. Possible modes of vibration of each configuration of GaN and Al-GaN clusters are depicted explicitly as stretching, bending, wagging and twisting, etc. The absence of imaginary frequency in table 3 implies that all configurations have local minima, *i.e.* they are stable and local minimum energy structures on the potential energy surface. We found that the molecules, which are Raman active at lowest frequency, range from 15 cm^{-1} to 251 cm^{-1}, and from 22 cm^{-1} to 154 cm^{-1}, for GaN and Al-GaN, respectively wherein the value (137 cm^{-1}) for GaN-cube-II is close to that of experimental results (144 cm^{-1} and 145 cm^{-1}) for GaN thin film and nanowire [60].

It is worth noting that at most of the frequencies, the clusters have strong Raman activity (weak or zero IR intensity), while at one frequency, the activity of mode is just reversed. For some frequencies, infrared and Raman activities are both significantly strong: there exists a vibration mode for both undoped and doped ring-I configuration, where neither shows IR activity nor Raman. One reason for this may be the significant figure of calculations. As listed in table 3, for the cubic configuration of GaN and Al-GaN cluster, Raman activity and IR intensity at the lowest frequency appear due to the bending and stretching mode of vibration and are showing an increasing behavior with an increase in the clusters size. On the other hand, ring configurations of GaN and Al-doped GaN have a number of vibrational frequencies; among them, the lowest frequency is 60 and 69 cm^{-1}, respectively, and because of the centrosymmetric D_{2h} point group, all modes are Raman-active without IR activity, except for the undoped ring-II configuration having non-zero dipole moment. The mode of vibrations is scissoring for the lowest frequency of GaN and Al-GaN. Thus, Raman activity and IR intensities are displaying variations with nanoclusters size, shape and stacking mode. Furthermore, at lowest frequency, out of the considered structures, Raman activity is found to be maximum for cubic-III GaN, which indicates that it is more polarizable than the others, and maximum IR intensity for rhombus Al-GaN results is due to the large change of dipole moment, vibrational mode of cluster with no change of dipole moment is infrared inactive. The values of lowest frequencies are decreasing in undoped and doped except for GaN cube-II clusters with clusters size; the lowest frequencies being 16 and 22 cm^{-1} for GaN and Al-GaN, belong to

Table 3. IR intensities, Raman activity and the vibrational mode for the stable clusters of GaN and Al-GaN clusters. Frequencies are in cm^{-1}, Raman activities in $Å^4$/amu and intensities are in km/mol.

Structures	Lowest frequency	Raman activity	IR intensity	Vibrational mode
Ga_4N_4 (Cube I)	91	21.43	4.46	Twisting
Ga_6N_6 (Cube II)	137	14.08	0.68	Twisting
Ga_8N_8 (Cube III)	16	187.96	48.89	Bending
$Ga_2Al_2N_4$ (Al_Cube I)	154	70.93	5.35	Diagonal stretching
$Ga_3Al_3N_6$ (Al_Cube II)	130	24.90	0.69	Stretching
$Ga_4Al_4N_8$ (Al_Cube III)	111	14.31	0.35	Stretching
Ga_4N_4 (Ring I)	72	0.00	0.00	Rocking
Ga_8N_8 (Ring II)	71	9.78	0.00	Scissoring
$Ga_{12}N_{12}$ (Ring3)	60	6.04	0.00	Scissoring
$Ga_2Al_2N_4$ (Al_Ring I)	89	0.00	0.00	Rocking
$Ga_4Al_4N_8$ (Al_Ring II)	82	10.29	0.04	Scissoring
$Ga_6Al_6N_{12}$ (Al_Ring III)	69	5.41	0.00	Scissoring
Ga_2N_2 Rhombus	251	40.01	0.00	Wagging
$Ga_1Al_1N_2$ (Al_ Rhombus)	124	2.72	106.91	Wagging
Ga_6N_6 (Sheet I)	54	13.98	0.00	Scissoring
Ga_8N_8 (Sheet II)	21	14.90	0.00	Scissoring
$Ga_{10}N_{10}$ (Sheet III)	44	4.93	0.02	Rocking
$Ga_{12}N_{13}$ (Sheet IV)	15	5.07	0.13	Rocking
$Ga_3Al_3N_6$ (Al_Sheet I)	55	4.17	1.54	Wagging
$Ga_4Al_4N_8$ (Al_Sheet II)	43	2.14	0.00	Scissoring
$Ga_5Al_5N_{10}$ (Al_Sheet III)	29	2.25	0.10	Scissoring
$Ga_6Al_6N_{13}$ (Al_Sheet IV)	22	6.14	0.13	Twisting

bending and twisting mode, which requires less energy than the other modes of vibration. For the undoped and doped cluster displaying the same configuration, the lowest vibrational frequency for the undoped cluster is found somewhat smaller than the doped one, which in agreement with the lower bond length exhibited by the doped clusters.

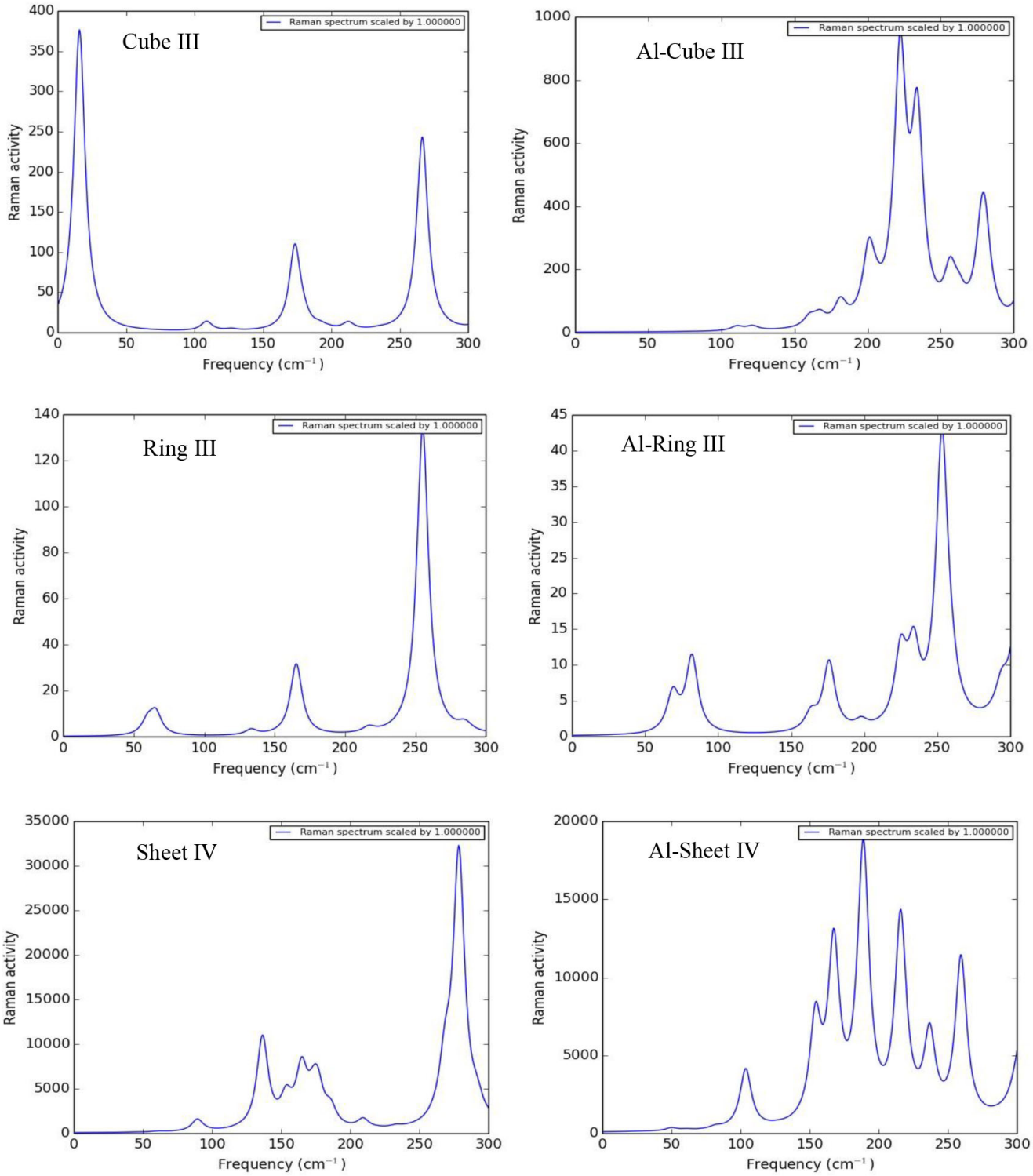

Fig. 8. Raman Activity for the most stable cube, ring, and sheet of GaN and Al-GaN clusters.

It is a cumbersome and difficult task to find out each of the modes due to vibrational complexity and hence we considered configurations of cube, ring, and sheet of pure and doped GaN clusters having lowest frequency in their respective family and illustrated the results of Raman and IR activity in figs. 8 and 9, respectively, wherein IR and Raman spectra are spanned through 14 to 300 cm^{-1}, and each frequency is related to a specific bending or stretching mode of vibration. Only a few peaks of absorption appear due to substantial coupling between vibrational modes with increasing number of atoms/subunits in the clusters. Triple cube configuration of GaN has five distinguished Raman-active vibrational modes with the most strong band at the lowest frequency 16 cm^{-1}, whereas other smaller peaks

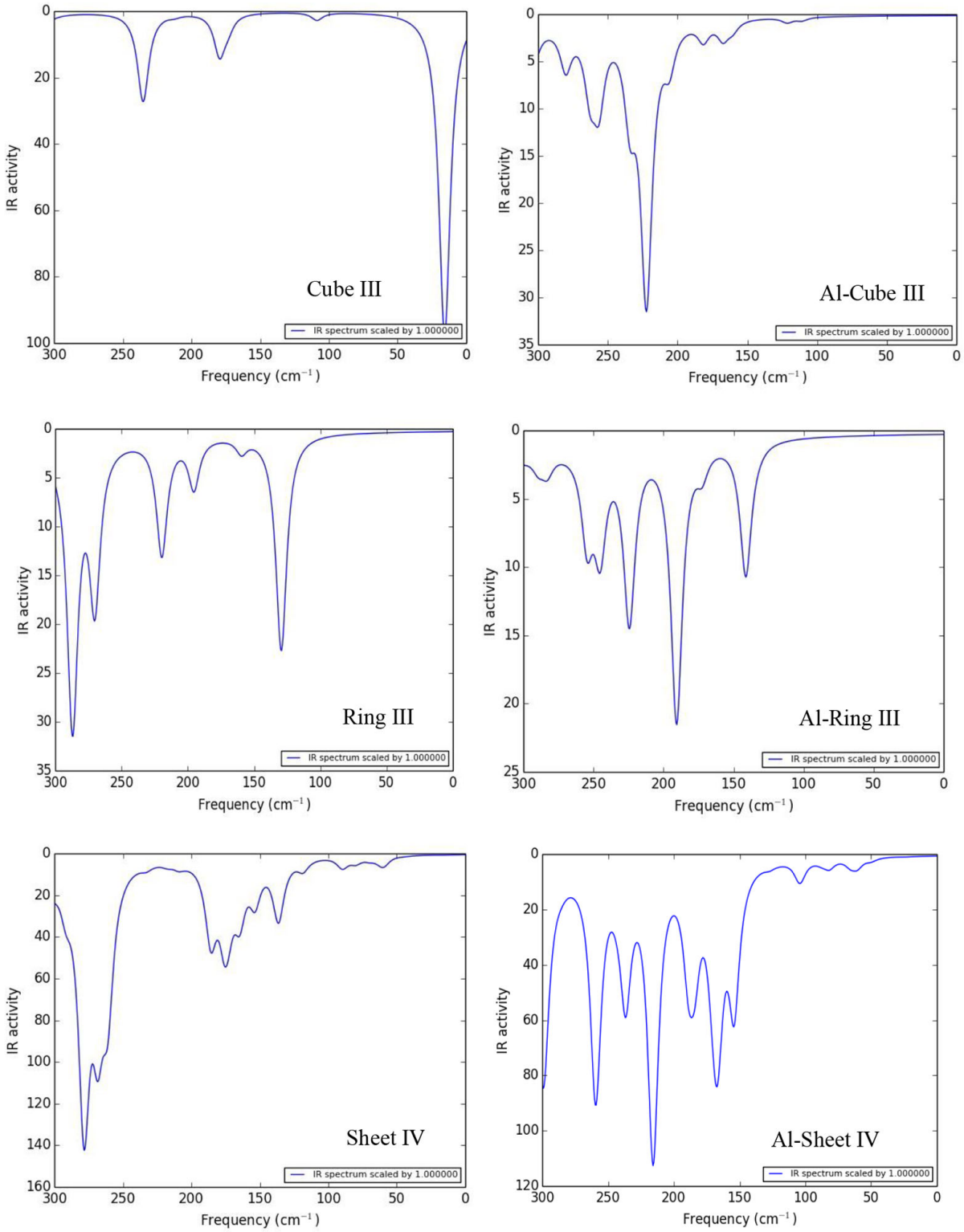

Fig. 9. IR Activity for the most stable cube, ring, and sheet of GaN and Al-GaN cluster.

are present towards high-frequency side. For the ring-III (tubular) structure, we observe six Raman intensity peaks, while the sheet configuration has 8 peaks; the highest peaks correspond to frequency 254 cm^{-1}, 277 cm^{-1}, respectively lying in the mid-IR region. It is interesting to see that there is an increase in the frequency (blue shift) of most intense Raman mode with an increase in the number of atoms and shape of the cluster. Looking at the IR intensity of structures considered, except for sheet configuration, an equal number of Raman peaks are observed in their spectra with the most prominent peaks at 16 cm^{-1}, 288 cm^{-1} and 279 cm^{-1}, respectively. Figures 8 and 9 clearly show that

with respect to Raman and infrared activity, the modes present a dependence on the stacking mode and increase in units of cube and rhombus. Also, clusters undergo a distinctive change in their vibrational spectra after substitution of Al atoms to the pure one; the variation of peak positions and intensity along with the appearance of additional bands in the Raman modes and IR spectra may be clearly seen. This may be due to various types of intermolecular interactions and their extent in mixtures with varying the Al content. Our calculated Raman spectra can be useful for analytical purposes and contribute significantly to spectral interpretation, and vibrational assignments also can provide methodical guidance for future measurements.

4 Conclusions

In this work, stacks of rhombus, rings, and cubes of GaN and Al-substituted GaN clusters are constructed and their structural stability, HOMO-LOMO energy gap, ionization potential, electron affinity, chemical potential and chemical hardness, dipole moment, IR and Raman spectra have been studied by DFT theory. The structures yield some interesting trends, and a strong size, shape and doping dependence of properties has been observed. An analysis of binding energies shows that final binding energy, even the numbers of atoms are same; varies with stacking mode or with an increase in the Al atoms. For all compositions and size of clusters, the cube type (GaN-cube-II) structure is found as the most stable structure.

A major variation in electronic properties is observed in different structures, few of them exhibit large band gaps and ionization potentials. Dopant Al considerably modifies the HOMO-LUMO energy gap of cubes and sheets. We observed that values of dipole moment are zero in the case of Al-GaN ring, whereas in different configurations, fluctuates randomly with either increasing the number of atoms or substitution of Al atom. A comparison of ionization potential and electron affinity reveals that Al doped cube-II clusters is most suitable for chemical sensors due to its high value of EA (4.15 eV). Furthermore, the doping modifies remarkably the vibrational spectra of nanoclusters. An important finding of the present study is that the linear stacking of stable units of the ring may undergo to GaN nanowires. Similarly, sideways stacking of several units of rhombus structure results in nanotube formation. Thus, using the coalescence of GaN nanocluster building blocks, nanomaterials with different dimensionalities can be constructed whose properties may be tailored through the choice of size, composition and doping, thereby providing a viable alternative pathway of creating materials using nanoclusters as building blocks.

The first author is highly thankful to the University Grant Commission (UGC), New Delhi, India for the financial support.

References

1. J.T. Hu, T.W. Odom, C.M. Lieber, Acc. Chem. Res. **32**, 435 (1999).
2. Y.H. Li, H.H. Pan, P.S. Xu, Acta Phys. Sin. **54**, 317 (2005).
3. A.H. Bar-Ilan, S. Zamir, O. Katz, B. Meyler, J. Salzman, Mater. Sci. Eng. A **14**, 302 (2001).
4. H.P. Zhao, G.Y. Liu, N. Tansu, Appl. Phys. Lett. **97**, 131114 (2010).
5. R.M. Farrell, P.S. Hsu, D.A. Haeger, K. Fujito, S.P. DenBaars, J.S. Speck, S. Nakamura, Appl. Phys. Lett. **96**, 231113 (2010).
6. H. Morkoc, S. Strite, G.B. Gao, M.E. Lin, B. Sverdlov, M. Burns, J. Appl. Phys. **76**, 1363 (1994).
7. W. Martienssen, H. Warlimont (Editors), *Springer Handbook of Condensed Matter and Materials Data* (Springer-Verlag, Berlin Heidelberg, 2005).
8. H. Morkoc, S. Strite, G.B. Gao, M.E. Lin, B. Sverdlov, M. Burns, J. Appl. Phys. **76**, 1363 (1994).
9. X.H. Wang, B.K. Chang, Y.J. Du, J.L. Qiao, Appl. Phys. Lett. **99**, 042102 (2011).
10. Y. Zhang, J. Singh, J. Appl. Phys. **85**, 587 (1999).
11. S.J. Pearton, J.C. Zolper, R.J. Shul, F. Ren, *GaN: Defect and Device Issues* (1998).
12. S. Nakamura, T. Mukai, M. Senoh, Appl. Phys. Lett. **64**, 1687 (1994).
13. P.N. Favennec, H.L. Haridon, M. Salvi, D. Moutonnet, Y. Le Guillou, J. Electron. Lett. **25**, 718 (1989).
14. Y.F. Wu, B.P. Keller, S. Keller, D. Kapolnek, P. Kozodoy, S. Denbaars, U.K. Mishra, J. Appl. Phys. Lett. J **69**, 1438 (1996).
15. R.J. Trew, M.W. Shin, V. Gatto, J. Solid-State Electron. **41**, 1561 (1997).
16. R. Gaska, M.S. Shur, A.D. Bykhovski, A.O. Oriov, G.L. Srider, J. Appl. Phys. Lett. **74**, 287 (1999).
17. E.R. Glaser, M. Murthy, J.A. Freitas, D.F. Storm, L. Zhou, D.J. Smith, Physica B **401**, 327 (2007).
18. F. Iskandar, T. Ogi, K. Okuyama, Mat. Lett. **60**, 73 (2006).
19. S. Jantrasee, S. Pinitsoontorn, P. Moontragoon, J. Electron. Mater. **43**, 1689 (2014).
20. P. Moontragoon, N. Vukmirovic, Z. Ikonic, P. Harrison, Microelectron. J. **40**, 483 (2009).
21. I. Akasaki, H. Amano, Y. Koide, K. Hiramatsu, N. Sawaki, J. Cryst. Growth **98**, 209 (1989).
22. P. Vennegues, M. Leroux, S. Dalmasso, M. Benaissa, P.D. Mierry, P. Lorenzini, B. Damilano, B. Beaumont, J. Massies, P. Gibart, Phys. Rev. B **6823**, 5214 (2003).

23. I. Takeshi, Y. Shigeru, I. Yoshifumi, M. Teruaki, J. Cryst. Growth **1**, 274 (2005).
24. E. Pournamdari, M. Khaleghian, J. Phys. Theor. Chem. **8**, 199 (2011).
25. S. Pezzagna, P. Vennegues, N. Grandjean, J. Massies, J. Cryst. Growth **269**, 249 (2004).
26. Y.J. Du, B.K. Chang, J.J. Zhang, X.H. Wang, B. Li, M.S. Wang, Optoelectron. Adv. Mat. **5**, 1050 (2011).
27. Ji Yan-Jun, Du Yu-Jie, Wang Mei-Shan, Chin. Phys. B **22**, 117103 (2013).
28. S.N. Lee, J.K. Son, T. Sakong, W. Lee, H. Paek, E. Yoon, J. Kim, Y.H. Cho, O. Nam, Y. Park, J. Cryst. Growth **272**, 455 (2004).
29. A.C. Reber, S.N. Khanna, J.S. Hunjan, M.R. Beltran, Eur. Phys. J. D **43**, 221 (2007).
30. S. Karthikeyan, E. Deepika, P. Murugan, J. Phys. Chem. C **116**, 5981 (2012).
31. K. Holczer, O. Klein, S. Huang, R.B. Kaner, K. Fu, R.L. Whetten, F. Diederich, Science **252**, 1154 (1991).
32. A.F. Hebard, M.J. Rosseinsky, R.C. Haddon, D.W. Murphy, S.H. Glarum, T.T.M. Palstra, A.P. Ramirez, A.R. Kortan, Nature **350**, 600 (1991).
33. M.J. Rosseinsky, A.P. Ramirez, S.H. Glarum, D.W. Murphy, R.C. Haddon, A.F. Hebard, T.T.M. Palstra, A.R. Kortan, S.M. Zahurak, A.V. Makhija, Phys. Rev. Lett. **66**, 2830 (1991).
34. P. Jena, S.N. Khanna, B.K. Rao, Mater. Sci. Forum **232**, 1 (1996).
35. A.W. Castleman Jr., S.N. Khanna, J. Phys. Chem. C **113**, 2664 (2009).
36. C.R.A. Catlow, S.T. Bromley, S. Hamad, M. Mora-Fonz, A.A. Sokol, S.M. Woodley, Phys. Chem. Chem. Phys. **12**, 786 (2010).
37. J. Kioseoglou, M. Katsikini, K. Termentzidis, I. Karakostas, E.C. Palour, J. Appl. Phys. **121**, 054301 (2017).
38. A. Szabo, N.S. Ostlund, *Modern Quantum Chemistry* (Dover Publications, New York, 1996).
39. M.J. Frisch, G.W. Trucks, H.B. Schlegel *et al.*, Gaussian 09, Revision D.01, Gaussian, Inc., Wallingford, Conn, USA (2009).
40. C. Lee, W. Yang, R.G. Parr, Phys. Rev. B **37**, 785 (1988).
41. A.D. Becke, J. Chem. Phys. **98**, 5658 (1993).
42. N.M. O'Boyle, A.L. Tenderholt, K.M. Langner, J. Comput. Chem. **29**, 839 (2008).
43. Chemcraft 1.8, `http://www.chemcraftprog.com`.
44. J.J. BelBruno, Heteroat. Chem. **11**, 281 (2000).
45. S. Bin, C. Pei-Lin, Chin. Phys. Lett. **9**, 1488 (2003).
46. A.K. Kandalam, M.A. Blanco, R. Pandey, J. Phys. Chem. B **106**, 1945 (2002).
47. L. Hedin, I.B. Lundqvist, J. Phys. C **4**, 2064 (1971).
48. T. Mattila, A. Zunger, J. Appl. Phys. **85**, 160 (1999).
49. Jijun Zhao, Baolin Wang, Xiaolan Zhou, Xiaoshuang Chen, Wei Lu, Chem. Phys. Lett. **422**, 170 (2006).
50. H.P. Maruska, J.J. Tietjen, Appl. Phys. Lett. **15**, 327 (1969).
51. W. Shan, J.W. Ager III, K.M. Yu, W. Walukiewicz, J. Appl. Phys. **85**, 8505 (1999).
52. B.S. Eller, Jialing Yang, R.J. Nemanich, J. Vac. Sci. Technol. A **31**, 050807 (2013).
53. S.P. Grabowski, M. Schneider, H. Nienhaus, W. Monch, R. Dimitrov, O. Ambacher, M. Stutzmann, Appl. Phys. Lett. **78**, 2503 (2001).
54. R.K. Shastri, D. Kumar, S.P. Goutam, R.R. Yadav, A.K. Yadav, Int. J. Adv. Res. **3**, 787 (2015).
55. R.K. Shastri, D. Kumar, D. Kumar, A.K. Yadav, Int. Adv. Res. J. Sci., Eng. Technol. **2**, 95 (2015).
56. X. Liao, X. Kuang, Eur. Phys. J. Plus **26**, 130 (2015).
57. D. Dundas, J.M. Rost, Phys. Rev. A **71**, 013421 (2005).
58. K.P. Huber, G. Herzberg, in *NIST Chemistry WebBook*, edited by P.J. Lindstrom, W.G. Mallard, Vol. **69** (NIST, 2003).
59. Y.K. Kim, Phys. Rev. A **66**, 012708 (2002).
60. M. Gopalakrishnan, V. Purushothaman, P.S. Venkatesh, V. Ramakrishnan, K. Jeganathan, Mater. Res. Bull. **47**, 3323 (2012).

Article

Advanced Science, Engineering and Medicine
Vol. 10, 1–5, 2018
www.aspbs.com/asem

A Density Functional Theory Study on Structural Stability and Electronic Properties of Co_xO_y $(x+y=4-12)$ Nanoclusters

Rajkamal Shastri, Nidhi Awasthi, Devesh Kumar, Anil Kumar Yadav*, Diptarka Roy, S. P. Goutam, and Anwesh Pandey

Department of Applied Physics, Babasaheb Bhimrao Ambedkar University, Lucknow 226025, UP, India

In this work, structural and electronic properties of cobalt oxide $(x+y=4-12)$ nanoclusters have been studied using first-principles calculations within the density functional theory (DFT). The effect of size, shape, and composition on properties was also investigated. DFT is one of the extensively employed methods for computing the structural and electronic properties of materials from first principle. The obtained results provide valuable information and reveal that the most stable configurations of different Co_xO_y nanoclusters depend on final binding energy and structures of nanoclusters. It was observed that the HOMO–LUMO gap is maximum for Co_xO_y $(x+y=10$ (A)) and binding energy is too maximum for the same configuration. Besides, dipole moment, point group symmetry and zero-point energy have also been computed for the clusters and analyzed.

Keywords: DFT, HOMO–LUMO, Structural, Stability, Electronic Properties, FBE.

1. INTRODUCTION

Transition metals in contact with oxygen atoms have been subject to intensive research in scientific realm due to their special physical, chemical, electronic, magnetic properties and wide applicability.[1–3] Among these, cobalt oxide (CoO) has engrossed special attention owing to its enormous potential for application in sensing, catalysis, electronics, electrode materials and magmatic materials.[4–6] An oxide of cobalt (CoO) is gray or blue–black powder; possessing three oxidation states[7] named as:

(i) Cobalt monoxide or cobalt [II] oxide (CoO, cubic crystal structure).
(ii) Cobalt [III] oxide (Co_2O_3).
(iii) Cobalt [II, III] oxide (Co_3O_4, cubic crystal structure).

These oxidation states of CoO and nanoscale cobalt systems have attracted a substantial attention due to their versatile properties which are most used in gas sensors, electrochromic devices, chemical and ceramic industries, and coloring glass etc.[7] In recent years, numbers of experimental and theoretical studies have been dedicated to clusters of metal oxide.[8–13] It has been reported that experimental data on cobalt oxide usually, belong to CoO.[14, 15] Xie and coworkers have studied the reaction of neutral cobalt oxide cluster (Co_mO_n) with NO, CO and C_2H_2[16] and found solid oxidation reaction dependency on cluster size. By performing the flow tube experiment Kapiloff et al. found that the response of smaller clusters of $(Co)_n^-$ (where $n=2-8$) with O_2 is maximum.[9] Dibble et al. observed photo dissociation mass spectra of Co_xO_y which show prominent stoichiometries of $x=y$.[17] DFT confirmed that CoO_4 possessed diperoxide $Co(O_2)$ structure and CoO_2 Co-dioxide structure.[18] Using DFT method Gutsev et al. has reported geometrical structure and electronic state of anion cobalt oxide cluster (CoO^-).[10] The stability of CoO clusters has been considered as a most attractive system which is revealed in many size-dependent properties like as abundance, ionization energies and dissociation energy.[19] In spite of the previous investigations on CoO, it is significant to extend the knowledge about structure, stability and electronic properties of these clusters for a better understanding of cluster reactivity and its role in sensing and catalysis.

Considering the above fact, we intended to study the cobalt oxide nanoclusters Co_xO_y $(x+y=4-12)$, their

*Author to whom correspondence should be addressed.

ISSN NO. 2320-5407

Journal homepage:http://www.journalijar.com

INTERNATIONAL JOURNAL OF ADVANCED RESEARCH

RESEARCH ARTICLE

Size dependent structural, electronic and vibrational properties of Cd_mS_n (m+n=2–6) nanoclusters: a DFT study

Rajkamal Shastri[1], Devesh Kumar[1], S.P.Goutam[1], R.R. Yadav[2] and Anil Kumar Yadav[1]*

1. Department of Applied Physics, Babasaheb Bhimrao Ambedkar University, Lucknow- 226025, U.P., India

2. Department of Physics, University of Allahabad, Allahabad- 211002, U.P., India

Manuscript Info

Manuscript History:

Received: 18 October 2015
Final Accepted: 26 November 2015
Published Online: December 2015

Key words:

Nanoclusters, Electronic, Vibrational, DFT, HOMO-LUMO, DOS, Binding energy, IP and EA

Corresponding Author

Dr. Anil Kumar Yadav

Abstract

We have performed first-principle calculations on the possible structures of cadmium sulphide Cd_mS_n (m+n=2–6) clusters; and equilibrium geometries, stabilities and electronic properties have been systematically investigated by density functional theory. Furthermore, binding energy (BE), highest-occupied and lowest-unoccupied molecular orbital (HOMO–LUMO) gap, density of states (DOS) have also been computed for Cd_mS_n nanoclusters. For the most stable structures, vibrational frequencies, infrared intensities (IR Int.), relative infrared intensities (Rel. IR Int.) and Raman scattering activities have been computed. The optimized geometries exhibit that the occurrence of the most stable configurations of the CdS nanoclusters is directly related to final binding energy. The nonlinear structured CdS_3 (rhombus) nanocluster with FBE 3.24 eV is found to be most stable as compared to others. We expect that findings of this study will stimulate further new experimental study on it.

INTRODUCTION

Nanoclusters represent the intermediate phase between small molecular species and the bulk state.The knowledge of atomic structure of nanoclusters is essential as their physical and chemical properties change significantly as size decreases from bulk level to nanoscale. Two basic reasons namely, quantum confinement effect and higher surface to volume ratio are viewed as vital for the dramatic change in their physical and chemical properties. To study the physical properties of such clusters it is indispensible to have an understanding about cluster evolution and possible structural changes that arise as a function of the nanocluster size because it can lead to the tailoring of novel materials with desirable properties [1]and sizes of the electronic devices have been reduced [2,3]. The basic idea behind structural study of the nanocluster is the assumption that it will follow structure with minimum energy. Therefore, global minimization techniques are used to predict the structure of nanoclusters. II–VI semiconductors such as ZnS, CdSe and CdTe are of enormous technological importance in different branches of science and technology. These semiconductors are widely used in solar cells, electronic sensors, hydrogen generation, photo catalysis and biological detections [4-9].Among the II–VI semiconductors, cadmium sulfide (CdS) is an important inorganic semiconductor owing to its unique photoelectric properties. It holds particle-size-dependent electronic spectrum [10,11] which could show the influence of size quantization effects. Its potential applications have been exhibited in many fields such as the nonlinear optics [12] the photo electro chemical cells and heterogeneous photo catalysis [13,14] etc.

There have been many experimental and theoretical studies using different computational approaches that are focused on the clusters of various compositions that have important and promising applications [3-8]. For binary clusters $(CdS)_n$, a number of theoretical studies have been performed to the search for the geometrical structure of the lowest total energy isomers [15-30]. It turns out from previous studies that the $(CdS)_n$ structures (n = 4–7)

ISSN (Online) 2393-8021
ISSN (Print) 2394-1588

International Advanced Research Journal in Science, Engineering and Technology
Vol. 2, Issue 11, November 2015

Quantum Chemical Studies on Zn_mO_n (m+n=2–8) Even Nanocluster's Stability

Rajkamal Shastri[1], Deep Kumar[2], Devesh Kumar[3] and Anil Kumar Yadav[4]

Research Scholar, Dept of Applied Physics, Babasaheb Bhimrao Ambedkar University, Lucknow, India[1, 2]

Associate Professor, Dept of Applied Physics, Babasaheb Bhimrao Ambedkar University, Lucknow, India[3]

Assistant Professor, Dept of Applied Physics, Babasaheb Bhimrao Ambedkar University, Lucknow, India[4]

Abstract: Present study shows a simple approach for constructing small computationally reasonable clusters and provides better understanding on structural motifs that stabilize the electronic structure of ZnO. The structural isomers of Zn_mO_n for m+n = (2-8), only even number, are optimized using Gaussian 09 program package with a B3LYP/LANL2DZ level basis set. In addition to this, other properties related to experimental data such as equilibrium geometry, point group symmetry, binding energy (BE), highest-occupied and lowest-unoccupied molecular orbital (HOMO–LUMO) gap, density of states (DOS), vibrational frequencies, infrared intensities (IR Int.) and Raman scattering activitieshave been computed for Zn_mO_n (m+n=2–8) nanoclusters using DFT theory. Our results show that the existence of the most stable configurations of the various ZnO nanoclusters depend on final binding energy (FBE) and the nonlinear structured nanoclusters are most stable. Also, the variation of HOMO–LUMO gap is decreasing and final binding energy (FEB) is increasing with clusters size. Finally, result would be very useful for new experimental studies on such significant nanoclusters.

Keywords: Nanoclusters, Final Binding Energy (FBE), ZnO, Density functional theory (DFT).

I. INTRODUCTION

Currently, when the world is surmounting on the pinnacle of technology, mostly on electronic equipment and thus creating quest to fabricate novel materials, which possess versatile properties. Semiconductors are very common material, which play very important role in the field of electronics and technology. Owing to need of speed and technology, many of the materials are being discovered and are using to serve the purpose. So there is requirement of such material to the world which possesses some unique properties such as larger band gap, higher electron mobility and higher breakdown field.

Zinc Oxide (ZnO) can be a better optional material. ZnO, II–VI group semiconductor, electronically play very important role due to the wide band gap. It has direct band gap energy of 3.37 eV and a large binding energy, 60 meV at the room temperature, very well satisfying the aforesaid properties [1]. ZnO is kind of semiconductor, which exhibit quantum confinement effect [2]. In recent time, ZnO-based low dimensional materials have produced great scientific interest because of their encouraging applications in the area of nanoscale optoelectronic devices, photo catalysis, photovoltaic solar cells, quantum devices, UV electronics, spintronic devices and sensor applications [3-10]. It has been commonly used in its polycrystalline form over hundred years in a wide range of applications and has emerged as a prominent material with potential optoelectronics, involve polycrystalline or nano structured ZnO [11-17].

The computational study may be a useful and dominant instrument for overcoming the existing disadvantages and predicting theoretical concept of such type of semiconductor material systems. Theoretical investigation of ZnO nano clusters will provide vital information for understanding the growth mechanisms of geometry and stability of ZnO nanoclusters having lowest energy of formation. Density functional theory (DFT) is a reliable theoretical method to study nanoclusters, particularly prediction of the structures that lie between molecular and bulk. This allows for much possible geometry and it is challenging to find a true global minimum energy structure. Though, there are a number of theoretical studies performed to investigate the properties of ZnO clusters [18–20],to best of our knowledge no precise quantum calculations have been performed, for considered nanoclusters using density function theory (DFT) calculations and basis set.

Therefore, the theoretical study of these systems is required. In present paper, ZnO nanocluster is get stabilized up to m+n=2-8, only for even nanoclusters for different structures and their structural stability, dipole moment, HOMO-LUMO energy gap, binding energy per atom, DOS, Ionization potential, Electron affinity and vibrational behaviour of these nanoclusters have been calculated and discussed.

II. COMPUTATIONAL TECHNIQUES

For optimization of ZnO nanocluster and to calculate their ground and excited state properties, we have used density functional theory. Structural optimizations (i.e. the geometrical parameters) have been done with no constraints imposed on the nanocluster structures during the optimization. We have constructed various possible structures for each ZnO cluster. For geometry optimization and vibrational analysis, B3LYP level of DFT method, Beck's three parameters with correlation function (Lee-Yang-Parr), and relativistic effective core potential with

ISSN (Online) 2393-8021
ISSN (Print) 2394-1588

International Advanced Research Journal in Science, Engineering and Technology
Vol. 2, Issue 11, November 2015

Structures Stabilities and Electronic Properties of GaAs Condensed Clusters

Deep Kumar[1], Rajkamal Shastri[2], Anil Kumar yadav[3], Devesh kumar[4]

Research Scholar, Dept of Applied Physics, School for Physical Sciences Babasaheb Bhimrao Ambedkar University, Lucknow, India[1, 2]

Assistant Professor, Dept of Applied Physics, School for Physical Sciences Babasaheb Bhimrao Ambedkar University, Lucknow, India[3]

Associate Professor, Dept of Applied Physics, School for Physical Sciences Babasaheb Bhimrao Ambedkar University, Lucknow, India[4]

Abstract: First-principal calculation are conceded out to appreciate the structural stability and electronic properties of nanotubes cluster and fundamental building blocks, Ga_nAs_n (n=1-3) small cluster by linear stacking of stable isomers, the condensed clusters, $(Ga_nAs_n)_m$ where n=1-3 and m =1-6 are modeled. The structure stability of condensed cluster their building blocks are achieved from the electron density of states. Electronic properties of all condensed cluster, with m≥4 are interesting in photo catalytic application as they have large energy gap than that of bulk. Our calculations also so that the $(Ga_3As_3)_m$ cluster are energetically more stable as compared with other condensed cluster.

Keyword: Carbon nanotubes, Density Functional Theory, Gallium arsenide.

I. INTRODUCTION

We are first going discussed carbon nano tubes (CNT) one dimension system gaining momentum with the invention of carbon nano tube (CNT). Appreciating that the potential application of CNT were due to their high mechanical strength ballistic transport and other novel properties (1) researches explored such as one dimensional system of inorganic compounds. For this above approach nanotubes and nanowires from Mo-S compound have been expansively studied and Even because of their many advantages for certain applications of CNTs has been suggested (2,3)as an alternative. Synthesis with unique structural and electronic properties and the ability to advance tune their properties by adding do pants (4). Recently, 1-D systems of CdS compounds have drawn much attention, leading to the synthesis of their nanowires,(5,6) nanotubes ,(7) and nanorods (8−10) with controlled dimensions.

As recently have proved that low dimensional semiconductor material have become a great interest to researcher in nanoscience among these material III-V group semiconductor compound have their paramount technological potential application such as photo electronic device, photonic integrations, ultrahigh frequency microwave and photovoltaic solar cells.

Gallium arsenide (GaAs) as substantial member of the III-V group semiconductor compounds has many distinctive properties as a low electronic effective mass high electron mobility and high saturation drift velocity which make it ideal for optoelectronic, low power and ultra high speed devices application more over it is an advantage material for making nanoscale devices because it surface Fermi level, pinning in the conduction band does not became an insulator due to depletion of carriers. Hence the post decades there have been a great number of studies investigating the chemical and physical properties of its nanostructure.

In the present work, we have investigated the atomic structure and electronic properties of condensed clusters and their infinite nanowires by first principles calculations within the construction of density functional theory.

II. COMPUTATIONAL

All GaAs and condensed clusters reported in this work are optimized by using the DFT with unrestricted B3LYP exchange-correlation potential. To superior describe the binding and geometrical feature of heavy atom, the basis set, effective core potential LanL2DZ, was adopted in this study for both arsenic (As) and gallium (Ga) atoms.. In this basis set the outermost electrons$3s^2\ 3p^6\ 4s^2\ 3d^{10}\ 4p^1$for Ga and $3s^2\ 3p^6\ 4s^2\ 3d^{10}\ 4p^1$ for As were described .the procedures of optimization were based on energy system convergence of energy was superior then10^{-6}(a.u. is atomic unit). In sequence to save time and improve efficiency the processes to optimize the structures with determined bond length ,bond angle, and dihedral angle of the initial value in the convergence criterion of 10^{-4}a.u. based on the optimized tube like clusters. All these calculation were implemented with the Gaussian 09 program package

The binding energy per atom (BE) of cluster is calculated from

$$\text{BE}=\frac{nE(Ga)+nE(As)-E(Ga_nAs_n)}{2n}$$

Where E(Ga), E(As)and $E(Ga_nAs_n)$ are the total energy of a single Ga atom, a single As atom and Ga_nAs_n clusters respectively and nis the number of Ga or As atoms.